UNIVERSIDADE DE SÃO PAULO
INSTITUTO DE FÍSICA DE SÃO CARLOS

Tiago Santiago do Espirito Santo

Quantum collective effects in a dilute cloud of two-level atoms interacting with a classical light

São Carlos

2020

Tiago Santiago do Espirito Santo

Quantum collective effects in a dilute cloud of two-level atoms interacting with a classical light

Thesis presented to the Graduate Program in Physics at the Instituto de Física de São Carlos, Universidade de São Paulo, to obtain the degree of Doctor in Science.

Concentration area: Theoretical and Experimental Physics

Advisor: Prof. Dr. Romain Pierre Marcel Bachelard

Corrected version

(Original version available on the Program Unit)

São Carlos

2020

Espirito Santo, Tiago
Quantum collective effects in a dilute cloud of two-level atoms interacting with a classical light / Tiago Espirito Santo; advisor Romain Bachelard - corrected version -- São Carlos 2020.
88 p.

Thesis (Doctorate - Graduate Program in Theoretical and Experimental Physics) -- Instituto de Física de São Carlos, Universidade de São Paulo - Brasil , 2020.

1. Two-level atom. 2. Superradiance. 3. Subradiance. 4. Ultracold atoms. 5. Cooperative effects. I. Bachelard, Romain, advisor. II. Title.

Dedico esse trabalho à minha mãe, que não pôde acompanhar minha trajetória por partir tão cedo. Porém, mesmo achando incomum eu ter me vislumbrado com o primeiro contato com a física, apoiou minha decisão e sempre me incentivou a fazer minhas próprias escolhas. Também dedico esse trabalho ao meu pai, que nos momentos difíceis sempre me aconselhou a persistir.

ACKNOWLEDGEMENTS

I would like to thank all my colleagues for the fruitful scientific discussions and all my friends for all the random talks and relaxing moments of stress release. I am eternally grateful for the effort of all the professors that instructed me during my life. A special thanks to Guido Pupillo and Johannes Schachenmayer for the supervision during my internship in Strasbourg (France) and to Robin Kaiser and William Guerin for the supervision during my internship in Nice (France).

This study was financed in part by the Coordenação de Aperfeiçoamento de Pessoal de Nível Superior - Brasil (CAPES) - Finance Code 001 and in part by grants from São Paulo Research Foundation (FAPESP) (Grants No. 2015/10763-7, No. 2017/10294-2, No. 2018/12653-2 and No. 2019/02071-9). Research was carried out using computational resources of the Center for Mathematical Sciences Applied to Industry (CeMEAI) funded by São Paulo Research Foundation (FAPESP) (Grant 2013/07375-0).

ABSTRACT

ESPIRITO SANTO, T. S. do **Quantum collective effects in a dilute cloud of two-level atoms interacting with a classical light**. 2020. 88p. Thesis (Doctor in Science) - Instituto de Física de São Carlos, Universidade de São Paulo, São Carlos, 2020.

The collective scattering of light by a large number of coupled scatterers yields a rich many-body physics, yet treating such a problem in the quantum regime is a challenge. In this thesis, we consider a large atomic cloud in free space and driven by a monochromatic light, where the vacuum modes induce long-range dipole-dipole interactions. In order to study clouds of hundreds of particles, higher order correlation terms are neglected, keeping only quantum correlations between pair of atoms: this allows to reduce the number of degrees of freedom from 2^{2N} in the full quantum model to N^2. Most of the works in the literature on dipole-dipole interactions have been performed in the linear optics limit, and our techniques allow to compare classical to beyond-semi-classical results. In particular, superradiance and subradiance have been reported in the decay dynamics of the cloud. Differently, by considering a system in the ground state and switching on the pump, we show that superradiance is also present in the Rabi oscillations at a rate obtained from using a single-dipole model for the radiated intensity. A frequency shift in the Rabi oscillations is also reported, which can be interpreted, in a linear dispersion theory, as a signature of a collective multimode vacuum Rabi splitting. While the classical dipoles model captures correctly the dynamics in the low-intensity regime, it fails for higher saturation, where semi-classical methods can be applied successfully. In particular, we observe a quantum subradiant decay in the intensity of the radiated field in the saturated regime. Furthermore, considering the decay dynamics starting from an initially strongly driven cloud, we observed that the states with $n < N/2$ excited atoms decays much slower than the ones with $n > N/2$: in other words, the upper part of the Dicke ladder is characterized by a superradiant emission, and the lower part by a subradiant one. Finally, investigating the fluorescence spectrum, we obtained quantum cooperative effects that modify the steady-state spectrum: additional sidebands at twice the Rabi frequency for the system driven at resonance and, out of resonance, an asymmetry in the peaks at the generalized Rabi frequency, and for all detection angles. We also present preliminary results of a sensor model that can capture the time evolution of the spectrum in the decay dynamics, a situation that the quantum regression theorem fails to describe. Several of these results were discussed in parallel with experimental data obtained by an experimental group of collaborators, and others aim to guide future experiments.

Keywords: Two-level atom. Superradiance. Subradiance. Ultracold atoms. Cooperative effects. Collective effects.

RESUMO

ESPIRITO SANTO, T. S. do **Efeitos coletivos quânticos em uma nuvem diluída de átomos de dois níveis interagindo com uma luz clássica**. 2020. 88p. Tese (Doutorado em Ciências) - Instituto de Física de São Carlos, Universidade de São Paulo, São Carlos, 2020.

O espalhamento coletivo da luz por um grande conjunto de espalhadores acoplados resulta em uma rica física de muitos corpos, contudo, é um grande desafio tratar esse problema no regime quântico. Nessa tese, consideramos uma grande nuvem atômica, com uma luz monocromática excitando o sistema, no espaço livre em que os modos de vácuo induzem interações dipolo-dipolo de longo alcance. Para estudarmos nuvens com centenas de partículas, negligenciamos correlações de ordem superior, mantendo apenas correlações quânticas entre pares de átomos: com isso reduzimos o número de graus de liberdade de 2^{2N} no modelo quântico completo para $\propto N^2$. Grande parte dos trabalhos presentes na literatura de interação dipolo-dipolo foram realizados no regime de óptica linear, nossas técnicas permitem comparar resultados clássicos com resultados semiclassicos e além. Em particular, superradiância e subradiância foram reportados na dinâmica de decaimento da nuvem. Em contra partida, considerando um sistema no estado fundamental e, ligando o bombeamento, nós mostramos que a superradiância também está presente nas oscilações de Rabi com uma taxa obtida ao se utilizar um modelo de um único dipolo superradiante para a intensidade irradiada. Um deslocamento de frequência na frequência de Rabi também foi observado, o qual pode ser interpretado, com teoria de dispersão linear, como uma assinatura de *vacuum Rabi splitting* coletivo multi-modo. Enquanto o modelo clássico captura corretamente a dinâmica para o regime de baixa intensidade, o mesmo falha aumentando-se a saturação, no entanto podemos aplicar com sucesso modelos semiclássicos. Em particular, observamos um decaimento subradiante quântico na intensidade do campo irradiado no regime saturado. Mais ainda, considerando a dinâmica de decaimento partindo de um estado saturado, observamos que os estados com $n < N/2$ átomos excitados decaem muito mais lentamente do que estados com $n > N/2$: em outras palavras, a parte superior da escada de Dicke é caracterizada pela emissão superradiante enquanto a inferior subradiante. Finalmente, investigando o espectro de fluorescência, obtemos efeitos cooperativos que modificam o perfil do espectro: bandas laterais adicionais presentes no dobro da frequência de Rabi para o regime ressonante e, fora de ressonância, uma assimetria dos picos presentes na frequência de Rabi generalizada obtida para todos os ângulos de detecção. Também apresentamos resultados preliminares de de um modelo de sensor que captura a evolução temporal do espectro na dinâmica de decaimento, situação na qual o teorema da regressão quântica não se aplica. Boa parte dos resultados foram discutidos em paralelo com dados experimentais, obtidos por um grupo experimental de

colaboradores, a outra parte visa guiar experimentos futuros.

Palavras-chave: Átomo de dois níveis. Superradiância. Subradiância. Átomos ultrafrios. Efeitos coletivos. Efeitos cooperativos.

CONTENTS

1 INTRODUCTION

The light-matter interaction is omnipresent in our every day life. The simple act of looking at our reflection in a mirror is possible due to the light reflection by a thin layer of polished metal. The colors we see around us comes from the reflected light at determined frequencies and the fact that different colors come to us in different ways (such as in a rainbow) shows that matter scatters each frequency differently. Also, this light can be converted in other forms of energy, like heat. The resonant cavity in a microwave is an example of heat generated from the electromagnetic energy interacting with matter, in this case the water molecules in the food. We could enumerate a series of other examples, infrared cameras or night-vision goggles, wi-fi technology, photovoltaic cells, tungsten lamps and also LED: the fact that the discovery of the blue LED, an efficient and long-lasting light source, has been rewarded in 2014 by a Nobel prize (in physics to Isamu Akasaki, Hiroshi Amano and Shuji Nakamura) shows that light scattering processes still hold many secrets and promises.

In this thesis, our focus will be at a fundamental level: the scattering of light by a sample of atoms. At a macroscopic level, light scattering is characterized by a change in the propagation direction of the electromagnetic wave. In the case of reflection, there is a deviation on the angle predicted by the law of reflection. Take, as an example, the formation of a rainbow. When the sunlight reaches a raindrop, part of the light enters the drop and, since water has a refractive index $n \approx 1.33$ and air $n \approx 1$, a change in the propagating direction of the light occurs at the interface of the two media, *i.e.* refraction. In water, the index of refraction is dependent on the light frequency, thus, the different color components are refracted at different angles. The color split their path, a phenomenon called dispersion. Then, part of the light is reflected in the droplet itself and, finally, part of the reflected light is refracted returning to the air and forming the rainbow. This whole process described is an example of coherent scattering, where the light is scattered by one raindrop. Another case is if the scatterer size is much smaller than the light wavelength, Rayleigh scattering takes place, a phenomenon where the light is emitted in all directions with little dependency on the frequency. In that case, the light colors are not well separated. Finally, the light can be scattered in a diffusive way, with many scattering events, so that all the colors end up mixing. That is what happens when light is scattered by water drops inside the clouds in the sky, and, it is also the reason why we see them white. Thus, changing the change in size of the scatterer or the number of scattering events, water drops in the clouds or forming rainbows, can modify substantially the way matter interact with light.

A mirror, with a polished layer of metal, is an example of a reflective surface.

However, if one has a rough surface, even if it looks smooth for the naked eye, the microscopic imperfections scatters the light in a diffusive way, *i.e.* in random directions. With such a surface one cannot see his/her own reflection. Thus, as one focuses on smaller scales, the presence of small scatterers and the presence of either order or disorder in the scattering medium becomes important.

In the case of a single atom, the light scattering can be understood as follows: the light is absorbed by one electron that reaches a higher energy level. Then, when the electron decays to a lower energy level, the light is re-emitted in a random direction. This is an example of single scattering, in which the light is scattered once, and this event is usually treated as a random process. For a cloud with a large number of atoms, the light scattered by one atom can be rescattered by another atom and so on. This is called multiple scattering and, in the case of a large number of events, it can be averaged out so one obtains a typical scattering pattern. Nevertheless, the absorption and emission of radiation by a particle is a complicated process that needs a quantum treatment[1], and the multiple scattering picture does not capture all the physics involved.

The quantum nature of the light was explained with the photoelectric effect by Albert Einstein (Nobel Prize in Physics 1921), where a quanta of light (that is, a photon), a package with specific energy $E = h\omega$ (h the Planck constant and ω the light frequency), is necessary to remove an electron from a material. In the case of an electron bounded to an atom, to excite the electron to a higher energy level, the quanta of light must have energy close to the energy difference between the levels. When the electron decays to a lower energy level, the photon is re-emitted, thus concluding the scattering process.

The study of the light-atom interaction gained great attention with the development of new technologies. The invention of the laser, for which we are able to generate light with a well-defined frequency, brought new tools to the quantum optics research field. The momentum of photons leads to mechanical forces of light and it can be applied to cool down a system (laser cooling, Nobel prize in physics in 1997 to Steven Chu, Claude Cohen-Tannoudji and William D. Phillips) and also to produce atomic lattices with magneto-optical trapping. The level of control reached such a precision that an individual quantum system could be manipulated (Nobel prize in physics in 2012 to Serge Haroche and David J. Wineland).

The electron bounded to an atom occupies a specific energy level. One can force a transition of an electron between two energy levels by providing photons with energy close to the energy of the transition, *i.e.* near-resonance. By optical pumping, with a driving laser, one can select an electronic transition and control the Hilbert space of the internal degrees of freedom (Nobel prize of physics 1966 to Alfred Kastler). As a consequence, one can work with a reduced Hilbert space, with one ground state and one excited state, of an object denominated two-level atom.

The two-level atom has the same algebra of the spin-1/2 and quantum dots. With the present level of control of the system, various geometries can be tested by manipulating the optical lattices and atoms trapping. Furthermore, Hamiltonians of interest can be simulated with cold atoms, and even the interaction and coupling parameters can be adjusted[2–5]. Thus, the possible applications are not limited to quantum optics but also to solid matter physics and quantum computing.

As the simplest case of light-atom interaction, the interaction of a two-level atom with a quantized field, a single mode in a cavity, was described by the Janes-Cummings model.[6] The field induces spontaneous emission, process in which the excited state decays to the ground state emitting a photon. When the atom is in free space, one has to consider the infinite number of vacuum modes instead of the single quantized mode. The existence of the vacuum modes also lead to Van Der Waals[7] and Casimir[8] forces, which will not be addressed in this thesis.

Our object of study is a large cloud of two-level atoms, driven by a monochromatic laser, decaying by spontaneous emission due to the vacuum modes. The light is scattered to the empty space, thus it is an open quantum system described with the master equation formalism. It is through atoms that photons can interact and become correlated, and the successive absorption and emission of light (using a multiple scattering picture), leads to a rich many-body physics. We consider ultracold atoms, *i.e.* fixed in position, which are obtained experimentally using laser cooling techniques: practically, we consider that the atoms move of a distance much smaller than the optical wavelength during the time of the experiment. The interaction between atoms is mediated by light with the successive emission and absorption of real and virtual photons. The interaction is long-ranged and, in the dilute regime under consideration, the field decay is proportional to $1/r_{nm}$ (r_{nm} the distance between atoms), thus atoms far away in position can be correlated.

As for other interacting systems, the optical response of a many-body system can substantially differ from the single-body case. Take one two-level atom, driven near-resonance by a monochromatic laser and measure the radiated field intensity to obtain an emission rate. For a large cloud of two-level atoms, cooperative effects can be observed: superradiance[9], an enhancement on the radiated field emission rate or, its counterpart, subradiance, a suppression on the emission.[10] Other collective effects, for example the modification in the radiation pressure force[11–13], collective backscattering and frequency shifts[14–16] have been reported. However, most of the work in the literature were performed in the linear optics limit, with at most one excitation in the system.[11–13,15–18] In this regime of low saturation, *i.e.* a low-intensity driving field, the classical dipoles model is considered and mostly the single scattering process is taking place. In the regime of strong driving, a single atom presents a unique quantum behavior: a three peak profile in the fluorescence power spectrum, known as Mollow triplet.[19] Some cooperative effects in the

quantum regime were studied with a few atoms[20–21], however, treating the many-body case in the saturated regime is a challenge. In this thesis, we investigate cooperative effects in a large dilute cloud by considering up to pair of atoms quantum correlations, a powerful technique to simulate large quantum systems. We also present a detailed description of the radiated field in the linear optics limit and show that, increasing the saturation, the classical dipole model fails to capture the dynamics.

In Chapter 2, we remind the physics of a single two-level atom interacting with light. The atom is driven near resonance by a monochromatic light, resulting in Rabi oscillations. When we consider the vacuum modes, we use the master equation formalism and obtain an open system with the spontaneous emission term given by a Lindbladian dissipative operator. Then, we present the model for N two-level atoms, in the dilute regime, in a cloud with ultracold atoms. We can calculate experimentally accessible observables, the radiated field intensity and the fluorescence power spectrum, by solving the atomic system dynamics.

Since the Hilbert space grows exponentially with the number of atoms, it is a challenge to treat, analytically and with exact simulations, a system with more than a dozen of scatterers. In Chapter 3, we present approximated methods to address larger systems at the price of neglecting higher-order terms. We find that, by considering quantum correlations between pair of atoms and, consequently, neglecting higher order connected correlations, a good approximation is obtained for the dilute regime. We also show that the linear classical dipole equation is recovered by making further approximations in the model. The non-linear mean-field approximation lies in between the classical and the quantum pair correlation method.

In Chapter 4 and 5 we explore experimentally accessible observables. For the radiated field intensity, we obtain results that shows cooperative phenomenon in the switch-on dynamics[22], in collaboration with an experimental group. We also show that, increasing the saturation parameter of the system, the linear optics regime is no longer valid: We enter in the non-linear and quantum regime, in which the mean-field equations and quantum pair correlation method can be applied successfully. We also propose, for the switch-off dynamics, a regime in which quantum subradiance in the decay of the radiated field is present. For the fluorescence power spectrum, we obtained signatures of quantum cooperativity in the modification of the Mollow triplet profile.[23] The results presented here might serve as a guideline to the elaboration of new experiments to detect quantum cooperative features in the scattering of light by a dilute atomic cloud.

2 THEORETICAL BACKGROUND & MODEL

Our object of study is a cloud of many atoms in free space and driven by a laser. We are interested in the collective effects due to the light-mediated long-range interaction in this many-body problem. By performing theoretical calculations and numerical simulations we obtain quantities that can be observed experimentally. Therefore, our goal is to understand recent experimental results and, going beyond, identify new quantum collective effects to propose new experiments. A sketch of the system, a dilute cloud with identical atoms driven by a monochromatic light, with wavevector $\mathbf{k_0}$ in the direction z, with a photon detector in a angle of $\theta = 35°$ can be observed in Fig. 1.

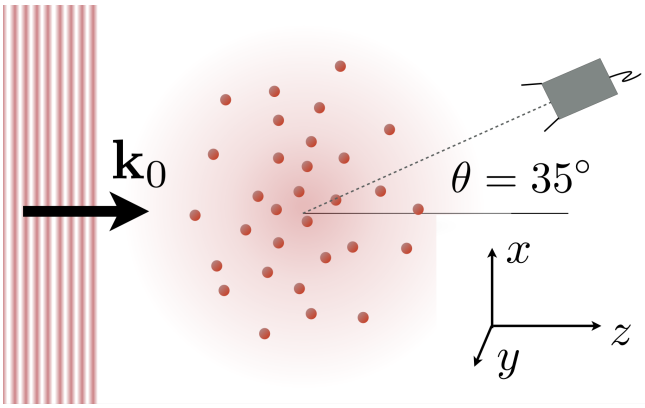

Figure 1 – Dilute cloud of N two-level atoms driven by a plane wave. The far-field detector is placed at a angle θ to measure only the scattered field.
Source: Adapted from ESPIRITO SANTO *et al.*[22]

It is a challenge to treat a quantum many-body problem due to the high number of degrees of freedom and many emission processes occurring concurrently, which result in an untractable set of differential equations for more than a dozen atoms. In that sense, a series of approximations are necessary to address the system in specific conditions. We consider a cloud with ultracold atoms, which means that we can neglect atomic movement due to thermal excitation (and also thermal excited photons) and frequency shifts due to Doppler effect. It is achieved experimentally with laser cooling by reaching a temperature below the Doppler limit. We also consider heavy atoms in the sense that moment kicks due to photon emission are neglected, so the atoms are fixed in position. We treat a dilute system, with distances between neighboring atoms larger than the optical wavelength, so light polarization and near-field terms are neglected. The cloud is composed by N identical two-level atoms, with atom-field interaction in the dipole approximation. The incident laser is treated as a monochromatic light, driven close to the atomic transition, while the free space is composed of an infinity number of vacuum modes. The long-range ($\propto 1/r_{nm}$, with r_{nm} the distance between two atoms) interaction is mediated by the light

with successive emission and absorption of real (light) and virtual (vacuum modes) photons. This many-body dynamics leads to a rich cooperative physics, which we shall discuss in this thesis.

For a better understanding of the approximations and the model, we first introduce the physics of a single atom interacting with the light. The two-level atom, dipole and rotating wave approximation (RWA) are defined in the context of the Rabi oscillations with the atom interacting with a monochromatic field. In the context of the interaction with a quantized field, the Born-Markov and secular (RWA in the master equation) approximations are necessary to obtain the Lindbladian master equation for the reduced density matrix that describes the spontaneous emission process. Finally, we present the many-body model that can be obtained with the same steps developed for a single atom, but additional terms for the dipole-dipole interaction and cooperative emission are present.

2.1 Single two-level atom interacting with light

Considering a single electron bounded to an atom, there are many energy levels that the electron can occupy (see Fig. 2 for the Hydrogen atom example).

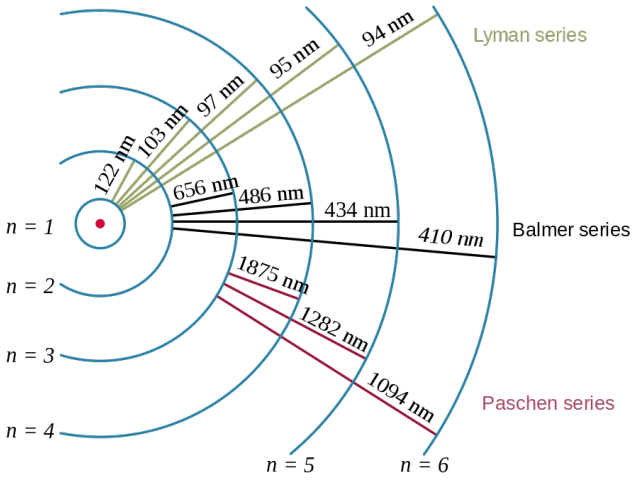

Figure 2 – Representation of the energy levels of a Hydrogen atom with corresponding transition wavelength. Each transition corresponds to a line in the emission spectrum.
Source: HYDROGEN...[24]

If sufficient energy is given to the electron, it can be removed from the atom and it is ionized, but if, the energy is of the order of an atomic transition, one can excite the electron to a specific level. When the electron decay to a lower energy state, a photon with energy $E_{fi} = \hbar\omega_{fi}$ is emitted. E_{fi} is the difference between the enegy levels and ω_{fi} the emitted light frequency, each energy can be associated with a frequency $E_i = \hbar\omega_i$. Each transition between two energy levels correspond to one line in the atomic spectrum (see Fig. 3 for the Hydrogen atom spectrum).

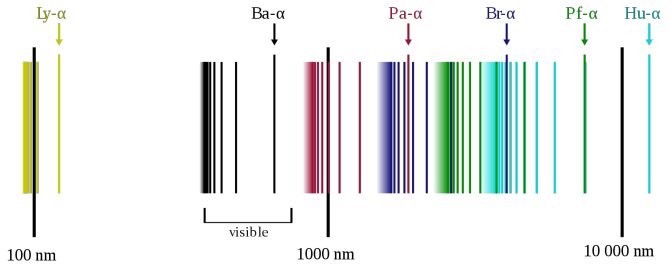

Figure 3 – Spectral lines of the hydrogen atom, on a logarithmic scale.
Source: HYDROGEN...[24]

If one selects a monochromatic light with frequency almost resonant with an atomic transition ($\omega \approx \omega_{fi}$) the transition dynamics behaves as a two-level system with one excited state $|e\rangle$ (higher energy E_e) and one ground state $|g\rangle$ (lower energy E_g), so one can neglect all the other levels. Let us define the state vectors

$$|e\rangle = \begin{pmatrix} 1 \\ 0 \end{pmatrix} \quad , \quad |g\rangle = \begin{pmatrix} 0 \\ 1 \end{pmatrix} \tag{2.1}$$

and the Hamiltonian for the atomic energies

$$\hat{H}_A = \begin{pmatrix} E_e & 0 \\ 0 & E_g \end{pmatrix} \tag{2.2}$$

Note that any two-level system follows the spin-1/2 algebra. We can define the Pauli matrices basis for the 2x2 Hilbert space

$$\mathbb{1} = |e\rangle\langle e| + |g\rangle\langle g| \quad , \quad \hat{\sigma}^x = |e\rangle\langle g| + |g\rangle\langle e| \quad , \quad \hat{\sigma}^y = i(|g\rangle\langle e| - |e\rangle\langle g|) \tag{2.3}$$

and also work with the ladder operators

$$\hat{\sigma}^+ = |e\rangle\langle g| \quad , \quad \hat{\sigma}^- = |g\rangle\langle e| \,. \tag{2.4}$$

$\hat{\sigma}^+$ is the rising operator, taking the atom from the ground state to an excited state, representing the absorption of a photon, and $\hat{\sigma}^-$ is the lowering operator, taking the excited state to the ground state representing the emission of a photon. Without loss of generality, one can rescale the energy setting $E_g = 0$, thus the free two-level atom Hamiltonian becomes

$$\hat{H}_A = \begin{pmatrix} \hbar\omega_{eg} & 0 \\ 0 & 0 \end{pmatrix} = \hbar\omega_{eg} |e\rangle\langle e| = \frac{\hbar\omega_{eg}}{2}(\mathbb{1} + \hat{\sigma}^z) = \hbar\omega_{eg}\hat{\sigma}^+\hat{\sigma}^-. \tag{2.5}$$

To include the atom-field interaction we consider the dipole approximation $H_I = -\mathbf{d}.\mathbf{E}$, with $\mathbf{d}$ the transition dipole moment and $\mathbf{E}$ the electric field, which is valid for field wavelengths much higher than the atomic size $\mathbf{k}.\mathbf{r}_a \ll 1$, with $\mathbf{k}$ the wavevector and $\mathbf{r}_a$ the atomic radius. A demonstration can be found in quantum optics textbooks[25–26], it is valid for both monochromatic light and quantum fields. Basically, any local variation of the field is neglected in the atomic extension.

2.1.1 Interaction with a monochromatic field and Rabi oscillations

Now let us consider a single two-level atom interacting with a single mode field in the dipole approximation $H_I = -\mathbf{d}.\mathbf{E}$. Calculating the expected value for this operator with a general wavevector $|\Psi\rangle = c_g |g\rangle + c_e |e\rangle$, one obtains:

$$-\langle\Psi| \mathbf{d}.\mathbf{E} |\Psi\rangle = -\left(|c_g|^2 \langle g| \mathbf{d}.\mathbf{E} |g\rangle + c_g^* c_e \langle g| \mathbf{d}.\mathbf{E} |e\rangle + c_g c_e^* \langle e| \mathbf{d}.\mathbf{E} |g\rangle + |c_e|^2 \langle e| \mathbf{d}.\mathbf{E} |e\rangle\right). \tag{2.6}$$

Since there is no permanent atomic dipole, $\langle g| \mathbf{d}.\mathbf{E} |g\rangle = \langle e| \mathbf{d}.\mathbf{E} |e\rangle = 0$, and the transition matrix for the dipole operator can be obtained:

$$\mathbf{d} = \begin{pmatrix} 0 & d_{eg} \\ d_{ge} & 0 \end{pmatrix}. \tag{2.7}$$

Considering the dipole phase term ϕ, $d_{eg} = |d_{eg}|e^{i\phi}$, with $d_{ge} = d_{eg}^*$ and the field linearly polarized in the x-axis $E = \mathcal{E}\cos(\omega t)$ we can define the Rabi frequency $\Omega = |d_{eg}|\mathcal{E}/\hbar$ and write the total Hamiltonian $\hat{H} = \hat{H}_A + \hat{H}_I$

$$\hat{H} = \hbar \begin{pmatrix} \omega_{eg} & \Omega e^{i\phi}\cos(\omega t) \\ \Omega e^{-i\phi}\cos(\omega t) & 0 \end{pmatrix}. \tag{2.8}$$

A sketch of the atomic transition is represented in Fig. 4.

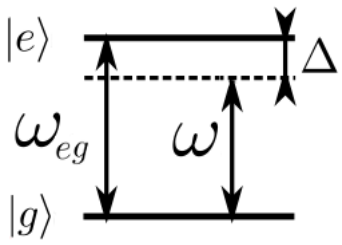

Figure 4 – Representation of the transition between excited and ground states of a two-level atom driven by a near-resonance monochromatic light with frequency ω.
Source: By the author

It is convenient to move from the Schrödinger to the interaction picture with $|\Psi'\rangle = e^{i\hat{H}_A t/\hbar}|\Psi\rangle$, $\hat{H}_I' = e^{i\hat{H}_A t/\hbar}\hat{H}_I e^{-i\hat{H}_A t/\hbar}$ and time-evolution $i\hbar(d/dt)|\Psi'\rangle = \hat{H}_I'|\Psi'\rangle$. For a general state $|\Psi'\rangle = c_g(t)|g\rangle + c_e(t)|e\rangle$, one has:

$$i\hbar\frac{d}{dt}\begin{pmatrix} c_g \\ c_e \end{pmatrix} = \hbar \begin{pmatrix} 0 & \Omega e^{i\phi}e^{i\omega_{eg}t}\cos(\omega t) \\ \Omega e^{-i\phi}e^{-i\omega_{eg}t}\cos(\omega t) & 0 \end{pmatrix}\begin{pmatrix} c_g \\ c_e \end{pmatrix}. \tag{2.9}$$

One can expand $\cos(\omega t) = (e^{i\omega t} + e^{-i\omega t})/2$. Near resonance $\omega \approx \omega_{eg}$, the term $\omega + \omega_{eg}$ oscillates much faster than $\omega - \omega_{eg}$ and it averages to zero for the dynamics time scale of interest. Thus, we neglect the fast oscillating term and keep only the near-resonance term

with the laser-atom detuning defined as $\Delta = \omega - \omega_{eg}$, which is known as the **Rotating Wave Approximation** (RWA). Rewriting the time evolution we obtain:

$$i\hbar\frac{d}{dt}\begin{pmatrix} c_g \\ c_e \end{pmatrix} = \hbar\begin{pmatrix} 0 & \Omega e^{i\phi}e^{-i\Delta t}/2 \\ \Omega e^{-i\phi}e^{i\Delta t}/2 & 0 \end{pmatrix}\begin{pmatrix} c_g \\ c_e \end{pmatrix}. \tag{2.10}$$

In order to remove the time dependency of the Halmiltonian and get rid of the phase term we use the unitary transformation $\hat{R} = e^{i(\Delta t-\phi)\hat{\sigma}^z/2}$. Remember that we transform the wave function $|\tilde{\Psi}\rangle = \hat{R}\,|\Psi'\rangle$, the operators $\tilde{A} = \hat{R}\hat{A}\hat{R}^\dagger$ and the Hamiltonian $\tilde{H} = \hat{R}\hat{H}'\hat{R}^\dagger + i\hbar(d\hat{R}/dt)\hat{R}^\dagger$, but when calculating the expected values of an operator we obtain the same results:

$$\langle\tilde{\Psi}|\,\tilde{A}\,|\tilde{\Psi}\rangle = \langle\Psi'|\,\hat{R}^\dagger\hat{R}\hat{A}\hat{R}^\dagger\hat{R}\,|\Psi'\rangle = \langle\Psi'|\,\hat{A}\,|\Psi'\rangle\,. \tag{2.11}$$

We finally obtain the Rabi Hamiltonian for the atom-field interaction

$$\hat{H}_{Rabi} = \frac{\hbar}{2}\begin{pmatrix} -\Delta & \Omega \\ \Omega & \Delta \end{pmatrix}. \tag{2.12}$$

We can also write the Hamiltonian in terms of the Pauli matrices. The total Hamiltonian for a single two-level atom interacting with a monochromatic field is obtained:

$$\hat{H} = -\hbar\frac{\Delta}{2}\hat{\sigma}^z + \hbar\frac{\Omega}{2}(\hat{\sigma}^+ + \hat{\sigma}^-). \tag{2.13}$$

Let us now consider an atom initially in the ground state ($c_g(0) = 1$ and $c_e(0) = 0$), we can solve the Schrödinger equation with the Hamiltonian in Eq. (2.13) to obtain:

$$\begin{cases} c_g(t) = \cos\left(\dfrac{\Omega_{GR}t}{2}\right) - i\dfrac{\Delta}{\Omega_{GR}}\sin\left(\dfrac{\Omega_{GR}t}{2}\right) \\ c_e(t) = -i\dfrac{\Omega}{\Omega_{GR}}\sin\left(\dfrac{\Omega_{GR}t}{2}\right) \end{cases} \tag{2.14}$$

with $\Omega_{GR} = \sqrt{\Delta^2 + \Omega^2}$ the generalized Rabi frequency. This oscillation between an excited and a ground state, which is equivalent to cycles of photon emission and absorption, is known as Rabi oscillations.

The problem of a single spin-1/2 interacting with a magnetic field was studied by Rabi in 1937.[27] He described the probability of a spin flip. The two-level atom problem has the same algebra of the spin-1/2. If one define the population inversion probability, $W = \langle\Psi|\,\hat{\sigma}^z\,|\Psi\rangle = |c_e|^2 - |c_g|^2$, the behavior presented in Fig. 5 is obtained. In the resonant case ($\Delta = 0$) it is possible to obtain a full inversion ($W = 1$) while out-of resonance it is not ($W < 1$). The larger the detuning $|\Delta|$, the smaller the probability to excite the two-level atom.

The dynamics of the atom-laser interaction is thus described by the Rabi oscillations with the parameters Ω and Δ. To include decoherence and dissipative processes, in our case

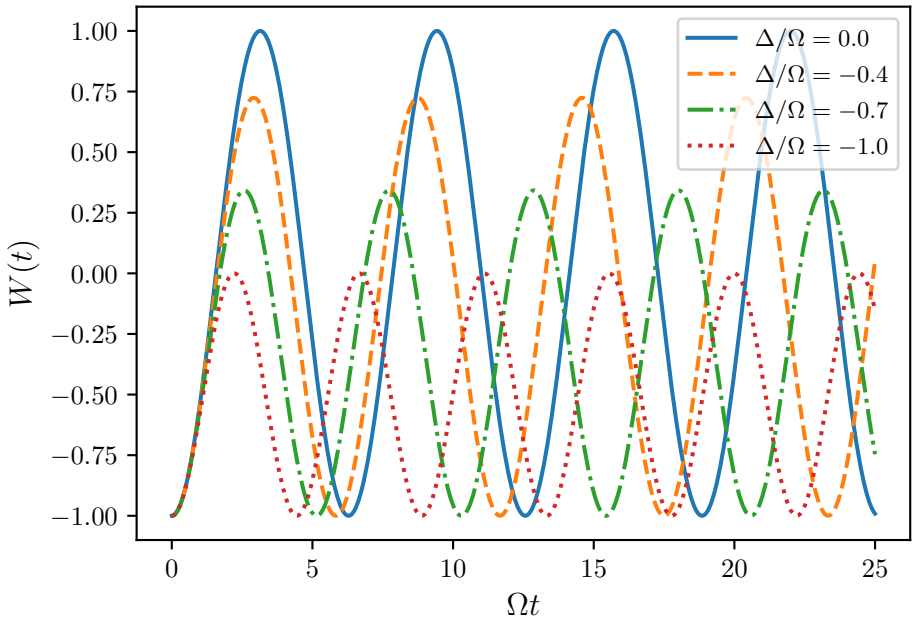

Figure 5 – Rabi oscillations of the inversion varying the detuning. A total inversion of the population ($W = 1$) is only achieved for a system on resonance ($\Delta = 0$).
Source: By the author

spontaneous emission, it is necessary to change to a statistical description with the density matrix formalism. For example, if one is treating a closed quantum system and prepares an initial state in an eigen-state, the system will remain in this state during the time evolution, only varying the phase term. But if an open quantum system is considered, the coupling with the enviroment will take the system to a mixture of states. In the following sections we will introduce the density matrix formalism and, by adding the interaction of the atom with the vacuum modes, we will obtain an open system with the dissipation due to spontaneous emission described by a Lindbladian operator.

2.1.2 Density matrix formalism

The density matrix is an operator that describes an ensemble of all possible states in the system. For a system with many particles or many degrees of freedom, it is often impossible to describe precisely the state and one must use a statistical description.[28] For example, imagine a system with n excited atoms decaying by spontaneous emission in a experimental setup where the sensors are photon detectors. If there is no photon detection at a certain time we know for sure that the system is still with n excited atoms. But if a photon is detected, the system now has $(n-1)$ excited atoms, but there is no way to determine which atom has decayed, thus a statistical mixture of all possible states with $(n-1)$ excited atoms must be considered.

Let us focus our attention on the two-level system. Suppose that due to experimental error or random fluctuation it is not possible to create an excited state with 100% certainty,

so an excited state $|e\rangle$ is achieved with a probability $p_e < 1$, for the other cases the atom is in the ground state $|g\rangle$ with probability $p_g = 1 - p_e$. So one might run the experiment several times and take the statistical average over all the realizations. While the Schrödinger equation evolves one state (wave function) the density matrix is constructed taking the outer product of the states and statistical mixtures are considered. If we have a pure state $|\Psi\rangle$ the density matrix is simply $\hat{\rho} = |\Psi\rangle\langle\Psi|$. For a mixed state $|\Psi\rangle = c_1 |\Psi_1\rangle + c_2 |\Psi_2\rangle$ we take the weighted sum with respective probabilities

$$\hat{\rho} = \sum_n p_n |\Psi_n\rangle\langle\Psi_n| , \tag{2.15}$$

where $p_n = |c_n|^2$ and $\mathrm{Tr}(\hat{\rho}) = \sum p_n = 1$ because it is a sum of probabilities. The time evolution is given by the Von-Neumann equation

$$\frac{d}{dt}\hat{\rho} = -\frac{i}{\hbar}\left[\hat{H}, \hat{\rho}\right] , \tag{2.16}$$

with $[\hat{A}, \hat{B}] = (\hat{A}\hat{B} - \hat{B}\hat{A})$ the commutator. And any operator expected value is obtained with the trace

$$\left\langle \hat{A} \right\rangle = \mathrm{Tr}\left(\hat{A}\hat{\rho}\right) . \tag{2.17}$$

One can choose any orthogonal basis $|\phi_k\rangle$ (with $\langle\phi_k|\phi_l\rangle = \delta_{kl}$, with δ_{kl} the Kronecker delta) to change the representation of the density matrix. The states are rewritten

$$|\Psi_n\rangle = \sum_l a_l^n |\phi_l\rangle \ ; \ \langle\Psi_n| = \sum_k (a_k^n)^* \langle\phi_k| , \tag{2.18}$$

with $\sum_l |a_l^n|^2 = 1$, due to the normalization. The density matrix in this basis becomes

$$\hat{\rho} = \sum_n \sum_l \sum_k p_n a_l^n (a_k^n)^* |\phi_l\rangle\langle\phi_k| , \tag{2.19}$$

with matrix elements

$$\hat{\rho}_{ij} = \langle\phi_i| \hat{\rho} |\phi_j\rangle = \sum_n p_n a_i^n (a_j^n)^* . \tag{2.20}$$

The trace of the density matrix is independent of the representation:

$$\mathrm{Tr}(\hat{\rho}) = \sum_i \hat{\rho}_{ii} = \sum_n p_n \sum_i |a_i^n|^2 = \sum_n p_n = 1. \tag{2.21}$$

For a pure state of a single two-level atom in the energy representation $|\Psi\rangle = c_e |e\rangle + c_g |g\rangle$ the density matrix

$$\hat{\rho} = \begin{pmatrix} \hat{\rho}_{ee} & \hat{\rho}_{eg} \\ \hat{\rho}_{ge} & \hat{\rho}_{gg} \end{pmatrix} = \begin{pmatrix} |c_e|^2 & c_e c_g^* \\ c_g c_e * & |c_g|^2 \end{pmatrix} \tag{2.22}$$

has a physical interpretation for each term. The diagonal ones have the populations of the excited and ground state while the off-diagonal terms are the expected values of the positive and negative frequency of the atomic transition dipole moment.

We can also define a matricial basis to expand the density matrix, in the energy representation the set $\{|e\rangle\langle e|\,;|e\rangle\langle g|\,;|g\rangle\langle e|\,;|g\rangle\langle g|\}$ or a set with Pauli matrices $\{\mathbb{1},\hat{\sigma}^x,\hat{\sigma}^y,\hat{\sigma}^z\}$, and define a state vector with the expected values of the operator to evolve the dynamics:

$$\frac{d}{dt}\mathbf{s}=\frac{d}{dt}\begin{pmatrix}\langle\hat{\sigma}^x\rangle\\ \langle\hat{\sigma}^y\rangle\\ \langle\hat{\sigma}^z\rangle\end{pmatrix}=\begin{pmatrix}\mathrm{Tr}\left(\hat{\sigma}^x(d\hat{\rho}/dt)\right)\\ \mathrm{Tr}\left(\hat{\sigma}^y(d\hat{\rho}/dt)\right)\\ \mathrm{Tr}\left(\hat{\sigma}^z(d\hat{\rho}/dt)\right)\end{pmatrix} \tag{2.23}$$

Some phenomenological dissipative process can be added to Eq. (2.16) with a relaxation matrix $\hat{\Gamma}$:[29]

$$\langle n|\,\hat{\Gamma}\,|m\rangle=\Gamma_n\delta_{nm} \tag{2.24}$$

and we obtain

$$\frac{d}{dt}\hat{\rho}=-\frac{i}{\hbar}\left[\hat{H},\hat{\rho}\right]-\frac{1}{2}\left\{\hat{\Gamma},\hat{\rho}\right\} \tag{2.25}$$

with $\{A,B\}=AB+BA$ the anti-commutator. Other dissipative processes are more complex, atoms collisions for example. For the two-level atom spontaneous emission, the dissipation is given by a Lindbladian operator

$$\frac{d}{dt}\hat{\rho}=-\frac{i}{\hbar}\left[\hat{H},\hat{\rho}\right]+\frac{\Gamma}{2}\left(2\hat{\sigma}^-\hat{\rho}\hat{\sigma}^+-\left\{\hat{\sigma}^+\hat{\sigma}^-,\hat{\rho}\right\}\right). \tag{2.26}$$

Eq. (2.26) is called a Lindbladian master equation. Using this equation with the single atom Hamiltonian in Eq. (2.13) and calculating the dynamics with the Pauli matrices basis Eq. (2.23) we obtain, for a two-level atom driven by a monochromatic light and decaying through spontaneous emission, the following set of equations:

$$\frac{d}{dt}\begin{pmatrix}\langle\hat{\sigma}^x\rangle\\ \langle\hat{\sigma}^y\rangle\\ \langle\hat{\sigma}^z\rangle\end{pmatrix}=\begin{pmatrix}-\Gamma/2 & \Delta & 0\\ -\Delta & -\Gamma/2 & -\Omega\\ 0 & \Omega & -\Gamma\end{pmatrix}\begin{pmatrix}\langle\hat{\sigma}^x\rangle\\ \langle\hat{\sigma}^y\rangle\\ \langle\hat{\sigma}^z\rangle\end{pmatrix}+\begin{pmatrix}0\\ 0\\ -\Gamma\end{pmatrix} \tag{2.27}$$

We can obtain the steady-state solution ($d\boldsymbol{\sigma}/dt=0$, with $\boldsymbol{\sigma}=(\langle\hat{\sigma}^x\rangle,\langle\hat{\sigma}^y\rangle,\langle\hat{\sigma}^z\rangle)^T$) where, defining the adimensional saturation parameter $s=2\Omega^2/(\Gamma^2+4\Delta^2)$, the population of the excited state is $|c_e|^2_{ss}=(1+\langle\hat{\sigma}^z_{ss}\rangle)/2=s/2(s+1)$. At resonance, the saturation is basically the ratio, in the steady-state, of the excitation rate due to the Rabi frequency Ω and the decay rate Γ of the excited population. Taking the limit of very high saturation ($s\to\infty$) $|c_e|^2_{ss}\to 0.5$, in terms of the inversion $W_{ss}\to 0$. For the limit of very low saturation ($s\to 0$) $|c_e|^2_{ss}\to 0$ and $W_{ss}\to -1$. The very low saturation case is known as the linear optics limit.

Solving Eq. (2.27) we obtain $\boldsymbol{\sigma}(t)=e^{Mt}(\boldsymbol{\sigma}_0-\boldsymbol{\sigma}_{ss})+\boldsymbol{\sigma}_{ss}$, and using the ground-state as initial condition we calculate the inversion for different values of saturation by varying the laser-atom detuning (see Fig. 6). We obtain the Rabi oscillation and also a damping in the population inversion due to the decay rate Γ. Note that, for high saturation $s=50$,

the long time inversion tends to 0 while for small saturation it tends to -1. By increasing $|\Delta|$ we observe a higher frequency of oscillations (higher generalized Rabi frequency) and a smaller value for the maximum inversion, as in Fig. 5.

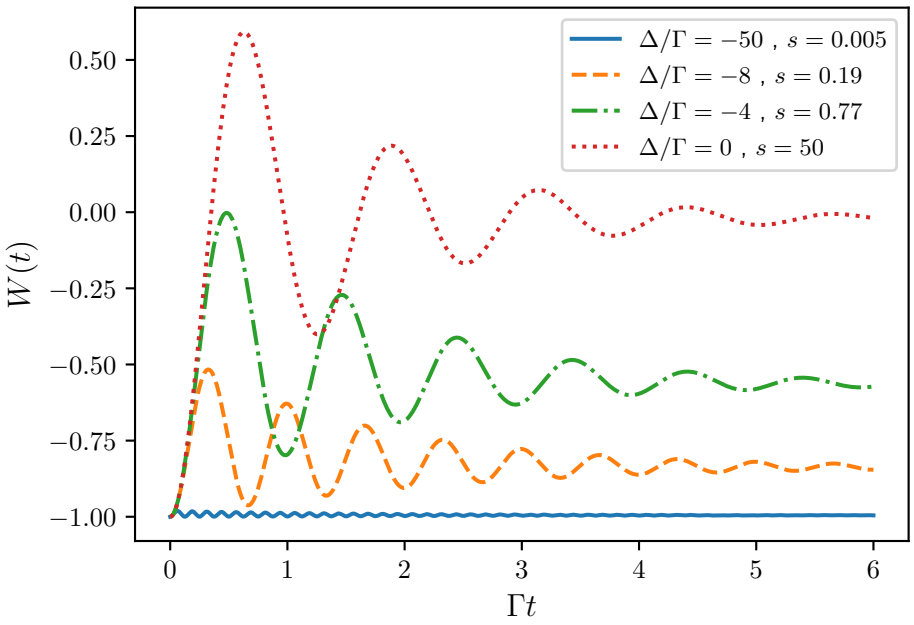

Figure 6 – Damping of the Rabi oscillations of the inversion W for a system with spontaneous emission, a constant Rabi frequency ($\Omega/\Gamma = 5$) and varying the saturation parameter. In the limit of high saturation, in the steady-state the maximum excited population tends to 0.5 ($|c_e|^2 \to 0.5$); in the limit of low saturation $W \approx -1$ and $|c_g|^2 \approx 1$ for all the dynamics which is the linear optics limit.
Source: By the author

For a better understanding of the spontaneous emission processes, all the approximations and physics involved, we will obtain in the following section the Lindbladian master equation by considering the interaction of a two-level atom with the vacuum modes. We will trace out the bath infinite number of degrees of freedom to work only with the atomic system reduced density matrix. We follow the microscopic derivation of the quantum master equation[29], but using the scalar light approximation in which polarization is neglected.

2.1.3 Interaction with the vacuum modes

The spontaneous emission process arise from the single atom interaction with the vacuum modes, a reservoir treated as a quantum field with an infinite number of degrees of freedom. The total Hamiltonian for a single two-level atom in the vacuum is given by $\hat{H} = \hat{H}_A + \hat{H}_R + \hat{H}_I$, with $\hat{H}_A = \hbar\omega_{eg}\hat{\sigma}^+\hat{\sigma}^-$ and $\hat{H}_R = \sum \hbar\omega_k \hat{b}_k^\dagger \hat{b}_k$, where $\hat{b}_k$ is the annihilation and $\hat{b}_k^\dagger$ the creation operator of a photon of frequency ω_k. The interaction is

considered in the dipole approximation $\hat{H}_I = -\mathbf{d}.\mathbf{E}$ with the quantized field

$$E = i\sum_k \sqrt{\frac{2\pi\hbar\omega_k}{V}}(\hat{b}_k - \hat{b}_k^\dagger), \tag{2.28}$$

V is the field volume quantization. Here we consider the scalar light model, for the optical transition $\Delta m = 0$, disregarding polarization effects. Recalling that the dipole operator is given by $\mathbf{d} = d_{eg}\hat{\sigma}^+ + d_{ge}\hat{\sigma}^-$, with $d_{eg} = |\mathbf{d}|e^{i\phi}$. The atomic transition dipole phase is arbitrary since it can be changed with a unitary transformation $\hat{U} = e^{-i\theta\hat{\sigma}^z/2}$ without changing the atomic Hamiltonian. For convenience, let us choose a phase factor in which $d_{eg} = i|\mathbf{d}|$ is a pure imaginary number. The interaction Hamiltonian, in the Schrödinger picture becomes

$$\hat{H}_I = \sum_k g_k \left(\hat{\sigma}^+ - \hat{\sigma}^-\right)\left(\hat{b}_k - \hat{b}_k^\dagger\right), \tag{2.29}$$

with $g_k = |\mathbf{d}|\sqrt{2\pi\hbar\omega_k/V}$ the atom-field coupling constant. Now we move to the interaction picture with the unitary transformation $\hat{U} = e^{-i(\hat{H}_A+\hat{H}_R)t/\hbar}$:

$$\hat{H}_I = \sum_k g_k \left(e^{i\omega_{eg}t}\hat{\sigma}^+ - e^{-i\omega_{eg}t}\hat{\sigma}^-\right)\left(e^{-i\omega_k t}\hat{b}_k - e^{i\omega_k t}\hat{b}_k^\dagger\right). \tag{2.30}$$

Performing the RWA and keeping only the slow varying term $(\omega_{eg} - \omega_k)$:

$$\hat{H}_I = \sum_k g_k \left(\hat{\sigma}^+\hat{B}_k(t) + \hat{\sigma}^-\hat{B}_k^\dagger(t)\right), \tag{2.31}$$

with $\hat{B}_k(t) = e^{i(\omega_{eg}-\omega_k)t}\hat{b}_k$. The dynamics in the interaction picture is given by the Von-Neumann equation

$$\frac{d}{dt}\hat{\rho} = -\frac{i}{\hbar}\left[\hat{H}_I, \hat{\rho}\right] \tag{2.32}$$

with $\hat{\rho}$ the total density matrix of the system interaction with the reservoir. Integrating the Eq. (2.32) one obtain

$$\hat{\rho}(t) = \hat{\rho}(0) - \frac{i}{\hbar}\int_0^t \left[\hat{H}_I(s), \hat{\rho}(s)\right] ds. \tag{2.33}$$

The reservoir being the vacuum state with no photons $|\varepsilon\rangle$, we consider that the interaction with the system is weak in the sense that any perturbation in the reservoir caused by the system can be neglected, thus, the vacuum state is stationary. In this limit of weak interaction, we can separate the atomic system and the reservoir density matrix in a product state

$$\hat{\rho}(t) = \hat{\rho}_A(t) \otimes \hat{\rho}_B \tag{2.34}$$

with $\hat{\rho}_B = |\varepsilon\rangle\langle\varepsilon|$. The weak-coupling approximation that leads to the product state is known as the Born approximation. Assuming that for $t = 0$ there is no interaction of the system with the reservoir, $\mathrm{Tr}_B\left(\left[\hat{H}_I(t), \hat{\rho}(0)\right]\right) = 0$, inserting Eq. (2.33) in Eq. (2.32) and tracing out the reservoir degrees of freedom we obtain

$$\frac{d}{dt}\hat{\rho}_A(t) = -\frac{1}{\hbar^2}\int_0^t \mathrm{Tr}_B\left(\left[\hat{H}_I(t), \left[\hat{H}_I(s), \hat{\rho}_A(s) \otimes \hat{\rho}_B\right]\right]\right) ds \tag{2.35}$$

a reduced master equation in which we only look at the dynamics of the atomic system. We can apply the Markov approximation by substituting $\hat{\rho}_A(s)$ by $\hat{\rho}_A(t)$, which means that the system has no memory, so the state at a time t will not depend on the system history. Now, substituting $s \to t - s$ and taking the limit $s \to \infty$ (that means that the system dynamics varies much slower than the reservoir correlations decay. Alias, when a photon is created, the perturbation in the vacuum decays before there is any appreciable change in the system state) we finally obtain the Markovian master equation:

$$\frac{d}{dt}\hat{\rho}_A(t) = -\frac{1}{\hbar^2}\int_0^\infty \mathrm{Tr}_B\left(\left[\hat{H}_I(t), \left[\hat{H}_I(t-s), \hat{\rho}_A(t)\otimes\hat{\rho}_B\right]\right]\right) ds. \tag{2.36}$$

Using Eq. (2.31) we obtain

$$\begin{aligned}
\frac{d}{dt}\hat{\rho}_A(t) = \frac{1}{\hbar^2}\int_0^\infty \sum_k\sum_{k'} g_k g_{\kappa'}\Big(&\hat{\sigma}^+\hat{\rho}_A(t)\hat{\sigma}^+\left(\left\langle \hat{B}_k(t)\hat{B}_{k'}(t-s)\right\rangle + \left\langle \hat{B}_{k'}(t-s)\hat{B}_k(t)\right\rangle\right) + \\
&-\hat{\sigma}^+\hat{\sigma}^-\hat{\rho}_A(t)\left\langle \hat{B}_k(t)\hat{B}^\dagger_{k'}(t-s)\right\rangle + \hat{\sigma}^-\hat{\rho}_A(t)\hat{\sigma}^+\left(\left\langle \hat{B}_k(t)\hat{B}^\dagger_{k'}(t-s)\right\rangle + \left\langle \hat{B}_{k'}(t-s)\hat{B}^\dagger_k(t)\right\rangle\right) + \\
&+\hat{\sigma}^+\hat{\rho}_A(t)\hat{\sigma}^-\left(\left\langle \hat{B}^\dagger_{k'}(t-s)\hat{B}_k(t)\right\rangle + \left\langle \hat{B}^\dagger_k(t)\hat{B}_{k'}(t-s)\right\rangle\right) - \hat{\rho}_A(t)\hat{\sigma}^-\hat{\sigma}^+\left\langle \hat{B}^\dagger_{k'}(t-s)\hat{B}_k(t)\right\rangle + \\
&-\hat{\sigma}^-\hat{\sigma}^+\hat{\rho}_A(t)\left\langle \hat{B}^\dagger_k(t)\hat{B}_{k'}(t-s)\right\rangle - \hat{\rho}_A(t)\hat{\sigma}^+\hat{\sigma}^-\left\langle \hat{B}_{k'}(t-s)\hat{B}^\dagger_k(t)\right\rangle + \\
&+\hat{\sigma}^-\hat{\rho}_A(t)\hat{\sigma}^-\left(\left\langle \hat{B}^\dagger_k(t)\hat{B}^\dagger_{k'}(t-s)\right\rangle + \left\langle \hat{B}^\dagger_{k'}(t-s)\hat{B}^\dagger_k(t)\right\rangle\right)\Big) ds.
\end{aligned} \tag{2.37}$$

Then, applying the stationary bath condition $\left\langle B^\alpha_k(t)B^{\alpha'}_{k'}(t-s)\right\rangle = \left\langle B^\alpha_k(s)B^{\alpha'}_{k'}(0)\right\rangle$ (for any reservoir correlation), and the relations, for the vacuum with no photon, $\left\langle \hat{b}_k\hat{b}_l\right\rangle = \left\langle \hat{b}^\dagger_k\hat{b}^\dagger_k\right\rangle = \left\langle \hat{b}^\dagger_k\hat{b}_l\right\rangle = 0$ and $\left\langle \hat{b}_k\hat{b}^\dagger_l\right\rangle = \delta_{kl}$:

$$\begin{aligned}
\frac{d}{dt}\hat{\rho}_A = \frac{1}{\hbar^2}\int_0^\infty \sum_k g_k^2\Big(&\hat{\sigma}^-\hat{\rho}_A\hat{\sigma}^+\left(\left\langle B_k(s)B^\dagger_k(0)\right\rangle + \left\langle B_k(0)B^\dagger_k(s)\right\rangle\right) + \\
&-\hat{\sigma}^+\hat{\sigma}^-\hat{\rho}_A\left\langle B_k(s)B^\dagger_k(0)\right\rangle - \hat{\rho}_A\hat{\sigma}^+\hat{\sigma}^-\left\langle B_k(0)B_k(s)\right\rangle\Big) ds,
\end{aligned} \tag{2.38}$$

with

$$\begin{cases}
\displaystyle\int_0^\infty \sum_k g_k^2\left\langle B_k(s)B^\dagger_k(0)\right\rangle ds = \int_0^\infty \sum_k g_k^2 e^{i(\omega_{eg}-\omega_k)s}\left\langle b_k b^\dagger_k\right\rangle ds \\
\displaystyle\int_0^\infty \sum_k g_k^2\left\langle B_k(0)B^\dagger_k(s)\right\rangle ds = \int_0^\infty \sum_k g_k^2 e^{-i(\omega_{eg}-\omega_k)s}\left\langle b_k b^\dagger_k\right\rangle ds
\end{cases} \tag{2.39}$$

By defining the constants

$$\begin{cases}
\Gamma = \dfrac{1}{\hbar^2}\displaystyle\int_{-\infty}^\infty \sum_k g_k^2 e^{i(\omega_{eg}-\omega_k)s}\left\langle b_k b^\dagger_k\right\rangle ds \\
\Lambda = \dfrac{1}{2i\hbar^2}\left(\displaystyle\int_0^\infty \sum_k g_k^2 e^{i(\omega_{eg}-\omega_k)s}\left\langle b_k b^\dagger_k\right\rangle ds - \int_{-\infty}^0 \sum_k g_k^2 e^{i(\omega_{eg}-\omega_k)s}\left\langle b_k b^\dagger_k\right\rangle ds\right)
\end{cases} \tag{2.40}$$

we can write the reduced master equation in the Lindblad form, dropping the atomic system index:

$$\frac{d}{dt}\hat{\rho} = -i\Lambda\left[\hat{\sigma}^+\hat{\sigma}^-, \hat{\rho}\right] + \frac{\Gamma}{2}\left(2\hat{\sigma}^-\hat{\rho}\hat{\sigma}^+ - \left\{\hat{\sigma}^+\hat{\sigma}^-, \hat{\rho}\right\}\right) \tag{2.41}$$

The integral for Λ is divergent and even with a relativistic quantum electrodynamics approach it does not converge. A renormalization theory is necessary.[25] It introduces a lineshift Λ, which is of the order of Γ ($\Lambda \ll \omega_{eg}$). It is known as Lamb shift and will be neglected in our model.

In order to calculate the decay constant Γ we go to the continuum limit with the dispersion relation $\omega = kc$ (c the velocity of the light)

$$\sum_k \to \frac{V}{(2\pi)^3}\int_0^{2\pi}\int_0^{\pi}\int_0^{\infty} k^2 \sin\theta dk d\theta d\phi = \frac{V}{2\pi^2 c^3}\int_0^{\infty}\omega^2 d\omega, \tag{2.42}$$

so we can write

$$\Gamma = \int_{-\infty}^{\infty}\int_0^{\infty}\frac{2|\mathbf{d}|^2\omega^3}{\hbar c^3 2\pi}e^{i(\omega_{eg}-\omega)s}d\omega ds. \tag{2.43}$$

Using the integral formula

$$\frac{1}{2\pi}\int_{-\infty}^{\infty} e^{i(\omega_{eg}-\omega)s}ds = \delta(\omega_{eg}-\omega), \tag{2.44}$$

with $\delta(\omega_{eg}-\omega)$ the Dirac delta, we finally obtain:

$$\Gamma = \frac{2|\mathbf{d}|^2\omega_{eg}^3}{\hbar c^3}. \tag{2.45}$$

Let us now consider the Hamiltonian driven by a monochromatic field in Eq. (2.13) and the Lindbladian operator in Eq. (2.41), we can write the master equation for the decay of a driven single two-level atom:

$$\frac{d}{dt}\hat{\rho} = i\frac{\Delta}{2}\left[\hat{\sigma}^z,\hat{\rho}\right] - i\frac{\Omega}{2}\left[\hat{\sigma}^+ + \hat{\sigma}^-,\hat{\rho}\right] + \frac{\Gamma}{2}\left(2\hat{\sigma}^-\hat{\rho}\hat{\sigma}^+ - \left\{\hat{\sigma}^+\hat{\sigma}^-,\hat{\rho}\right\}\right). \tag{2.46}$$

We conclude that the interaction with the vacuum modes leads to the phenomenon of spontaneous emission. Looking at the excited state population $(1+\langle\hat{\sigma}^z\rangle)/2$ with initial condition the ground-state $|c_g|^2 = 1$ we observe, in Fig. 7, an overdamped behavior for $\Omega_{GR} \approx \Gamma$ (almost no Rabi oscillations) and a damped oscillatory dynamics for $\Omega_{GR} > \Gamma$.

If a thermal equilibrium reservoir is considered, one should use the bath correlation relations

$$\left\langle b_k^\dagger b_{k'}\right\rangle = \delta_{kk'}\mathcal{N}(\omega_k) \quad , \quad \left\langle b_k b_{k'}^\dagger\right\rangle = \delta_{kk'}\left(1+\mathcal{N}(\omega_k)\right) \tag{2.47}$$

with

$$\mathcal{N}(\omega_k) = \frac{1}{e^{\beta\hbar\omega_k}-1} \tag{2.48}$$

the Planck distribution for the average number of thermally excited photons in the mode ω_k[29] and $\beta = k_B T$ (k_B the Boltzmann constant and T the temperature). More terms of Eq. (2.37) should be kept and, neglecting the Lamb shift, one obtains

$$\frac{d}{dt}\hat{\rho} = \left(1+\mathcal{N}(\omega_{eg})\right)\frac{\Gamma}{2}\left(2\hat{\sigma}^-\hat{\rho}\hat{\sigma}^+ - \left\{\hat{\sigma}^+\hat{\sigma}^-,\hat{\rho}\right\}\right) + \mathcal{N}(\omega_{eg})\frac{\Gamma}{2}\left(2\hat{\sigma}^+\hat{\rho}\hat{\sigma}^- - \left\{\hat{\sigma}^-\hat{\sigma}^+,\hat{\rho}\right\}\right). \tag{2.49}$$

However, in the presented ultracold atom model, we neglect thermally excited photons.

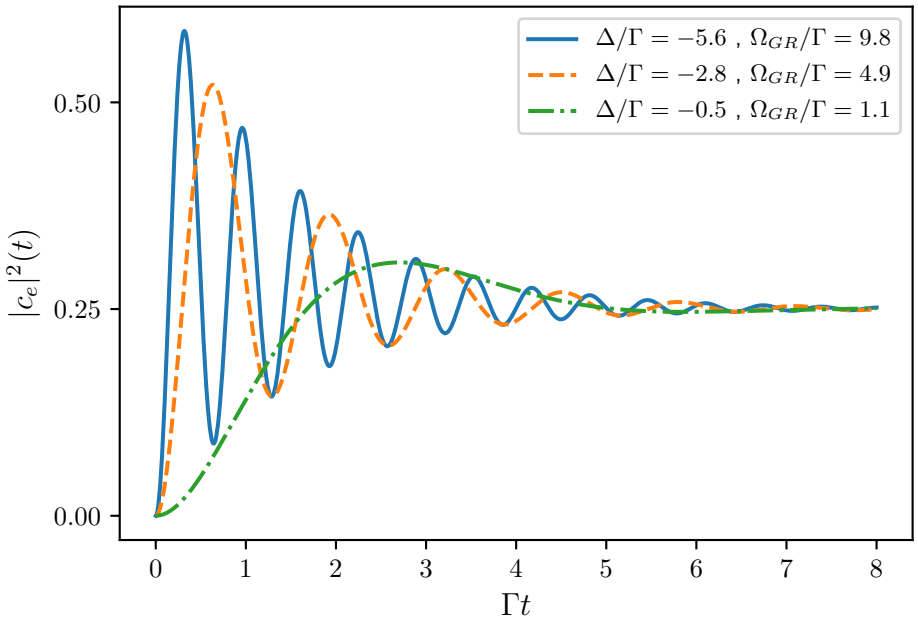

Figure 7 – Population of the excited state varying Ω_{GR}. We set a constant saturation parameter $s = 1$ since it defines the steady-state value of $|c_e|^2 = s/2(s+1)$. We observe an overdamped behavior for $\Omega_{GR} \approx \Gamma$ and Rabi oscillations for $\Omega_{GR} > \Gamma$.
Source: By the author

2.2 Many two-level atoms

Now, let us consider a cloud of N identical two-level atoms, fixed in position, driven by a monochromatic laser and decaying due to the vacuum modes (Fig. 1). The Hilbert space of a single two-level atom has dimension 2×2, which means that the dimension of the system with N atoms, obtained with the tensor (Kronecker) product, has dimension $(2 \times 2)^N$. We label the atoms in an ordered manner and construct an operator acting only on the Hilbert space of an atom at position $\mathbf{r}_n$ via a Kronecker product of 2×2 identity operators, except for the ordered label position n where the atomic operator is placed. For example,

$$\hat{\sigma}_n^+ = \mathbb{1} \otimes \mathbb{1} \otimes \ldots \mathbb{1} \otimes \hat{\sigma}^+ \otimes \mathbb{1} \cdots \otimes \mathbb{1} \tag{2.50}$$

with $\hat{\sigma}^+$ the 2×2 single atom ladder operator. That way, each operator is a $2^N \times 2^N$ matrix, with the same dimension of the Hilbert space. The atomic operators have the commutation relations $[\hat{\sigma}_n^+, \hat{\sigma}_m^-] = \delta_{nm}\hat{\sigma}_n^z$, $[\hat{\sigma}_n^\pm, \hat{\sigma}_m^z] = \mp 2\delta_{nm}\hat{\sigma}_n^\pm$. The interaction Hamiltonian is given by[12], after a change in the rotation frame

$$\begin{aligned}\hat{H} = &-\hbar\frac{\Delta}{2}\sum_n \hat{\sigma}_n^z + \hbar\frac{\Omega}{2}\sum_n \left(e^{-i\mathbf{k}_0.\mathbf{r}_n}\hat{\sigma}_n^- + e^{i\mathbf{k}_0.\mathbf{r}_n}\hat{\sigma}_n^+\right) + \\ &+ \hbar\sum_n\sum_k g_k \left(e^{i\omega_{eg}t}\hat{\sigma}_n^- + e^{-i\omega_{eg}t}\hat{\sigma}_n^+\right)\left(e^{-i\omega_k t + i\mathbf{k}.\mathbf{r}_n}\hat{b}_k + e^{i\omega_k t - i\mathbf{k}.\mathbf{r}_n}\hat{b}_k^\dagger\right)\end{aligned} \tag{2.51}$$

where the phase terms, $e^{i\mathbf{k}.\mathbf{r}_n}$, due to the atomic positions are added. $\mathbf{k}_0$ is the incident laser wavevector and $\mathbf{k}$ the vacuum mode k wavevector. Each atom interact individually with the light, the two terms at the beginning describe the interaction with the monochromatic laser and the last term the interaction with the vacuum modes. By tracing out the vacuum modes, performing the same approximations presented in the single atom case, we obtain the reduced master equation for the atomic system:

$$\begin{aligned}\frac{d\hat{\rho}}{dt} = &\frac{i\Delta}{2}\sum_n \left[\sigma_n^z, \hat{\rho}\right] - \frac{i\Omega}{2}\sum_n \left[e^{-i\mathbf{k}_0.\mathbf{r}_n}\hat{\sigma}_n^- + e^{i\mathbf{k}_0.\mathbf{r}_n}\hat{\sigma}_n^+, \hat{\rho}\right] + \\ &- i\sum_n\sum_{m\neq n}\Delta_{nm}\left[\hat{\sigma}_n^+\hat{\sigma}_m^-, \hat{\rho}\right] + \frac{1}{2}\sum_n\sum_m \gamma_{nm}\left(2\hat{\sigma}_m^-\hat{\rho}\hat{\sigma}_n^+ - \left\{\hat{\sigma}_n^+\hat{\sigma}_m^-, \hat{\rho}\right\}\right)\end{aligned} \tag{2.52}$$

with

$$\Delta_{nm} = -\frac{\Gamma}{2}\frac{\cos(k_0 r_{nm})}{k_0 r_{nm}} \quad ; \quad \gamma_{nm} = \Gamma\frac{\sin(k_0 r_{nm})}{k_0 r_{nm}} \tag{2.53}$$

the long-range ($1/r_{nm}$, with $r_{nm} = |\mathbf{r}_n - \mathbf{r}_m|$) light-mediated dipole-dipole coupling. These coupling terms are derived from the exponential interaction kernel with the scalar light approximation.[30] Since we are in the dilute regime, the near-field effects are neglected. For dense systems one can include more terms in the dipole expansion ($\propto 1/r_{nm}^3$). The Markov approximation ($s \to \infty$) also requires a system size not too large ($s \gg \max\{r_{nm}/c\}$) in the sense that the time required for a photon to travel through the cloud is much shorter than the cooperative emission time[18] ($s \gg \max\{r_{nm}/c\} < 1/\max\{\gamma_{nm}\}$). Δ_{nm} is the dipole-dipole interaction cooperative lineshift and γ_{nm} the cooperative emission term.

By solving Eq. (2.52) numerically we obtain the density matrix dynamics and we can access the expected value of any operator $\left\langle \hat{O}(t)\right\rangle = \mathrm{Tr}\left(\hat{O}\hat{\rho}(t)\right)$. We can calculate observables of the dynamics to compare with and propose experiments to observe quantum effects in this system.

2.3 Observables

There are some quantities that one accesses more easily experimentally, related to the system dynamics. For example, the Lieb-Robinson bounds establish an upper limit for the propagation of the information in quantum spin systems[31], with a exponential decay for the correlations. The propagation of the perturbation as a function of space and time, in regular lattices, form a linear light cone for short-range interactions and, for long-range interactions, the velocity can increase with the traveled distance forming a logarithmic profile for the propagation of the perturbation.[32] One way to observe the Lieb-Robinson bounds is to create a linear lattice of two-level atoms, apply a local perturbation (total population inversion in a small region of the lattice) and monitor the

propagation of the total excited population ($P = \sum_n \langle \hat{\sigma}_n^+ \hat{\sigma}_n^- \rangle$) or the connected correlations ($C_{nm} = \langle \hat{\sigma}_n^z \hat{\sigma}_m^z \rangle - \langle \hat{\sigma}_n^z \rangle \langle \hat{\sigma}_m^z \rangle$).[33]

However, probing the atomic state or the connected correlations is a difficult experimental task. An observable much more accessible is the radiated electric field and also the fluorescence power spectrum, which will be more detailed in the following sections.

2.3.1 Electric field in the far-field limit

The radiated field properties can be determined from the atomic system operators. The Markov approximation cannot be considered for the field density operator, so the route we used to obtain the atomic system reduced master equation cannot be used to determine the field properties. Another route should be used, we refer the reader to Ref. Agarwal[34]. The positive frequency radiated electric field operator, in the far-field limit, in a direction $\hat{n} = (\sin\theta\cos\phi, \sin\theta\sin\phi, \cos\theta)$, with angles defined for spherical coordinates with the incident laser wave vector $\mathbf{k}_0$ in the z-axis direction, is proportional to

$$\hat{E}^+(t) \propto \sum_{n=1}^{N} \hat{\sigma}_n^-(t) e^{-ik_0 \hat{n}.\mathbf{r}_n}. \tag{2.54}$$

The intensity in the far-field is given by

$$I(\theta,\phi) \propto \sum_{n=1}^{N}\sum_{m=1}^{N} \left\langle \hat{\sigma}_n^+ \hat{\sigma}_m^- \right\rangle e^{ik_0 \hat{n}.(\mathbf{r}_n - \mathbf{r}_m)} \tag{2.55}$$

To reduce fluctuations, in absence of polarization the average intensity depends only on the angle to the pump beam θ, we take the mean value over ϕ. In a experimental setup, one can assume multiple realizations are considered:

$$I(\theta) \propto \sum_{n=1}^{N}\sum_{m=1}^{N} \left\langle \hat{\sigma}_n^+ \hat{\sigma}_m^- \right\rangle e^{ik_0 z_{nm}\cos\theta} I_0\left(\sqrt{-k_0^2 \sin^2\theta ({x_{nm}}^2 + {y_{nm}}^2)}\right) \tag{2.56}$$

with I_0 the modified Bessel function of first kind of order 0 and (x_{nm}, y_{nm}, z_{nm}) the Cartesian coordinates of $(\mathbf{r}_n - \mathbf{r}_m)$.

A common experimental protocol (Fig. 8) is to switch on the external laser at $t = 0$, drive the system to the steady-state (or at least very close letting the laser on for long times $\Gamma t \gg 1$), then switch off the driving laser and observe the field decay. Hereafter the intensity is normalized by the steady-state value.

In Fig. 9 we compare the normalized radiated intensity for a single atom and 5 atoms. For the field decay we observe distinct behaviors: the single atom decay with a constant rate Γ while for $N = 5$ there is a faster decay, with the cooperative decay rate $\Gamma_N > \Gamma$ (superradiance) in the beginning ($\Gamma t \approx 15$) and a slower decay (subradiance)

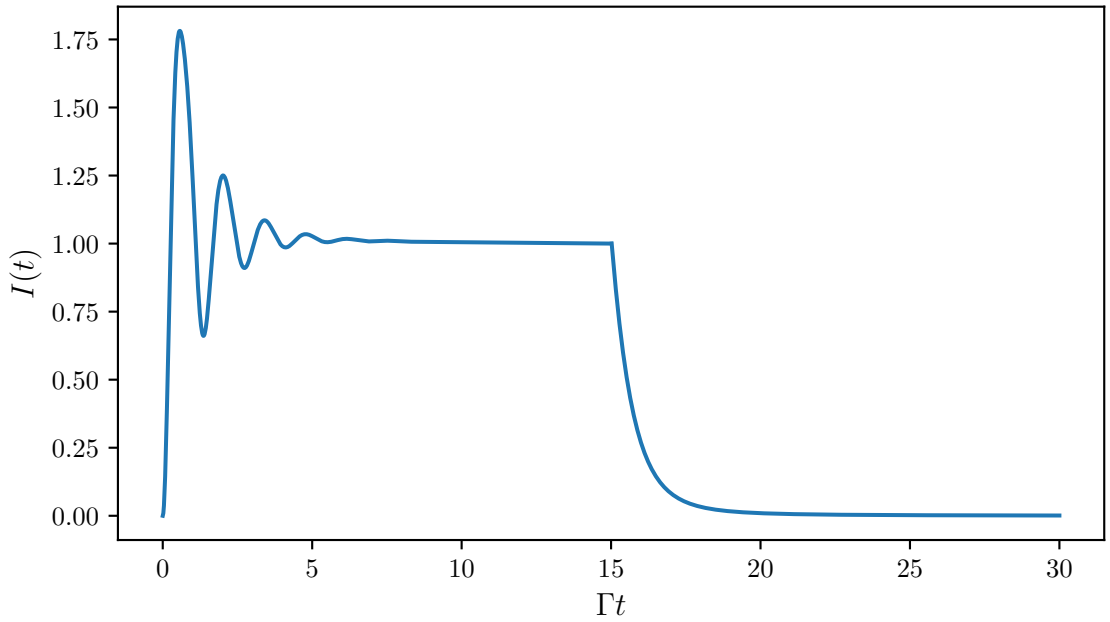

Figure 8 – Switch-on / switch-off radiated intensity protocol calculated with Eq. (2.52) and Eq. (2.56).

Source: By the author

at later times. This is an example of cooperative effect and the decay constant can be obtained from an exponential fitting ($e^{-\Gamma_N t}$) of the radiated field intensity.

Apart from superradiance, most of the works on cooperative effects in the literature so far, for dilute atomic clouds, were performed in the linear optics limit (low saturation parameter $s \ll 1$) and for the switch-off dynamics. Little is known for higher saturation where quantum effects can modify the system behavior. In chapter 4 we present a detailed study of the switch-on dynamics in the linear optics limit and show, with simulations and experimental comparison, that, increasing the saturation, a nonlinear mean-field model is, at first, an extension of the linear optics case and, beyond that, we can add quantum pair correlations. All these cited models can be obtained from Eq. (2.52). Since for the full quantum model the degrees of freedom scales exponentially with the number of atoms, approximations are necessary to simulate larger systems (see chapter 3).

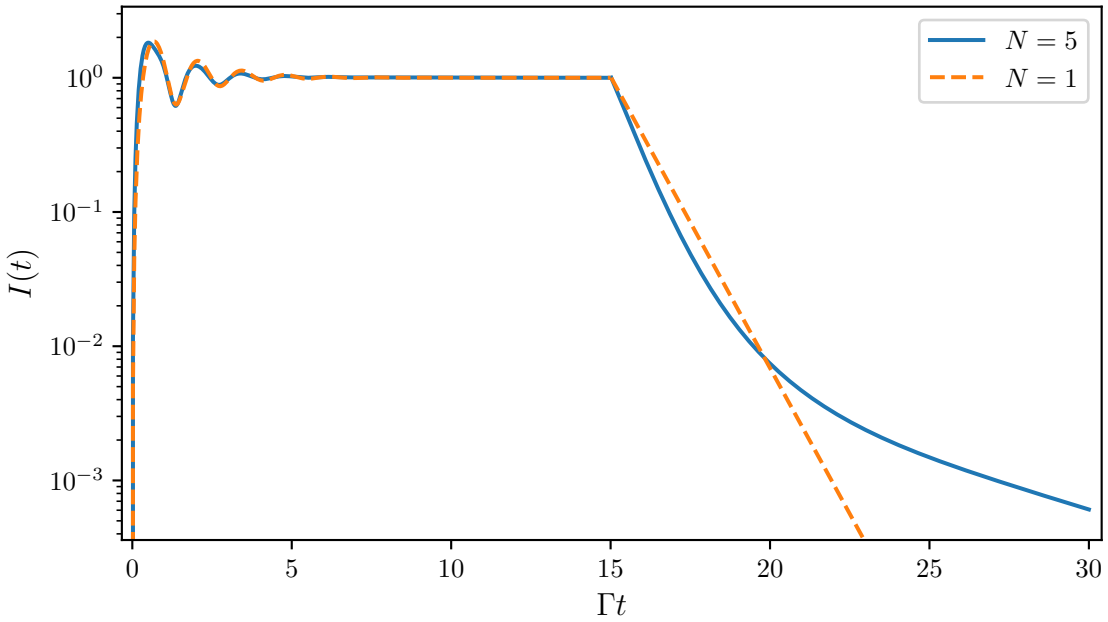

Figure 9 – Switch-on / switch-off radiated intensity calculated with Eq. (2.52) and Eq. (2.56) for $N \in (1, 5)$, $\Delta/\Gamma = -2$, and $s = 2$. The system is driven from the ground-state to the steady-state in the switch-on dynamics and, then, the laser is turned-off in the steady-state for the switch-off dynamics. There are slight deviations for the normalized intensity in the switch-on case, while for the field decay (switch-off) there is a substantially different behavior.

Source: By the author

2.3.2 Fluorescence power spectrum

The previous section addressed the dynamics of the radiated field intensity, another experimentally accessible quantity is the power spectrum in the regime of resonant fluorescence. From a theoretical point of view the atomic system is driven to the steady-state and the spectrum obtained from the first order optical coherence function, which measures the field correlations of the radiated light. For a single two-level atom, Benjamin Mollow investigated the power spectrum for a high intensity incident field (saturated regime)[19], identifying the presence of a 'triplet' of inelastically scattered light, today referred as the Mollow triplet. He obtained the spectrum

$$S(\omega) = 2\pi|\alpha_\infty|^2\delta(\omega-\omega_0)+\frac{D_0}{(\omega-\omega_0)^2+s_0^2}+\frac{M-(\omega-\omega_0+\Omega')N}{(\omega-\omega_0-\Omega')^2+\sigma^2}+\frac{M+(\omega-\omega_0+\Omega')N}{(\omega-\omega_0+\Omega')^2+\sigma^2} \tag{2.57}$$

with

$$|\alpha_\infty| = \frac{\Omega\Gamma}{2\Omega^2+\Gamma^2} \quad , \quad s_0 = -\frac{1}{2}\Gamma \quad , \quad \sigma = -\frac{3}{4}\Gamma \quad , \quad \Omega' = \left(\Omega^2 - \frac{1}{16}\Gamma^2\right)^{1/2} \tag{2.58}$$

and

$$D_0 = \frac{1}{2}\Gamma\bar{n}_\infty \quad , \quad M = \frac{3}{8}\Gamma\bar{n}_\infty\left(\frac{\Omega^2-\Gamma^2/2}{\Omega^2+\Gamma^2/2}\right) \quad , \quad N = \frac{1}{8}\frac{\Gamma\bar{n}_\infty}{\Omega'}\left(\frac{5\Omega^2-\Gamma^2/2}{\Omega^2+\Gamma^2/2}\right) \tag{2.59}$$

where $\bar{n}_\infty = \Omega^2/(2\Omega^2+\Gamma)$. The Dirac delta in Eq. (2.57) corresponds to the elastic scattering. The power spectrum for the inelastic scattering has a profile composed of three peaks, one centered on the incident field frequency and two dislocated at $\omega_0 \pm \Omega'$. An example of such spectrum is presented in Fig.10.

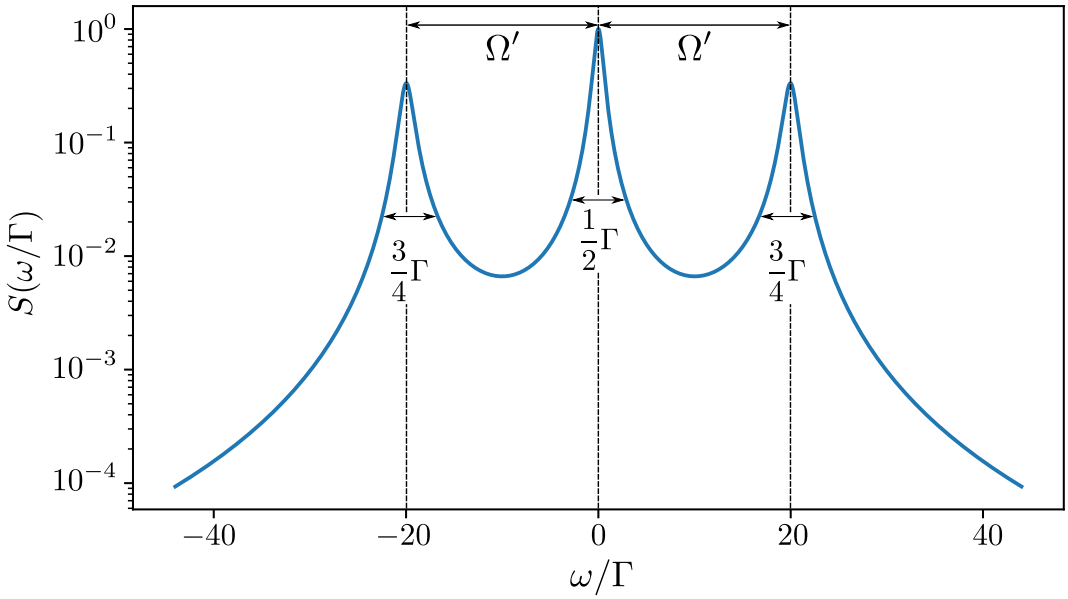

Figure 10 – Fluorescence power spectrum for $N = 1$, $\Omega/\Gamma = 20$ and $\Delta/\Gamma = 0$. The pattern of three peaks is known as the Mollow triplet.
Source: By the author

One way to calculate the fluorescence power spectrum is to take the Fourier transform of the first order optical coherence function $g^{(1)}$:

$$S(\omega) = \lim_{T\to\infty}\int_{-T}^{T} g^{(1)}(\tau)e^{-i\omega\tau}\,\mathrm{d}\tau \tag{2.60}$$

The first-order coherence function corresponds to two-time correlation of the electric field $\hat{E}^+$ and can be obtained for the many-atom case using Eq. (2.54):

$$g^{(1)}(t,\tau) = \frac{\left\langle \hat{E}(t)\hat{E}^+(t+\tau)\right\rangle}{\left\langle \hat{E}(t)\hat{E}^+(t)\right\rangle} \tag{2.61}$$

In that sense, $g^{(1)}$ is a quantity that depends on two-time and two-atom correlations $\langle\sigma_n^-(t)\sigma_m^+(t+\tau)\rangle$, so that quantum collective effects might be visible in this observable.

Let us consider a general master equation

$$\frac{\partial\hat{\rho}}{\partial t} = \mathcal{L}\hat{\rho}. \tag{2.62}$$

One can argue that the time correlation function can be obtained by the mean value equation for the system with initial density operator $\hat{O}\hat{\rho}$ to derive the quantum regression theorem.[25] $\hat{O}\hat{\rho}$ is not a density operator but the argument is still valid. It is convenient to write the equations in terms of the expected values of a complete set of system operators $\hat{A}_\mu$. For an arbitrary operator $\hat{O}$ and for each $\hat{A}_\mu$:

$$\mathrm{Tr}\left(\hat{A}_\mu \mathcal{L}\hat{\rho}\hat{O}\right) = \sum_\lambda M_{\mu\nu}\,\mathrm{Tr}\left(\hat{A}_\lambda \hat{\rho}\hat{O}\right), \tag{2.63}$$

where $M_{\mu\nu}$ are constants. In particular:

$$\left\langle \dot{\hat{A}}_\mu \right\rangle = \mathrm{Tr}\left(\hat{A}_\mu d\hat{\rho}/dt\right) = \mathrm{Tr}\left(\hat{A}_\mu \mathcal{L}\hat{\rho}\right) = \sum_\lambda M_{\mu\nu}\left\langle \hat{A}_\lambda \right\rangle. \tag{2.64}$$

In a vector notation, one can write:

$$\left\langle \dot{\hat{A}} \right\rangle = \mathcal{M}\left\langle \hat{A} \right\rangle, \tag{2.65}$$

where $\hat{A}$ is the column vector of operators $\hat{A}_\mu$. Now, for the evolution of the two-time correlation operator, in the case $\tau \geq 0$:

$$\begin{gathered}\frac{d}{d\tau}\left\langle \hat{O}(t)\hat{A}_\mu(t+\tau)\right\rangle = \mathrm{Tr}\left(\hat{A}_\mu(0)\left(\mathcal{L}e^{\mathcal{L}\tau}\left(\hat{\rho}(t)\hat{O}(0)\right)\right)\right) = \\ \sum_\lambda M_{\mu\lambda}\,\mathrm{Tr}\left(\hat{A}_\lambda(0)e^{\mathcal{L}\tau}\left(\hat{\rho}(t)\hat{O}(0)\right)\right) = \sum_\lambda M_{\mu\lambda}\left\langle \hat{O}(t)\hat{A}_\lambda(t+\tau)\right\rangle.\end{gathered} \tag{2.66}$$

In vector form, it rewrites as:

$$\frac{d}{d\tau}\left\langle \hat{O}(t)\hat{A}(t+\tau)\right\rangle = \mathcal{M}\left\langle \hat{O}(t)\hat{A}_\mu(t+\tau)\right\rangle, \tag{2.67}$$

where $\hat{O}$ can be any operator. Eq. (2.67) is the desired quantum regression theorem.

Now, let us consider the master equation (Eq. (2.46)) for a single two-level atom driven by a laser, the objective is to calculate the first-order coherence function $g^{(1)} = \langle\hat{\sigma}^+(t)\hat{\sigma}^-(t+\tau)\rangle$, using as initial condition the steady-state ($t \to \infty$). A convenient matrix basis to represent the state vector is

$$\mathbf{s} = \begin{pmatrix} \hat{\sigma}^- \\ \hat{\sigma}^+ \\ \hat{\sigma}^+\hat{\sigma}^- \end{pmatrix}. \tag{2.68}$$

Calculating $d\langle \mathbf{s} \rangle / dt$, similar to Eq. (2.23) we obtain

$$\frac{\partial}{\partial t}\begin{pmatrix} \langle \hat{\sigma}^- \rangle \\ \langle \hat{\sigma}^+ \rangle \\ \langle \hat{\sigma}^+ \hat{\sigma}^- \rangle \end{pmatrix} = \begin{pmatrix} i\Delta - \Gamma/2 & 0 & i\Omega \\ 0 & -i\Delta - \Gamma/2 & -i\Omega \\ i\Omega/2 & -i\Omega/2 & -\Gamma \end{pmatrix} \begin{pmatrix} \langle \hat{\sigma}^- \rangle \\ \langle \hat{\sigma}^+ \rangle \\ \langle \hat{\sigma}^+ \hat{\sigma}^- \rangle \end{pmatrix} + \begin{pmatrix} -i\Omega/2 \\ i\Omega/2 \\ 0 \end{pmatrix} \tag{2.69}$$

or, in vector form:

$$\frac{d\langle \mathbf{s} \rangle}{dt} = \mathcal{M}\langle \mathbf{s} \rangle + \mathbf{b} \tag{2.70}$$

Applying the quantum regression theorem for the operator $\hat{\sigma}^+$ and, as initial condition the steady-state (ss), one obtains:

$$\frac{d\langle \hat{\sigma}^+_{ss}\mathbf{s}(\tau) \rangle}{d\tau} = \mathcal{M}\left\langle \hat{\sigma}^+_{ss}\mathbf{s}(\tau) \right\rangle + \left\langle \hat{\sigma}^+_{ss} \right\rangle \mathbf{b}, \tag{2.71}$$

where the first term of $\langle \hat{\sigma}^+_{ss}\mathbf{s}(\tau) \rangle$ is the desired $g^{(1)} = \langle \hat{\sigma}^+_{ss}\hat{\sigma}^-(\tau) \rangle$. Note that, since $\mathrm{Tr}(\hat{\rho}) = 1$ and we are replacing $\hat{\rho}$ by $\hat{\rho}\hat{\sigma}^+$ in the quantum regression theorem, we have to add $\langle \hat{\sigma}^+_{ss} \rangle$ multiplying the vector $\mathbf{b}$ (see the first line of Eq. (2.66)). To obtain the steady-state, we must calculate:

$$\left\langle \hat{\sigma}^+_{ss}\mathbf{s}(0) \right\rangle = \begin{pmatrix} \langle \hat{\sigma}^+\hat{\sigma}^- \rangle_{ss} \\ \langle \hat{\sigma}^+\hat{\sigma}^+ \rangle_{ss} \\ \langle \hat{\sigma}^+\hat{\sigma}^+\hat{\sigma}^- \rangle_{ss} \end{pmatrix} = \begin{pmatrix} \langle \hat{\sigma}^+\hat{\sigma}^- \rangle_{ss} \\ 0 \\ 0 \end{pmatrix}. \tag{2.72}$$

That way, to obtain $g^{(1)}(\tau)$, the steady-state is calculated as $\mathbf{s}(t \to \infty)$, where the dynamics is evolved using the same equations as for the system matrix base with a standard numerical integrator.

In a dilute cloud with many atoms, it was reported, using a first order pertubative approach for the dipole coupling terms, that the cooperative effects leads to an asymmetry in the fluorescence power spectrum in the forward direction $\theta \approx 0$ (see Fig. 11).[35] But this approach does not capture new sidebands in the dilute regime since it does not include two-body two-time correlations.

For a system with a high spatial density, the emergence of new sidebands at multiples of the generalized Rabi frequency has been described.[36–37] Nevertheless, even for two atoms, using exact simulations, this effect is substantial only for distances smaller than the incident laser wavelength λ (Fig. 12).

In the chapter 5 we show that, including quantum pair correlation in the model, we observe additional sidebands at $2\Omega_{GR}$ even in dilute systems and that the asymmetry in the Mollow triplet is also present outside the frontal lobe ($\theta \neq 0$). We also discuss

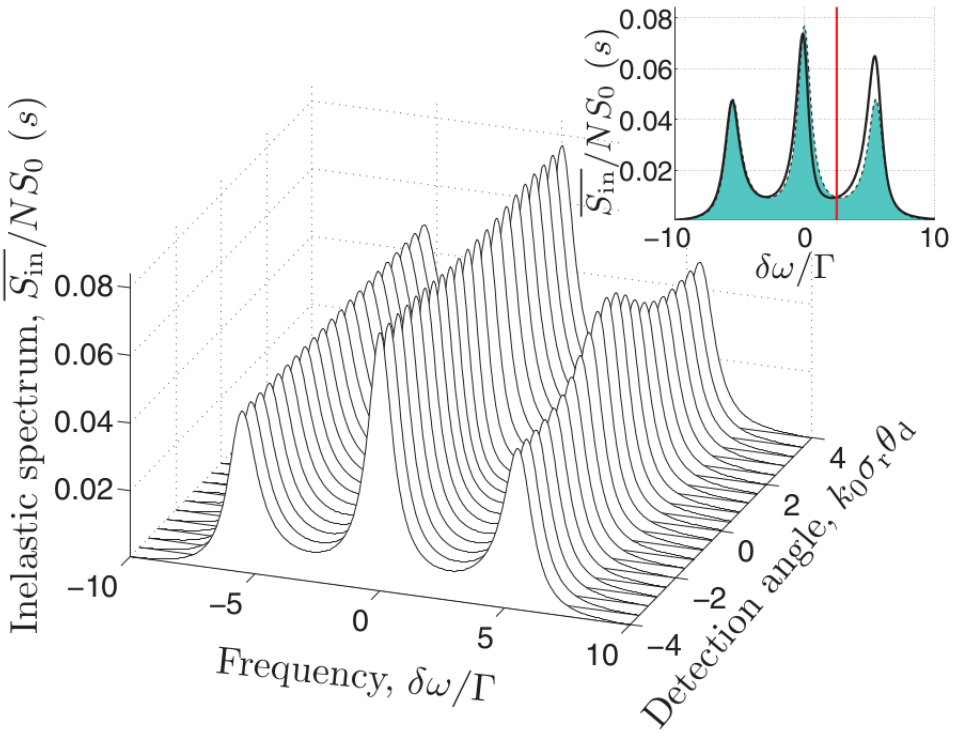

Figure 11 – Asymmetry in the Mollow triplet for $N = 25000$, $\Omega/\Gamma = 5$ and $\Delta/\Gamma = -2.5$ using a perturbatie approach. The asymmetry was observed in the forward direction ($\theta = 0$).

Source: Adapted from OTT *et al.*[35]

preliminary results for an atomic sensor model in which a time-dependent spectrum can be obtained, so the triplet dynamics (not only the steady-state one) can be observed.

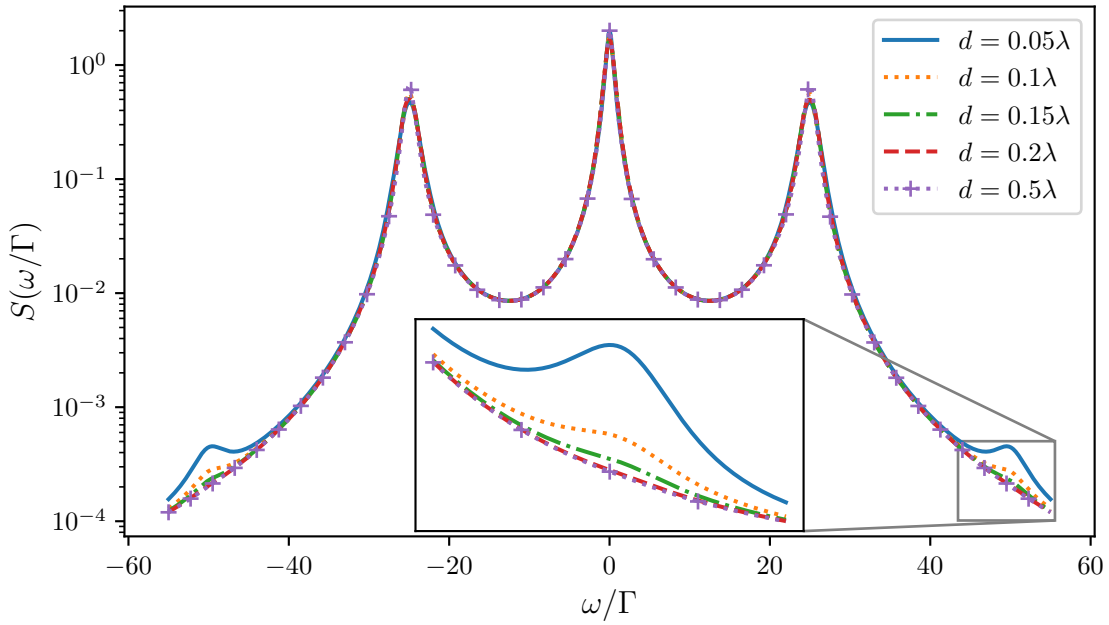

Figure 12 – Fluorescence power spectrum for $N = 2$, $\Omega/\Gamma = 25$, $\Delta/\Gamma = 0$ and separated by a distance d. For atoms much closer than a wavelength additional sidebands appears at $2\Omega/\Gamma$.

Source: By the author

3 SIMULATION OF MANY-BODY OPEN QUANTUM SYSTEMS

The simulation of a quantum many-body problem is a challenge due to the exponential growth of the Hilbert space with the number of particles. In the case of N two-level atoms, the Hilbert space of the reduced density matrix Eq.(2.52) scales as $\propto 2^N \times 2^N = 2^{2N}$. Modern computers are able to simulate up to a dozen of atoms and even using the quantum jumps method or cloud computing with clusters, only $N \approx 20$ can be achieved. To address larger systems approximations are necessary, paying the price of neglecting higher order terms.

Hereafter, the dynamics of the full Lindbladian master equation Eq. 2.52 will be referred as **exact simulation** (**E**) and has been used to study cooperative effects in systems with a few atoms.[20–21] We have run exact simulations with the toolbox QuTiP[38] (Quantum toolbox in python), and compared them with approximated methods obtained by means of a truncation in the BBGKY (Bogoliubov–Born–Green–Kirkwood–Yvon) hierarchy. The method consist in taking partial traces over the Lindbladian master equation

$$\frac{\partial \hat{\rho}_n}{\partial t} = \mathrm{Tr}_{\neq n}\left(\frac{\partial \hat{\rho}}{\partial t}\right) \quad , \quad \frac{\partial \hat{\rho}_{nm}}{\partial t} = \mathrm{Tr}_{\neq n,m}\left(\frac{\partial \hat{\rho}}{\partial t}\right) \quad , \quad \ldots \tag{3.1}$$

to obtain a hierarchy of n-atom reduced density matrices (RDM) $n \in [1, 2, \ldots, N]$.[23,39–40] The dynamics of the one-atom RDM ($\hat{\rho}_n$) depends on the two-atom RDM ($\hat{\rho}_{nm}$), which depends on the three-atom RDM and so on. The complete set of equations is equivalent to the full master equation and, by truncating the hierarchy we are able to simulate larger systems neglecting higher order terms. Indeed the set of equations up to n-atom RMD scales as $\propto N^n$.

3.1 Classical dipoles equation

The **classical dipole** (**CD**) equation is obtained in the linear optics regime of low saturation ($s \ll 1$). It can be derived from Eq. (2.51) and Eq. (2.52) by considering $\langle \hat{\sigma}_n^z \rangle \approx -1$ and defining $\beta_n = \langle \hat{\sigma}_n^- \rangle$:[12–13,18]

$$\frac{\partial \beta_n}{\partial t} = \left(i\Delta - \frac{\Gamma}{2}\right)\beta_n - i\frac{\Omega}{2}e^{i\mathbf{k_0}\cdot\mathbf{r}_n} + i\frac{\Gamma}{2}\sum_{m\neq n}\frac{e^{ik_0|\mathbf{r}_n-\mathbf{r}_m|}}{k|\mathbf{r}_n-\mathbf{r}_m|}\beta_m. \tag{3.2}$$

The same equation can be obtained fully classically from Maxwell equations for classical harmonic oscillators.[41] We show in the next section that the CD equation is readily obtained from the mean-field equation with the approximation $\langle \hat{\sigma}_n^z \rangle \approx -1$. Note from Fig. 6 that this approximation ($\langle \hat{\sigma}_n^z \rangle = W(t) \approx -1$) is valid in the regime of low saturation.

3.2 Mean-field approximation

In order to obtain the **mean-field** (**MF**) equation we keep only the one-atom RDM in the hierarchy Eq. (3.1) and consider a product state Ansatz for the N-atom density matrix at all times: $\hat{\rho} = \bigotimes \hat{\rho}_n$. As a consequence we neglect any kind of entanglement in the system, so this model only includes factorized coherences between sites $\langle \hat{\sigma}_n^+ \hat{\sigma}_m^- \rangle = \langle \hat{\sigma}_n^+ \rangle \langle \hat{\sigma}_m^- \rangle$. With the N-atom density matrix we can access any collective operator expected value in the usual way by taking the trace $\mathrm{Tr}\left(\hat{O}\hat{\rho}\right)$. The product state Ansatz has been used in the context of the Maxwell-Bloch description, in the low intensity driving laser, and showed good agreement in the low density regime.[42] Expanding $\hat{\rho}_n$ in the Pauli matrices basis leads to

$$\hat{\rho}_n = \frac{1}{2}\left(\mathbb{1}_n + \langle \boldsymbol{\sigma}_n \rangle . \hat{\boldsymbol{\sigma}}_n\right), \tag{3.3}$$

with $\hat{\boldsymbol{\sigma}}_n = (\hat{\sigma}_n^x, \hat{\sigma}_n^y, \hat{\sigma}_n^z)$. By substituting in Eq. (2.52), we obtain a set of $3N$ coupled non-linear equations for the coefficients:

$$\begin{aligned}\frac{\partial \langle \hat{\sigma}_n^a \rangle}{\partial t} = &-\Delta \varepsilon_{azc} \langle \hat{\sigma}_n^c \rangle + \Omega \cos(\mathbf{k_0}.\mathbf{r}_n) \varepsilon_{axb} \left\langle \hat{\sigma}_n^b \right\rangle - \Omega \sin(\mathbf{k_0}.\mathbf{r}_n) \varepsilon_{ayd} \left\langle \hat{\sigma}_n^d \right\rangle + \\ &\sum_{m \neq n} \Delta_{nm} \left(\langle \hat{\sigma}_m^x \rangle \varepsilon_{axb} \left\langle \hat{\sigma}_n^b \right\rangle + \langle \hat{\sigma}_m^y \rangle \varepsilon_{ayd} \left\langle \hat{\sigma}_n^d \right\rangle \right) - \frac{\Gamma}{2} \left(\langle \hat{\sigma}_n^a \rangle + \delta_{az} (2 + \langle \hat{\sigma}_n^z \rangle) \right) \\ &+ \frac{1}{2} \sum_{m \neq n} \gamma_{nm} \left(\langle \hat{\sigma}_m^x \rangle \varepsilon_{ayd} \left\langle \hat{\sigma}_n^d \right\rangle - \langle \hat{\sigma}_m^y \rangle \varepsilon_{axb} \left\langle \hat{\sigma}_n^b \right\rangle \right)\end{aligned} \tag{3.4}$$

with $a \in (x, y, z)$, δ_{nm} the Kronecker delta and ε_{abc} the Levi-Civita symbol. Considering the equations for σ_n^-, it can be rewritten as

$$\begin{cases} \dfrac{\partial}{\partial t} \left\langle \hat{\sigma}_n^- \right\rangle = \left(-\dfrac{\Gamma}{2} + i\Delta \right) \left\langle \hat{\sigma}_n^- \right\rangle + \left(i\dfrac{\Omega}{2} e^{i\mathbf{k_0}.\mathbf{r}_n} - i\dfrac{\Gamma}{2} \displaystyle\sum_{m \neq n} \frac{e^{ik_0|\mathbf{r}_n - \mathbf{r}_m|}}{k_0 |\mathbf{r}_n - \mathbf{r}_m|} \left\langle \hat{\sigma}_m^- \right\rangle \right) \langle \hat{\sigma}_n^z \rangle \\ \dfrac{\partial}{\partial t} \langle \hat{\sigma}_n^z \rangle = \left(\left(-i\Omega e^{i\mathbf{k_0}.\mathbf{r}_n} + \displaystyle\sum_{m \neq n} \frac{i\Gamma e^{ik.|\mathbf{r}_n - \mathbf{r}_m|}}{k_0 |\mathbf{r}_n - \mathbf{r}_m|} \left\langle \hat{\sigma}_m^- \right\rangle \right) \left\langle \hat{\sigma}_n^+ \right\rangle + c.c. \right) - \Gamma \left(\langle \hat{\sigma}_n^z \rangle + 1 \right). \end{cases} \tag{3.5}$$

It becomes clear that, in the MF approximation, the field acting on atom n is composed of the incident laser $\propto e^{i\mathbf{k_0}.\mathbf{r_n}}$ plus the field emitted by all other atoms in the form of a spherical wave $\propto e^{ik_0 r_{nm}}/k_0 r_{nm}$. The system of non-linear equations can be integrated numerically for thousands of atoms ($N \approx 10^4$).

Note that going to the linear optics limit by seting $\langle \hat{\sigma}_n^z \rangle = -1$ and $\langle \hat{\sigma}_n^- \rangle = \beta_n$ in Eq. (3.5) we obtain the CD equation Eq. (3.2).

3.3 Quantum pair correlations

Now, to go beyond semi-classical physics and include quantum correlations, we consider pair of atoms connected correlations: $\langle\hat{\sigma}_n^+\hat{\sigma}_m^-\rangle - \langle\hat{\sigma}_n^+\rangle\langle\hat{\sigma}_m^-\rangle \neq 0$ for $n \neq m$ (it is put to zero in the MF approximation). The idea is the same as for the cumulant expansion[43–45] but instead of a bottom-up approach we use a top-down approach by truncating the BBGKY hierarch in Eq. 3.1 using a cluster expansion

$$\begin{cases} \hat{\rho}_{nm} = \hat{\rho}_n \otimes \hat{\rho}_m + \hat{\chi}_{nm} \\ \hat{\rho}_{nml} = \hat{\rho}_n \otimes \hat{\rho}_m \otimes \hat{\rho}_l + \hat{\rho}_n \otimes \hat{\chi}_{ml} + \hat{\rho}_m \otimes \hat{\chi}_{nl} + \hat{\rho}_l \otimes \hat{\chi}_{nm} + \hat{\chi}_{nml}. \end{cases} \tag{3.6}$$

We consider up to two-atom correlations and truncate the series of equations by neglecting higher-order terms: $\hat{\chi}_{nml} = 0$. We keep the one-atom $\hat{\rho}_n$ and two-atom RDM $\hat{\rho}_{nm}$. Expanding the two-atom RDM in terms of the Pauli operators, we get

$$\hat{\rho}_{nm} = \frac{1}{4}\left(\mathbb{1}_n \otimes \mathbb{1}_m + \mathbb{1}_n \otimes \langle\hat{\boldsymbol{\sigma}}_m\rangle \,.\hat{\boldsymbol{\sigma}}_m + \langle\hat{\boldsymbol{\sigma}}_n\rangle \,.\hat{\boldsymbol{\sigma}}_n \otimes \mathbb{1}_m + \sum_{ab} B_{nm}^{ab}\hat{\sigma}_n^a \otimes \hat{\sigma}_m^b\right) \tag{3.7}$$

with $B_{nm}^{ab} = \left\langle\hat{\sigma}_n^a \otimes \hat{\sigma}_m^b\right\rangle$. Then we define $c_{nm}^{ab} = \left(\left\langle\hat{\sigma}_n^a \otimes \hat{\sigma}_m^b\right\rangle - \langle\hat{\sigma}_n^a\rangle\left\langle\hat{\sigma}_m^b\right\rangle\right)/4$ to obtain the two-atom correlation operator $\hat{\chi}_{nm} = \hat{\rho}_{nm} - \hat{\rho}_n \otimes \hat{\rho}_m$:

$$\hat{\chi}_{nm} = \sum_{ab} c_{nm}^{ab}\hat{\sigma}_n^a \otimes \hat{\sigma}_m^b. \tag{3.8}$$

By evolving the dynamics of the coupled equations for the coefficients $\langle\hat{\sigma}_n^a\rangle$ and c_{jk}^{ab}, we can obtain the N-atom density matrix and access any collective operator expected value $\mathrm{Tr}(\hat{A}\hat{\rho})$ where

$$\hat{\rho} = \bigotimes_{n=1}^{N}\hat{\rho}_n + \sum_{l=2}^{N}\sum_{m<l}\bigotimes_{n=1}^{m-1}\hat{\rho}_n \otimes \hat{\chi}_{ml} \otimes \bigotimes_{n=m+1,n\neq l}^{N}\hat{\rho}_n. \tag{3.9}$$

We call this approximation the **quantum pair correlations** (**QPC**) method, which provides a set of equations, whose number scales as $\propto N^2$. The full equation for this model can be found in Appendix A of PUCCI *et al.*[23]

3.4 Other methods

In this section we discuss two other methods: the quantum jumps (QJ) and the discrete truncated Wigner approximation (dTWA). While the QJ evolves the state vector instead of the density matrix, a random jump projects the system in a random state, in the dTWA a random sampling of the initial state in a discrete phase space is taken into account and, that way, higher order corrections are included in the dynamics.

3.4.1 Quantum Jumps

The quantum jumps method can be applied to the spontaneous emission problem[46] and is implemented with a Monte Carlo simulation for the evolution of the state vector $|\Psi(t)\rangle$.[47–49] After a time step δt, there is a probability δp of a random jump that projects the system ($\hat{C}_n$ the jump operator) in a random state. Consider a first order expansion of the state at a time $t + \delta t$[50]:

$$\langle\Psi(t+\delta t)|\Psi(t+\delta t)\rangle = 1 - \delta p, \tag{3.10}$$

with

$$\delta p = \delta t \sum_n \left\langle \Psi(t+\delta t) \left| \hat{C}_n^\dagger \hat{C}_n \right| \Psi(t+\delta t) \right\rangle, \tag{3.11}$$

δt is chosen so $\delta p \ll 1$. The probability of the system staying in the state $|\Psi(t)\rangle$ at $t + \delta t$ is given by $1 - \delta p$ and δp is the probability of a quantum jump event. If there is a jump, the wave function goes to a state given by the projection of $|\Psi(t)\rangle$

$$|\Psi(t+\delta t)\rangle = \frac{\hat{C}_n |\Psi(t)\rangle}{\sqrt{\left\langle \Psi(t) \left| \hat{C}_n^\dagger \hat{C}_n \right| \Psi(t) \right\rangle}}. \tag{3.12}$$

When we consider multiple jump operators, in the Monte Carlo method, we sample a random number with probability δp and, if a jump occurs, we sample another random number to choose a jump operator with probability p_n. For each jump operator we can calculate the probability p_n:

$$p_n(t) = \frac{\left\langle \Psi(t) \left| \hat{C}_n^\dagger \hat{C}_n \right| \Psi(t) \right\rangle}{\delta t}. \tag{3.13}$$

In the spontaneous emission problem, the quantum jump trajectory has a straightforward physical interpretation.[51] Let us consider a continuous measurement with photon detectors. If a photon is measured, it means that a quantum jump took place, whereas if there is no photon detection, the system remained in the same state. In that sense we obtain information on the system even when there is no detection. Now, suppose that the atomic system has M excited atoms, if a photon is detected, we know that the system has now $M - 1$ excited atoms. However, there is no information on which atom has decayed. So we must run multiple quantum jumps trajectories and calculate the average to obtain the correct expected values of the system operators.

To apply this method to the Lindbladian master equation Eq. (2.52) we must write the dissipation operators in a diagonal form (see Section 3.4.1.1):

$$\frac{d\hat{\rho}}{dt} = -i\left[\hat{H}, \hat{\rho}\right] + \sum_{n=1}^{N} \frac{1}{2}\left(2\hat{C}_n \hat{\rho} \hat{C}_n^\dagger - \left\{\hat{C}_n^\dagger \hat{C}_n, \hat{\rho}\right\}\right). \tag{3.14}$$

This equation can be rewritten in the following form:

$$\frac{d\hat{\rho}}{dt} = -i\left(\hat{H}_{eff}\hat{\rho} - \hat{\rho}\hat{H}_{eff}^{\dagger}\right) + \sum_{n=1}^{N}\hat{C}_n\hat{\rho}\hat{C}_n^{\dagger}, \tag{3.15}$$

with effective Hamiltonian

$$\hat{H}_{eff} = \hat{H} - \frac{i}{2}\sum_{n}\hat{C}_n^{\dagger}\hat{C}_n \tag{3.16}$$

and recycling therm

$$\sum_{n=1}^{N}\hat{C}_n\hat{\rho}\hat{C}_n^{\dagger}. \tag{3.17}$$

The wave function $|\Psi(t=0)\rangle$ is evolved with the Schrödinger equation using the effective Hamiltonian and, at each time step δt, one checks by drawing a random sampling number if a quantum jump occurs. The system is evolved for n_{traj} trajectories (*i.e.* realizations) and, for each trajectory, the expected value of a desired operator $\hat{O}$ is calculated as follows:

$$\left\langle \hat{O}(t) \right\rangle = \langle\Psi(t)|\,\hat{O}\,|\Psi(t)\rangle\,. \tag{3.18}$$

Finally, the operator expected value is obtained from averaging over all the trajectories. For an infinite number of trajectories $n_{traj} \to \infty$ the master equation result is recovered, showing the equivalence between both methods.[51] For a finite number of trajectories the statistical error is given by:[50]

$$\text{err} = \frac{\delta O}{\sqrt{n_{traj}}}, \tag{3.19}$$

with δO the statistical standard deviation for the operator expected value averaged over the trajectories. In that sense, the precision of the method varies with the number of trajectories (see Fig. 13) and with the operator choice.

One strong point of the quantum jumps method (QJ) is that we can perform exact simulations with $N \approx 20$ atoms since the state vector has dimension 2^N, whereas the density matrix has dimension 2^{2N}. On the other hand, it is not possible with the quantum jumps method to start from an entangled initial state since, to add decoherences $|\Psi_n\rangle\langle\Psi_m|$, with $n \neq m$, we need the density matrix formalism. If the initial state is a mixed state $|\Psi(0)\rangle = \sum a_n\,|\Psi_n\rangle$, one has to run the simulation for each state $|\Psi_n\rangle$ and calculate the operator expected value $\left\langle \hat{O} \right\rangle$ with the probabilities weights $|a_n|^2$.

Since we aim to simulate hundreds or thousands of atoms, we applied the QJ method with the MF equation and a random sampling on the initial state, we hopped to, that way, obtain quantum corrections, however the results did not present any good agreement.

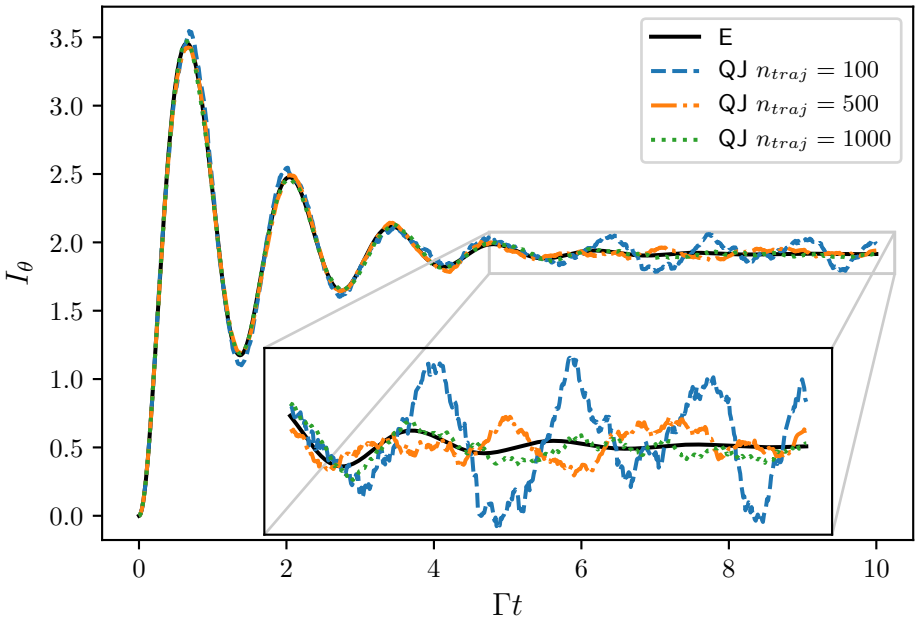

Figure 13 – Comparison of the far-field radiation at $\theta = 35°$ for exact simulation (E) and quantum jumps (QJ) with $N = 5$, $s = 2$, $\Delta = -2$ and one random position realization for a spherical distribution with $kR = 5$. Increasing the number of trajectories n_{traj}, the QP prediction becomes closer to the (E) result.
Source: By the author

3.4.1.1 Lindblad operator diagonalization

Let us consider the following Lindbladian operator:

$$\mathscr{L}(\hat{\rho}) = \frac{1}{2}\sum_{n=1}^{N}\sum_{m=1}^{N}\gamma_{nm}\left(2\hat{\sigma}_n^-\hat{\rho}\hat{\sigma}_m^+ - \left\{\hat{\sigma}_m^+\hat{\sigma}_n^-, \hat{\rho}\right\}\right). \tag{3.20}$$

In order to apply the quantum jumps formalism, one needs to cast it under a diagonal form. To that end, we need to diagonalize the damping matrix γ in Eq. (2.53). Defining the vector with eigenvalues of the damping matrix as $\boldsymbol{\gamma}$ with λ_n the n-th eigenvalue we can write:

$$\boldsymbol{\gamma}.\mathbb{1} = U^\dagger \gamma U, \tag{3.21}$$

with U the unitary transformation obtained with the damping matrix eigenvectors. We then write

$$\gamma = U\boldsymbol{\gamma}.\mathbb{1}U^\dagger, \tag{3.22}$$

and we can rewrite the coefficients of the matrix γ

$$\gamma_{nm} = \sum_{\alpha}^{N}\sum_{\beta}^{N} U_{n\alpha}\lambda_\alpha\delta_{\alpha\beta}U_{\beta m}^\dagger, \tag{3.23}$$

in order to substitute it in the Lindbladian operator:

$$\mathscr{L}(\rho) = \frac{1}{2}\sum_{\alpha}^{N}\sum_{\beta}^{N}\lambda_\alpha\delta_{\alpha\beta}\left(\sum_{n=1}^{N}\sum_{m=1}^{N}U_{n\alpha}U_{m\beta}^\dagger\left(2\hat{\sigma}_n^-\hat{\rho}\hat{\sigma}_m^+ - \left\{\hat{\sigma}_m^+\hat{\sigma}_n^-, \hat{\rho}\right\}\right)\right). \tag{3.24}$$

Now, we define the transformed operator $\hat{A}$ as follows:

$$\hat{A}_\alpha = \sum_n^N U_{n\alpha}\hat{\sigma}_n^-, \tag{3.25}$$

and rewrite Eq. (3.24) to obtain the Lindbladian in the form:

$$\mathscr{L}(\rho) = \frac{1}{2}\sum_\alpha^N\sum_\beta^N \lambda_\alpha\delta_{\alpha\beta}\left(2\hat{A}_\alpha\hat{\rho}\hat{A}_\beta^\dagger - \left\{\hat{A}_\beta^\dagger\hat{A}_\alpha,\hat{\rho}\right\}\right). \tag{3.26}$$

By applying the Kronecker delta $\delta_{\alpha\beta}$, with $\alpha = \beta = n$, and defining $\hat{C}_n = \sqrt{\lambda_n}\hat{A}_n$ we obtain the desired Lindblad operator in diagonal form of Eq. (3.14). Note that, each eigenvalue λ_n is associated with an operator $\hat{A}_n$, which is a linear combination of all atomic lowering operators Eq. (3.25); in that sense, we can say that we have N collective decay channels in the system, which define the jump operators $\hat{C}_n$ for the collective spontaneous emission of the light.

3.4.2 Discrete truncated Wigner approximation

By exploring the phase space representation of the quantum dynamics, one can search for truncated methods or other approximations to represent a many-body system. One method is based on a perturbative approach with an expansion that adds quantum fluctuations to a classical limit.[52] In the truncated Wigner approximation (TWA), quantum corrections are obtained by random sampling the initial state, due to statistical uncertainty, and, then, averaging the dynamics over the multiple classical trajectories. For spin systems (same algebra of the two-level atom), the TWA can be applied in the Bloch limit in which the angular momentum is treated as classical rotators. This approximation is obtained from the Heisenberg representation by using the Feynman's path integral with the Keldrysh technique and the Wigner-Weyl quantization.[52] This technical derivation is out of the scope of this text. In short, there is a transformation, denominated Weyl symbol, that maps the operator in the Hilbert space to the phase space. The Wigner function is the representation of the density matrix in the phase space, while the Moyal product is the Weyl symbol of the product of two operators. By taking the Weyl symbol of the commutator, and the limit $\hbar \to 0$, one obtains the Poisson bracket of the corresponding classical functions multiplied by $i\hbar$. In that sense, the classical trajectory equation to apply the TWA method can be obtained from the Von-Neumann equation in the classical limit. The TWA method recovers the exact result for quadratic potentials in the limit of infinite trajectories. For other potentials, it is an approximation method and one can add quantum fluctuations with stochastic quantum jumps in the discrete phase space dynamics.[52]

Let us consider a system with a finite number of orthogonal states. One can represent the Hilbert space of dimension D^2 with D^2 points in a discrete phase space.[53] This discrete phase space is defined using modular arithmetic $\mod(D)$ and has a non-intuitive definition of lines: $ma_1 + na_2 = p, \mod(D)$. a_1 and a_2 are the points coordinates

while n, m, p are integers $\in (0, D-1)$. Two lines are parallel if they only differ by the value of p. A set of parallel lines is denominated foliation. Each foliation is associated to an operator in the Hilbert space and the sum of the Wigner function in a line is an expected value of the operator.[53]

In the single two-level atom case, Hilbert space dimension 2^2, we need 4 points in the discrete phase space, as shown in Fig. 14(a). In Fig. 14(b) we represent the 6 possible lines (pair of circled points) for the two-level atom, the 3 possible foliations (lines inside the dashed rectangle). The sum of the Wigner function in one line gives the probability of measurement of an observable, for example, p^z_{-1} is the line that corresponds to $(1-\langle\hat{\sigma}^z\rangle)/2$. Although the Wigner function is allowed to assume negative values, the sum over a line is a positive quantity that gives an observable expected value. This is the reason why it is called a pseudo-probability function.

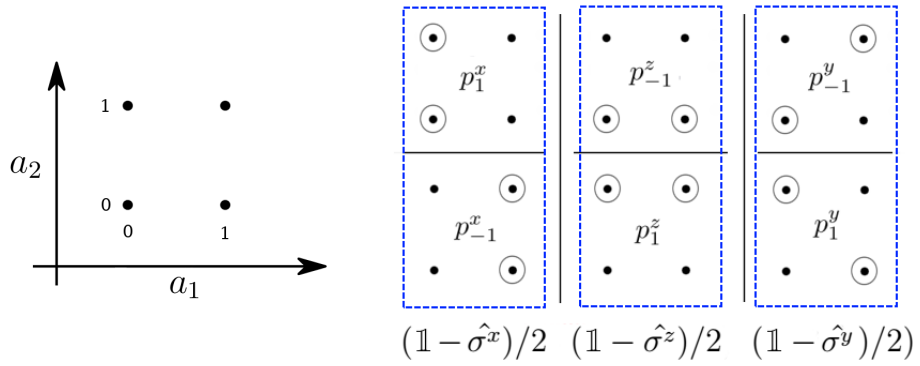

(a) (b)

Figure 14 – (a) Representation of a two-level atom in the discrete phase space, (b) we can associate each foliation to one observable of the Hilbert space.
Source: By the author

For N two-level atoms, we could map the $D^2 = 2^{2N}$ Hilbert space in the phase space, but that way the complexity of the problem is not reduced and there is no computational gain. The main idea of the discrete truncated Wigner approximation (dTWA) is to represent each spin by 4 points in the phase space (analogous to the product state Ansatz for the MF method) and, by evolving the dynamics with a classical or semi-classical equation, to obtain quantum correction using a random sampling of the initial state.

In Fig. 15 we present a scheme of the dTWA method. In (a) there is a Bloch sphere with spin $N/2$ formed by N spin-1/2 particles. In (b) we see a compact representation of Fig. 14(b). In (c) the initial state in the phase space for a spin-up $\langle\hat{\sigma}^z\rangle = 1$ is given and, in (d), one random configuration is obtained by choosing one point for each spin-1/2 in the phase space (so there is 4^N possible trajectories). Then, n_t trajectories are evolved with the classical equation (that can be obtained with the Poisson braket) and the expected value of the observable is calculated with the average over the n_t trajectories.

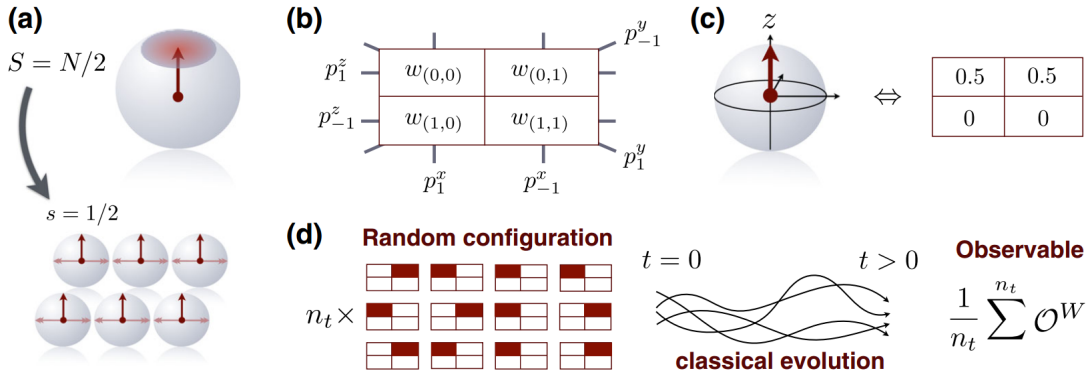

Figure 15 – Scheme of the dTWA method to simulate a many-body spin system.
Source: Adapted from: SCHACHENMAYER; PIKOVSKI; REY.[54]

The dTWA method was proven to work well for spin systems solving the quantum dynamics[54–55] and giving results that go beyond the MF approximation.[56] However, it has been applied only to Hermitian Hamiltonians, without dissipation. When applied to our dissipative system using the MF equation (as semi-classical evolution) it seems to capture correctly the Rabi oscillations in the switch-on configuration (see Fig. 16(a)). Nevertheless, it does not capture correctly the dissipative component in the overdamped regime (see Fig. 16(b)). In particular, if we have no laser, the dTWA appears to fail completely (Fig. 16(c)). Differently, the QPC method presents, overall, a good agreement with exact simulations (the total population is defined as $\text{Pop} = \sum_n (1 + \langle \hat{\sigma}^z_n \rangle)/2$).

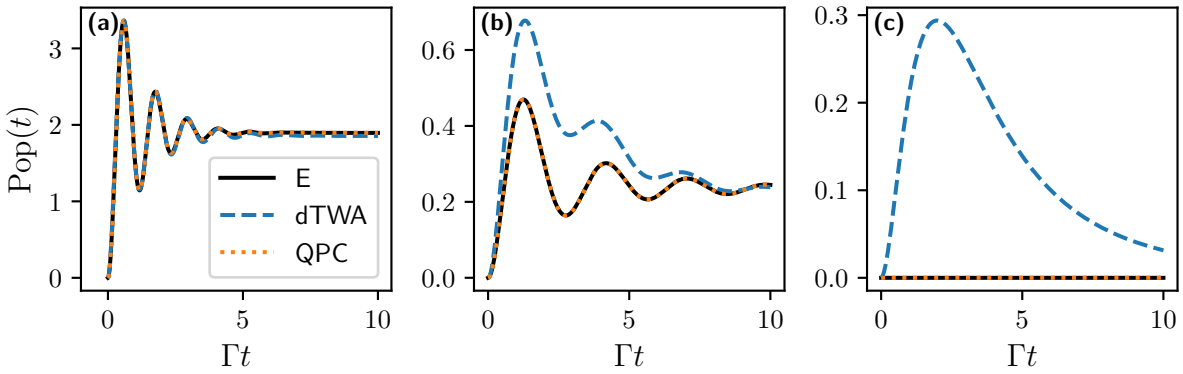

Figure 16 – Comparison of the total population Pop for one random positions realization with a uniform sphere with spatial density $k^3\rho = 0.05$, $N = 5$ and $\Delta/\Gamma = -2$. In (a) $\Omega/\Gamma = 5$ and we have the dynamics dominated by the Rabi oscillations. In (b) $\Omega/\Gamma = 1$ and we are in the overdamped regime, the dTWA method fails. In (c) $\Omega/\Gamma = 0$ and no dynamics is expected, but the dTWA method shows a wrong behavior.

Source: By the author

We conclude that, for our model with the MF equations, the dTWA method does not work properly. It might be related to the evolution of the product of two random variables, $\langle \hat{\sigma}^a_n \rangle \left\langle \hat{\sigma}^b_m \right\rangle$ in Eq. (3.4), that appears from the Lindbladian operator in the MF

approximation. One could also speculate that, when deriving the dynamics in the phase space with the Feynman integral[52], the process is considered time-reversible. However, when deriving the master equation Eq. (2.52), with the Born-Markov approximation, the time-reversal symmetry is broken.[39] More investigations are necessary to apply this method for dissipative systems. One alternative is to obtain the classical equations from the Moyal bracket in the limit of $\hbar \to \infty$, or with a perturbative approach.

We also did apply the dTWA using the QPC equations for the fluorescence power spectrum[23]. Yet for dilute systems the QPC equations already show a very good agreement and the computational cost is much smaller than using the QPC plus dTWA random sampling. For this reason, we have focused on the QPC method to include quantum corrections in our simulations, and abandoned, at least temporarily, the dTWA method. In the future, one could apply stochastic quantum jumps in the dynamics of the phase space to include quantum fluctuations, given that a proper semi-classical evolution equation is obtained.

4 APPLICATION TO THE DYNAMICS OF THE RADIATED INTENSITY

In Section 2.3.1 we introduced the radiated far-field intensity Eq. (2.56) which is an observable that can be obtained experimentally with CCD cameras. The collective optical response of a cloud of cold atoms differs substantially from the single-atom case and it has been explored in recent studies.[57–58] The cooperative scattering of light[18] leads to many-body effects with a rich physics. Since Dicke's work on coherence in the spontaneous emission superradiance[9,15,59–60], an enhancement in the field emission with collective decay rate larger than the single atom one $\Gamma_N > \Gamma$, and its counterpart subradiance[10,61–63] $\Gamma_N < \Gamma$ have been studied both from the theoretical[12,64–65] and experimental[10,66–67] side. However, most of the work in the literature were performed in the linear optics limit, with at most one excitation in the system and, in particular for the radiated far-field intensity, its decay dynamics is well understood in the switch-off protocol, thus there is no Rabi oscillations after the laser is turned off.[10,61,66,68–69]

In this chapter we present a detailed study of the switch-on dynamics in the linear optics limit and show, with simulations and experimental comparison, that a first extension of the CD model beyond linear optics is a nonlinear MF model.[22] We also present preliminary results with the QPC model demonstrating the role of quantum correlations in the subradiant decay dynamics of the atomic excitation.

4.1 Switch-on dynamics

Let us describe the problem of the dilute atomic cloud driven by a monochromatic light (see Fig. 1) in the switch-on regime in which all atoms are in the ground state at $t = 0$, when the driving laser is turned on, and the system evolves to the steady-state. The Rabi oscillations of the atomic states leaves their trace in oscillations of the intensity of the radiated far field that can be accessed experimentally, an example is presented in Fig. 17. We apply the simulation methods discussed in chapter 3 to study this problem in the theoretical side. With the CD model Eq. (3.2) we reproduce the experimental data in the linear optics limit and by fitting a phenomenological function we obtain a collective Rabi frequency and decay rate. We show that superradiance can also be observed in the switch-on dynamics and not only on the switch-off case as studied before.

We also observe a frequency shift, which can be described by a linear dispersion theory with a multimode vacuum Rabi splitting.[70] Beyond the linear optics model we show that the MF nonlinear equations presented in Eq. (3.5) reproduce the experimental data, when the CD model fails. Going further, by considering quantum correlations with the QPC model (section 3.3), we show, as a preliminary result, that a slope in the far-field decay can be explained by a subradiant mode pumping.

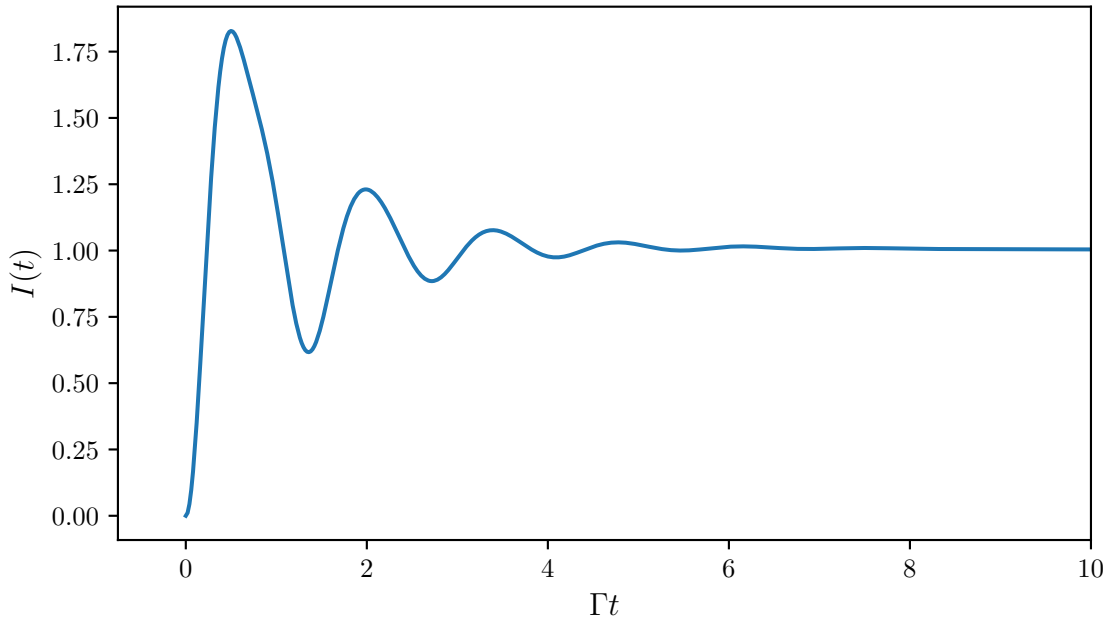

Figure 17 – Example of far-field observation for the switch-on dynamics. At $t = 0$ the driving laser is turned-on with the system in the ground state. There are oscillations in the field due to the Rabi oscillations. The field is normalized by the steady-state value.
Source: By the author

4.1.1 Switch-on dynamics in the linear optics limit

To solve the classical dipoles equation in the switch-on case (the atoms are initially in the ground-state) it is convenient to define the complex amplitude vector $\boldsymbol{\beta}(t) = (\beta_1(t), \beta_2(t), \ldots, \beta_N(t))^T$ and a vector with the Rabi frequencies $\boldsymbol{\Omega} = (-i/2)\,(\Omega_1, \Omega_2, \ldots, \Omega_N)^T$, with $\Omega_n = \Omega e^{i\mathbf{k_0}\cdot\mathbf{r_n}}$ taking into account the phase term due to the atom position. Then we can rewrite Eq. (3.2) in a vector form:

$$\frac{d\boldsymbol{\beta}(t)}{dt} = \mathbf{M}\boldsymbol{\beta}(t) + \boldsymbol{\Omega}, \tag{4.1}$$

with matrix elements

$$M_{nm} = \delta_{nm}\left(i\Delta - \frac{\Gamma}{2}\right) + (1-\delta_{nm})\, i\frac{\Gamma}{2}\frac{e^{ik_0 r_{nm}}}{k_0 r_{nm}}. \tag{4.2}$$

Using the initial condition the ground-state ($\boldsymbol{\beta}(0) = (0, 0, \ldots, 0)^T$) we obtain the formal time-dependent solution for the switch-on dynamics:

$$\boldsymbol{\beta}(t) = \left(e^{\mathbf{M}t} - \mathbb{1}\right)\mathbf{M}^{-1}\boldsymbol{\Omega}. \tag{4.3}$$

That way we can calculate the dynamics with an optimized matrix exponential algorithm or by a standard 4^{th} order Runge-Kutta integrator using Eq. (4.1).

4.1.1.1 Experimental setup

All the experimental data presented in this chapter were obtained by collaborators in the *Institut de Physique de Nice* (INPHYNI, France), in Robin Kaiser's Cold Atoms Group. A detailed description of the experimental setup can be found in (66).

In brief, they produce a 3D Gaussian cloud of rms $\approx$ 1mm of $N \approx 10^9$ randomly distributed ^{87}Rb atoms. The atoms are treated as two-level systems using the atomic transition $F = 2 \rightarrow F' = 3$ (which we assume to be closed), with wavelength $\lambda = 782.4$nm and linewidth $\Gamma/2\pi = 6.07$MHz. The cloud is driven by a linearly polarized monochromatic probe beam with waist $w \approx 5.7$mm, frequency ω_L, detuning $\Delta = \omega - \omega_{eg}$ from the atomic transition and it is propagating along the z-direction $\mathbf{k}_0 = k_0(0, 0, 1)^T$ ($k_0 = 2\pi/\lambda$). The recorded signal is taken by a photon detector in the far field at a 35° angle with the z-axis (see sketch on Fig. 1).

The intensity is normalized to one in the steady-state and the signal is averaged over $\approx 5 \times 10^5$ realizations. Also, the normalized intensity is divided by a normalized temporal signal without the atoms, with only the laser on and a white paper as a scattering medium. This procedure and the mean over realizations reduces the noise and fluctuations in the signal and allows to attenuate the contributions from unwanted photons.

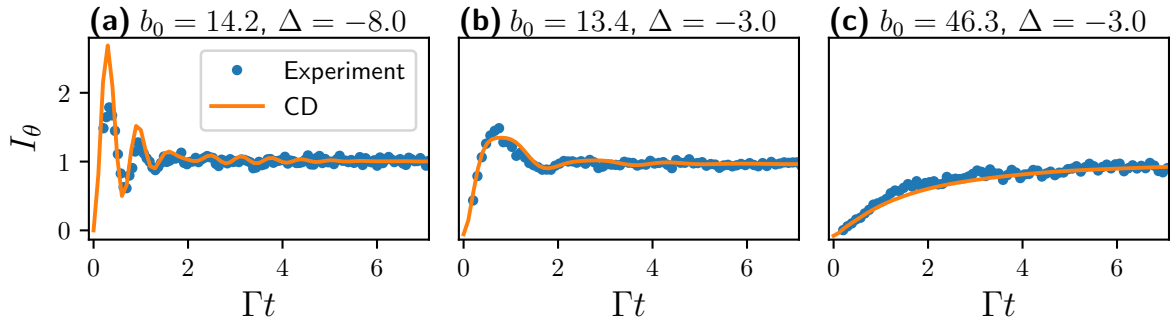

Figure 18 – Experimentally recorded time-dependent intensity after the laser switch-on for various cloud and laser parameters. Different parameters lead to an increasingly large resonant optical thickness b_0. Large b_0 and small Δ lead to an increasingly damped excitation behavior (a) $b_0 = 14.2$ and $\Delta = -8\Gamma$ (b) $b_0 = 13.4$ and $\Delta = -3\Gamma$ (c) $b_0 = 46.3$ and $\Delta = -3\Gamma$. The lines denote a numerical simulation of linear optics dynamics equations and reproduce the experiment very well, in case of a low saturation parameter ($s \approx 0.02$).

Source: Adapted from ESPIRITO SANTO *et al.*[22]

In Fig. 18 we compare the experimental results with numerical simulations for the time-dependent field dynamics. Treating $N = 10^9$ atoms numerically is not feasible due to hardware limitations on the modern desktop computers or very long time consuming simulations if powerful clusters are utilized. We choose $N_{eff} = 5000$ for the CD simulations and define the Gassian cloud rms radius to match the experimental optical thickness $kR = \sqrt{2N_{eff}/b_0}$, $k = 2\pi/\lambda$ the wave vector of the driving laser, λ the wavelength and

b_0 the optical thickness. We also define a hard sphere condition with minimal distance between atoms $d_{min} = 0.1\rho_0^{-1/3}$ (ρ_0 the atomic density at the center of the cloud) to avoid strong contributions from very close atoms. The dynamics is evolved with Eq. (3.2) with a standard 4^{th} order Runge-Kutta method and the field is calculated with Eq. (2.56). We take the mean over 100 random atoms position realizations to reduce fluctuations.

In Fig. 18(a)-(c) there are very different regimes of b_0 and Δ, one can note that the oscillations are reduced when decreasing $|\Delta|$ (from (a) to (b)) or when increasing b_0 (from (b) to (c)). Despite the very different number of atoms from the simulation to the experimental setup we obtain a very good agreement, which confirms the role of the optical thickness b_0 as the control parameter for cooperative effects. We also tested other values of N_{eff} and d_{min} for the simulations and the results are still in good agreement. The main difference of CD and the experiment is in the first peak of the oscillation in panel (a), typically lower for the experiment in this regime, this might be due to the finite switch-on time for the laser in the experiment (of $\approx$ 6ns, which is short compared to the ^{87}Rb excited state lifetime $\tau_{at} = \Gamma^{-1} = 26.2$ns, but not completely negligible).

4.1.1.2 Superradiant dipole

The far-field intensity dynamics, in the linear optics limit, behaves approximately as a single superradiant dipole. Both experimental and simulation data can be fitted, with good agreement, by a phenomenological function:[42,70]

$$I_\theta = I_s \left| 1 - e^{(i\Omega_N - \Gamma_N/2)t} \right|^2 , \tag{4.4}$$

where Γ_N is the collective decay rate and Ω_N the generalized Rabi frequency of the effective mode.

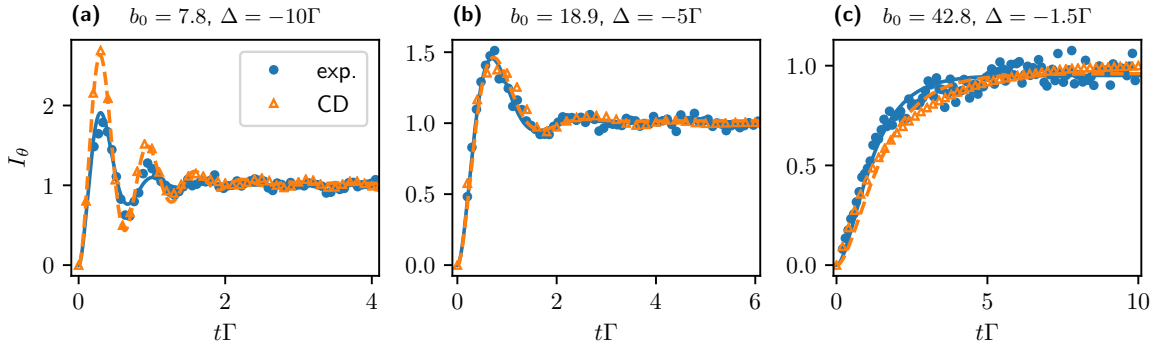

Figure 19 – Comparison of an effective mode fitting Eq. (4.4) to signals from the experiment (points: data; solid lines: fit) and to CD simulations (triangles: simulation; dashed lines: fit) in different regimes: In the underdamped case (a) the fit to the CD theory is nearly perfect. In the more damped cases (b),(c) small deviations from the effective mode (also in CD simulations) are visible.

Source: Adapted from ESPIRITO SANTO *et al.*[22]

In Fig. 19 we have fitted the Eq. (4.4) (plain lines) to the experimental signal and CD simulations (dashed lines). We obtain a very good agreement for the different regimes of b_0 and Δ (panels (a)-(c)), which allows us to extract the effective mode collective parameters Γ_N and Ω_N. In the following we discuss the superradiant dipole in the single and multimode cases.

4.1.1.3 Single mode

The dynamics in the linear optics limit, where the atomic excitation is considered small and the atomic population are neglected (when assuming $\langle\hat{\sigma}_n^z\rangle \approx -1$), is dominated by the driving laser. For this reason, it is convenient to move to the laser frame with the transformation

$$\tilde{\beta}_n = e^{-i\mathbf{k_0}\cdot\mathbf{r_n}}\beta_n, \tag{4.5}$$

we rewrite Eq. (4.1) in the form:

$$\frac{d\tilde{\boldsymbol{\beta}}(t)}{dt} = \tilde{\mathbf{M}}\tilde{\boldsymbol{\beta}}(t) + \tilde{\boldsymbol{\Omega}}, \tag{4.6}$$

where the Rabi vector is now homogeneous , $\tilde{\boldsymbol{\Omega}} = (-i\Omega/2)(1, 1, \ldots, 1)^T$, and the coupling matrix terms

$$\tilde{M}_{nm} = \delta_{nm}\left(i\Delta - \frac{\Gamma}{2}\right) + (1-\delta_{nm})\, i\frac{\Gamma}{2}\frac{e^{ik_0 r_{nm}}}{k_0 r_{nm}} e^{i\mathbf{k_0}\cdot(\mathbf{r_m}-\mathbf{r_n})}. \tag{4.7}$$

Taking advantage of the homogeneous driving, we consider an effective mode approach by replacing the excitation amplitude by its average over the number of atoms ($\tilde{\beta}_n \approx \bar{\beta} = (1/N)\sum \beta_n$) and we obtain an equation similar to the single dipole case

$$\frac{d\bar{\beta}}{dt} = \left(i\Delta - \frac{\Gamma}{2} + C\right)\bar{\beta} - i\frac{\Omega}{2}, \tag{4.8}$$

with C a geometrical factor:

$$C = \frac{1}{N}\sum_n \sum_{m\neq n} i\frac{\Gamma}{2}\frac{e^{ik_0 r_{nm}}}{k_0 r_{nm}} e^{i\mathbf{k_0}\cdot(\mathbf{r_m}-\mathbf{r_n})}. \tag{4.9}$$

Then we obtain the solution

$$\bar{\beta}(t) = \frac{i\Omega}{2i\Omega_N - \Gamma_N}\left(1 - e^{(i\Omega_N - \Gamma_N/2)t}\right), \tag{4.10}$$

with modified damping and frequency

$$\begin{aligned} \Gamma_N &= \Gamma + 2\mathrm{Re}(C) \\ \Omega_N &= \Delta - \mathrm{Im}(C). \end{aligned} \tag{4.11}$$

The field intensity now simply writes $I = \bar{\beta}^* \bar{\beta}$, and computing it we recover the same result of the phenomenological Eq. (4.4). To estimate the value of C we go to the continuum density limit by using a Gaussian distribution for the atoms position and integrating over all the space

$$\begin{aligned} C &= \frac{N}{(2\pi)^3 R^6} \int d\mathbf{r} \int d\mathbf{r}' \frac{e^{ik_0|\mathbf{r}-\mathbf{r}'|}}{k|\mathbf{r}-\mathbf{r}'|} e^{i\mathbf{k_0}\cdot(\mathbf{r}-\mathbf{r}')} e^{-(r^2+r'^2)/2R^2} \\ &= -\frac{\Gamma}{2}\frac{b_0}{8}\left(2i\frac{\mathrm{D}(2k_0R)}{\sqrt{\pi}} - \left(1 - e^{-4k_0^2R^2}\right)\right), \end{aligned} \tag{4.12}$$

with $\mathrm{D}(x)$ the Dawson integral that behaves asymptotically as $\mathrm{D}(x \to \infty) \approx 1/2x$. In the limit of a large dilute cloud ($kR \gg 1$ and $\rho_0/k^3 \ll 1$), $C = -(\Gamma/2)b_0/8$ gives a scaling linear in b_0 for the collective damping:[17–18]

$$\Gamma_N = \Gamma\left(1 + b_0/8\right). \tag{4.13}$$

Note that since C is real in the dilute approximation, the frequency shift is negligible. Nevertheless, this single-mode approach reproduces the scaling decay rate due to a single photon superradiance after a weak pump excitation.[17–18]

4.1.1.4 Multiple modes

Let us now consider the multiple modes case Eq. (4.6) without further approximations. Note that the matrix $\tilde{\mathbf{M}}$ is complex symmetric and can always be written in a diagonal form by a unitary transformation $\mathbf{U}\tilde{\mathbf{M}}\mathbf{U}^{\mathbf{T}} = \mathbf{D}$, with $\mathbf{D}$ complex diagonal. We suppose $\mathbf{U}\mathbf{U}^{\mathbf{T}} = \mathbb{1}$, which is always true for random distributions of positions. Introducing the transformed amplitudes $\mathbf{b}(t) = \mathbf{U}\tilde{\boldsymbol{\beta}}$ and transformed Rabi frequency vector $\mathbf{w} = \mathbf{U}\tilde{\boldsymbol{\Omega}}$ we obtain the solution

$$\mathbf{b}(t) = \left(e^{\mathbf{D}t} - \mathbb{1}\right)\mathbf{D}^{-1}\mathbf{w} \tag{4.14}$$

which gives an exponential decay for the amplitude of each mode

$$b_n(t) = \frac{w_n}{\lambda_n}\left(e^{\lambda_n t} - 1\right), \tag{4.15}$$

with w_n the nth element of the vector $\mathbf{w}$, λ_n the associated eigenvalue of $\tilde{\mathbf{M}}$ with real and imaginary parts $\lambda_n = -\Gamma_n/2 - i\Omega_n$ that define the damping and oscillation of the mode n. That way, the dynamics of the amplitudes b_n depends on a geometrical factor w_n and the spectral distribution λ_n. Thus not only the geometrical factor for each mode w_n, but also the presence of multiple modes in the dynamics, lead to more fluctuations for the radiated far-field, which presents a large deviation from one atomic position realization to another. Nevertheless the average over random realizations can still be fitted with the phenomenological function Eq. (4.4) with a remarkably good agreement (see Fig. 20).

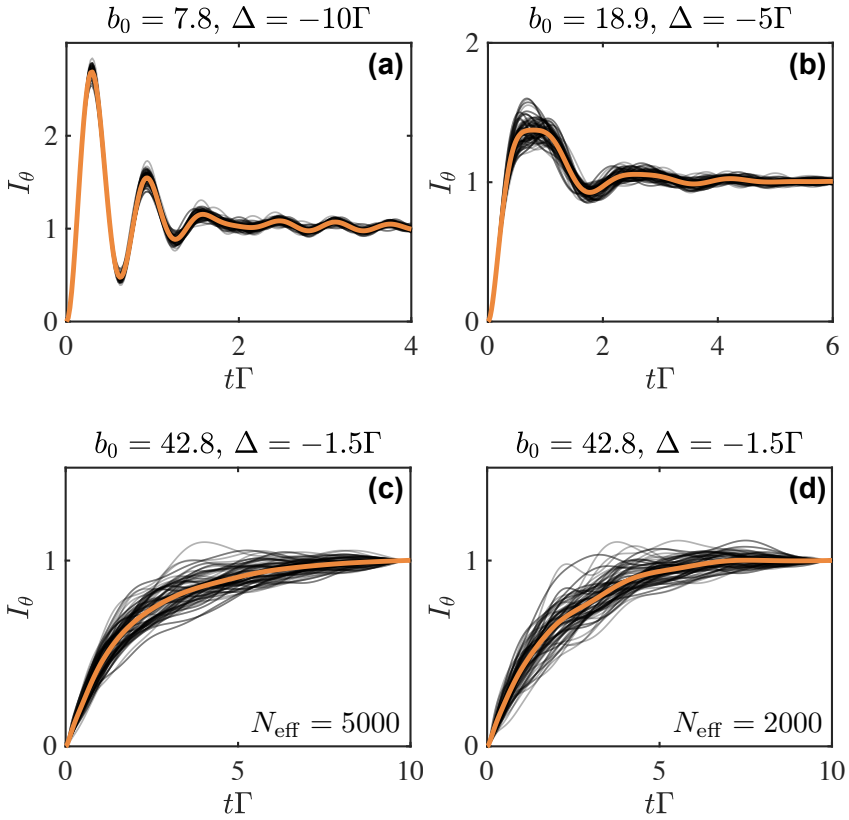

Figure 20 – CD simulations for the parameters from Fig. 19. Besides the realization averaged curves (orange lines), we also show 100 single realization results (thin gray lines). (a-c) $N_{eff} = 5000$ (d) $N_{eff} = 2000$. For small $|\Delta|$ and large b_0 we observe large fluctuations that are independent of N_{eff}.

Source: Adapted from ESPIRITO SANTO *et al.*[22]

4.1.1.5 Collective superradiance and frequency shift observation

We ran CD simulations to compare them with the experimental data in the linear optics limit, with a constant low saturation parameter ($s \approx 2.2 \pm 0.6 \times 10^{-2}$), varying the optical thickness b_0 and the laser-atom detuning Δ. All the simulations were done with $N_{eff} = 5000$ atoms, the Gaussian cloud kR adjusted to match the experimental b_0 and we took the average over 100 realizations of random positions to reduce fluctuations.

By fitting Eq. (4.4) we extract the collective damping constant Γ_N and the generalized Rabi frequency Ω_N. For the damping, the out-of-resonance optical thickness $b(\Delta) = b_0/(1 + 4(\Delta/\Gamma)^2)$ appears to be the control parameter to describe the superradiant behavior. Our results (Fig. 21), obtained with the switch-on dynamics, has the same behavior of the well-known superradiant decay obtained for the switch-off case.[66]

In Fig. 21 we compare the CD simulations (a) with the experimental results (b) for the collective damping rate. We only kept the values for which the fit is rather good: $R^2 > 0.85$. A superradiant decay is indeed observed ($\Gamma_N > \Gamma$), note that, for small $b(\Delta)$, Γ_N scales with b_0 following the single mode result of Eq. (4.13) (Fig. 21(a) solid lines). For

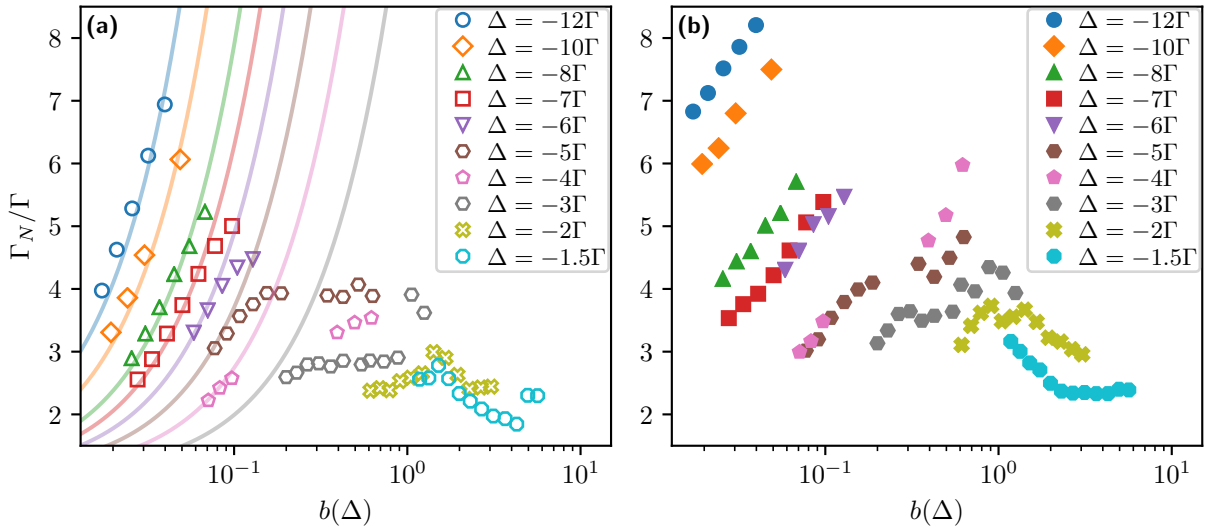

Figure 21 – Collective decay rate Γ_N showing superradiant behavior. (a) Fits to CD simulations. (b) Fits to experimental data. We only kept the data for which the fitting function Eq. (4.4) has a value of $R^2 > 0.85$. For small $b(\Delta)$ the CD theory agrees with the single-mode prediction (lines from Eq. (4.13)). Generally, the experiment exhibits a more damped behavior.

Source: Adapted from ESPIRITO SANTO *et al.*[22]

$b(\Delta) \geq 1$ the decay rate gets smaller due to attenuation and multiple scattering, which can be explained by the reduced superradiant states population near-resonance.[71] The experimental data Fig. 21(b) shows a very similar behavior compared with the CD results (a). We attribute the deviations to systematic errors and to the finite switch-on time of the laser.

In Fig. 22 we present the frequency shift $(\Omega_N - \Delta)/\Gamma$. Note that, for small optical thickness there is almost no shift, in agreement with the single mode approximation. Increasing b_0 there is a shift that also varies with the detuning Δ. This shift can be interpreted as a multi-mode vacuum Rabi splitting: it can be calculated with linear dispersion theory (solid lines in Fig. 22), and is related to the coupling strength of the light modes to the atomic cloud.[70]

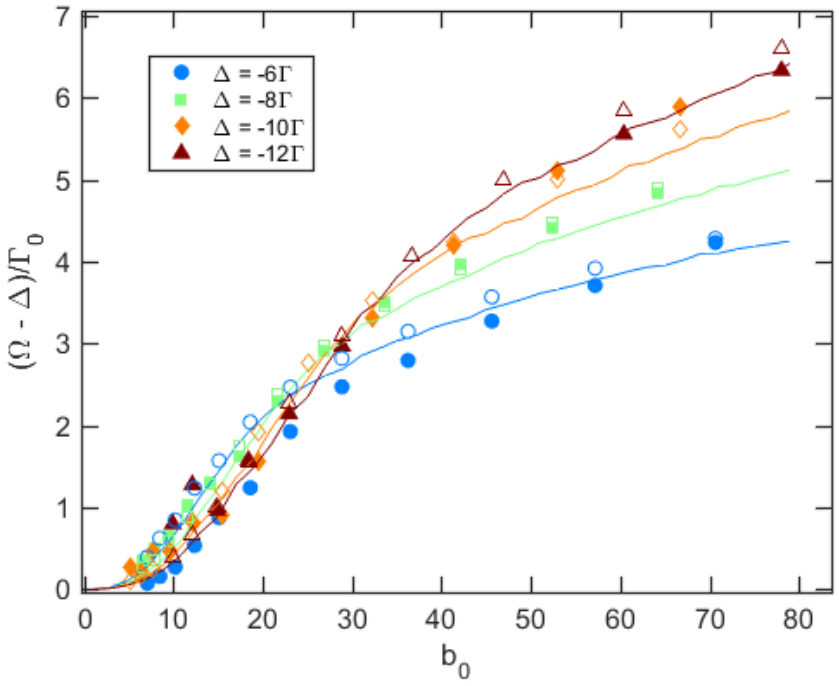

Figure 22 – Splitting amplitude extracted from the experiment (full symbols), from the coupled-dipole simulations (empty symbols) and from the linear-dispersion theory (lines), for different detunings and optical thicknesses. For the CD simulation the collective decay rate Ω in the label is obtained with Ω_N from Eq. (4.4).
Source: Adapted from GUERIN *et al.*[70]

4.1.2 Beyond linear optics

When increasing the saturation parameter in the system, the linear optics regime in which the low saturation is assumed ($\langle\hat{\sigma}_n^z\rangle \approx -1$) breaks down and we cannot neglect the atomic population anymore. The nonlinear MF equations Eq. (3.5), that includes the σ_n^z operators is a good candidate to describe the field dynamics if one assumes that the quantum correlations between atoms can be neglected. Since the MF equations scale linearly with N ($3N$ equations instead of N for linear optics), numerical simulations can still be performed with thousands of atoms.

In Fig. 23 we compare exact simulations (E), *i.e.*, that addresses the full Hilbert space, with MF and CD results. We use a toy-model with $N = 6$ atoms with a uniform sphere distribution for the atomic positions. It is a toy-model in the sense that, even though the model is derived for the low spatial density regime (scalar approximation for the light), by choosing a sphere radius $R = 1k^{-1}$, there is a high density $\rho = 1.4k^3$. But since we are working with a small number of atoms we extrapolate the spatial density to obtain a high optical thickness. Even for this high density case, with a small saturation parameter $s = 0.1$ (Fig. 23(a)) all three models are in good agreement, as can be expected from the low-excitation regime. Increasing the saturation (see Fig. 23(b)) the CD simulations deviate strongly from the exact ones, while the MF results captures correctly the oscillatory

dynamics, although it does not capture the slope in the decay. Going back to the dilute regime (see Fig. 23(c), $R = 5k^{-1}$ and $\rho \approx 0.01k^3$) the slope is not present and the MF results are in good agreement with the exact simulation.

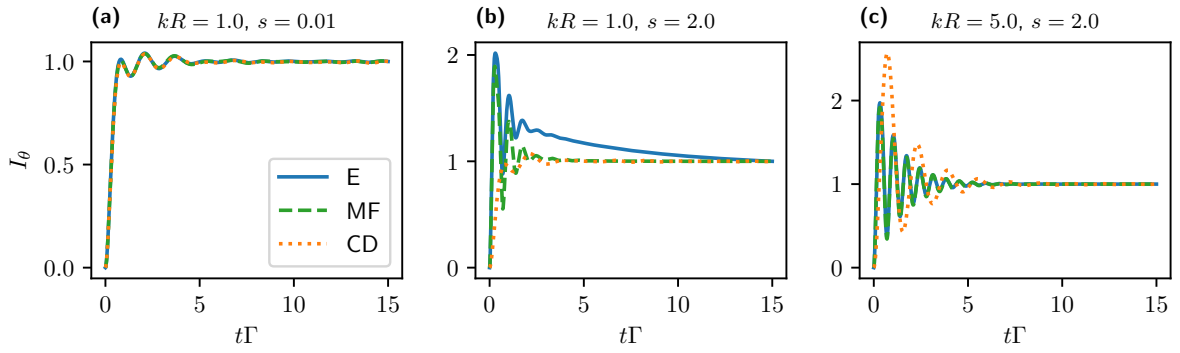

Figure 23 – Comparison between exact simulations of the master equation (E), Eq. (2.52), mean-field simulations (MF), Eq. (3.5), and the coupled-dipole model (CD), Eq. (3.2). The intensity is normalized to the long-time value. We use a small cloud with uniform density ($N_{eff} = 6$). Here, $\Delta = -4\Gamma$ and we use two sphere radii $kR = 1$ (a),(b) and $kR = 5$ (c). We tune the Rabi frequency to obtain small and large saturation parameters, $s = 0.01$ (a) and $s = 2$ (b),(c), respectively. MF is superior to CD in reproducing the full quantum results for high saturation (c) and only fails for dense clouds and high saturation (b). Exclusion distance $kd_{min} = 0.1$; average performed over 21 realizations.

Source: Adapted from ESPIRITO SANTO *et al.*[22]

Overall, we find a very good agreement between exact and MF simulations for the switch-on dynamics, with small deviations for $\Omega \approx \Gamma$. This regime is the one where quantum correlations are expected to be the strongest, as the atoms are strongly driven by the laser, yet the radiation they exchange between each other is comparable to that.

In Fig. 24 we compare the experimental signal with MF and CD simulations for higher saturation parameter s. From the experimental side, the same setup described in section 4.1.1.1 is used with some upgrades.[61–62] The experiment is still in development for high saturation parameter and some issues, for example, higher temperature in the system and higher laser switch-on time (17ns), are being addressed to study this regime with a better control of the different parameters. Note that, increasing the saturation parameter (Fig. 24(a)-(c)) the CD model fails to describe the signal whereas the data from the non-linear MF model are in good agreement with the experimental results.

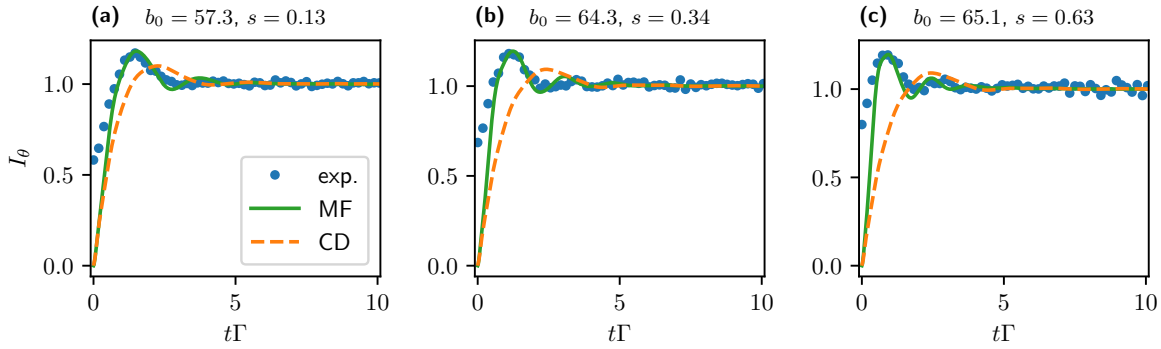

Figure 24 – Comparison between the normalized intensity evolution from the experiment with MF and CD simulations in a large saturation regime ($s \gtrsim 0.1$) and with $b_0 \sim 60$: (a) $s = 0.13$, (b) $s = 0.34$, (c) $s = 0.63$. Here, $\Delta = -4\Gamma$. For the simulations $N_{eff} = 5000$, and the results were averaged over 78 random distributions.
Source: Adapted from ESPIRITO SANTO *et al.*[22]

4.1.3 Single mode in the mean-field approximation

Let us now apply the single mode approximation (see section 4.1.1.3) for the MF equations. Here we not only replace the excitation amplitudes by it average value $\bar{\beta}$ but also the average of the σ_n^z operators $\bar{z} \approx (1/N)\sum \sigma_n^z$ to obtain:

$$\begin{cases} \dfrac{d}{dt}\bar{\beta} = \left(i\Delta - \dfrac{\Gamma}{2}\right)\bar{\beta} - i\dfrac{\bar{\Omega}(t)}{2}\bar{z} \\ \dfrac{d}{dt}\bar{z} = i\dfrac{\bar{\Omega}^*(t)}{2}\bar{\beta} - i\dfrac{\bar{\Omega}(t)}{2}\bar{\beta}^* - \Gamma\left(\bar{z}+1\right) \end{cases} \tag{4.16}$$

with

$$\bar{\Omega}(t) = \Omega - i\Gamma\frac{b_0}{8}\bar{\beta}(t). \tag{4.17}$$

Eq. (4.16) is identical to the single dipole equation but with a time-dependent Rabi frequency Eq. (4.17). The mean electric field generated by the cloud acts like an additional pumping stimulating the successive emission and absorption of light by the atoms.

4.1.4 Optical pumping of a subradiant mode

The slow decay that induces the slope behavior observed in the toy-model on Fig. 23(b) is intriguing and was also observed in some of the experimental results, in the dilute regime and high b_0, for higher saturation parameter. Let us first take a closer look at the decay matrix, which elements are defined by the collective emission terms

$$\gamma_{nm} = \Gamma\frac{\sin(kr_{nm})}{kr_{nm}}, \tag{4.18}$$

obtained by diagonalizing this matrix. We thus obtain N decay constants γ_n (eigenvalues) associated with each decay channel (see section 3.4.1.1). At this point, we analyze the geometrical dependency of the γ_n without directly studying the dynamics. Note that,

due to the trace conservation of a similarity transformation (Eq. (3.22)) $\sum \gamma_n = N\Gamma$, the maximum possible exponential decay at the system is $N\Gamma$ for any channel.

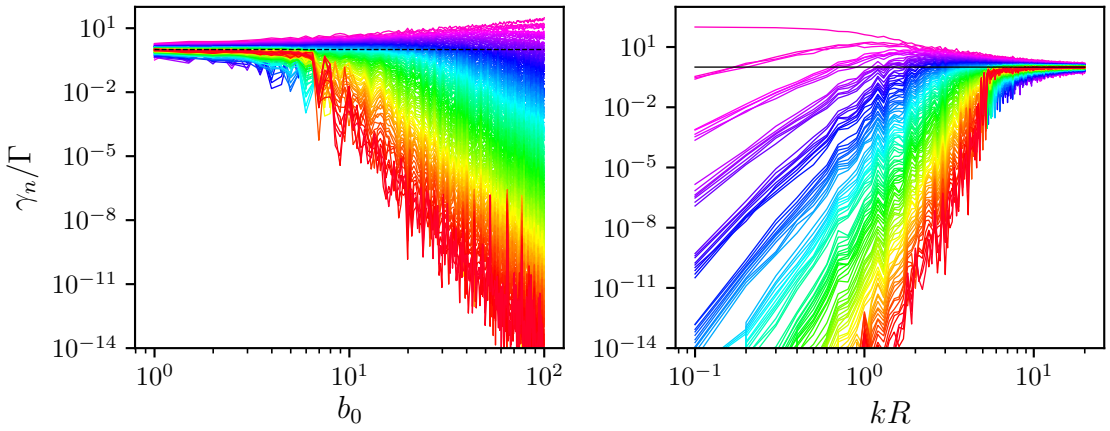

Figure 25 – Decay channels γ_n obtained from the decay matrix diagonalization as a function of (a) the optical thickness b_0 and (b) the Gaussian cloud RMS kR. $N = 100$ and average over 50 random atoms position realizations.The color gradient indicates the γ_n) valuers from lower (red) to higher (violet).
Source: By the author

In Fig. 25 we compare the behavior of the N decay constants γ_n when increasing the system size kR on one hand, and the optical thickness b_0 on the other hand. The number of atoms is fixed, $N = 100$, so the spatial density ρ is also varying. For each value of parameters we took the average over 50 realizations with a Gaussian distribution. Note that, for very small kR or high b_0 there is one strong superradiant decay channel ($\gamma_n \gg \Gamma$) and most of the others channels become subradiant ($\gamma_n < \Gamma$). In particular in Fig. 25(b), for a very small kR we observe two decay constants, Γ_{sup} of the order of $N\Gamma$ and one small Γ_{sub} (neglecting $\gamma_n < 10^{-3}$). For high values of kR or small b_0 there seems to be $\sim N/2$ superradiant channels and $\sim N/2$ subradiant ones with γ_n of the order of Γ. For a very dilute cloud ($kR \gg 1$) the atoms are very distant and the interaction is small, we expect that all the decay channels tends to the independent atoms case with $\gamma_n \to \Gamma$. Also remember that, this model was derived for the dilute regime; in that sense the $kR \ll 1$ limit should in principle be studied using a vectorial light model.

Now, inspired by the small kR case where it seems to be one superradiant rate and one subradiant rate (neglecting $\gamma_n < 10^{-3}$), or one can think of averaging the super/subradiant decay, let us consider a three-level system with one superradiant mode and one subradiant mode: this system is an idealization of the full system, which contains $\sim 2^N$ modes, yet its aim is to capture the ingredients necessary to explain the slope discussed above. The pump addresses mainly the superradiant mode, since these modes are those that most couple to a planewave[72]. From the superradiant state, it can decay to the ground-state or decay (pumping) to the subradiant mode. A sketch of this model is

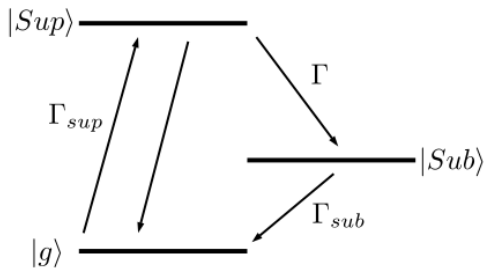

Figure 26 – Three-level system with a superadiant and a subradiant states.
Source: By the author

presented in Fig. 26. One can write the rate equations for this three-level system, with $\rho_{sup\to g}$ the transition $|sup\rangle \to |g\rangle$, the following equations are obtained:

$$\begin{cases} \dfrac{d\rho_g}{dt} = -i\dfrac{\Omega}{2}(\rho_{sup\to g} - \rho_{g\to sup}) + \Gamma_{sup}\rho_{sup} + \Gamma_{sub}\rho_{sub}, \\ \dfrac{d\rho_{sup\to g}}{dt} = (i\Delta - \Gamma_{sup}/2)\,\rho_{sup\to g} + i\dfrac{\Omega}{2}(\rho_{sup} - \rho_g), \\ \dfrac{d\rho_{sup}}{dt} = i\dfrac{\Omega}{2}(\rho_{sup\to g} - \rho_{g\to sup}) - \Gamma_{sup}\rho_{sup} - \Gamma\rho_{sup}, \\ \dfrac{d\rho_{sub}}{dt} = \Gamma_{sup}\rho_{sup} - \Gamma_{sub}\rho_{sub}. \end{cases} \tag{4.19}$$

Averaging out the fast oscillations to describe only the slope which occurs on long time scales ($t \gg 1/\Gamma$), by considering

$$\frac{d}{dt}\rho_{sup\to g} = \frac{d}{dt}\rho_{g\to sup} = 0 \tag{4.20}$$

we obtain the rate equations

$$\begin{cases} \dfrac{d\rho_g}{dt} = -\dfrac{\Gamma_{sup}\Omega^2}{\Gamma_{sup}^2 + 4\Delta^2}(\rho_{sub} - \rho_{sup}) + \Gamma_{sup}\rho_{sup} + \Gamma_{sub}\rho_{sub}, \\ \dfrac{d\rho_{sup}}{dt} = \dfrac{\Gamma_{sup}\Omega^2}{\Gamma_{sup}^2 + 4\Delta^2}(\rho_g - \rho_{sup}) - \Gamma_{sup}\rho_{sup} - \Gamma\rho_{sup}, \\ \dfrac{d\rho_{sub}}{dt} = \Gamma\rho_{sup} - \Gamma_{sub}\rho_{sub}. \end{cases} \tag{4.21}$$

This system of equation can be rewritten in the form

$$\frac{d}{dt}\begin{pmatrix} \rho_g \\ \rho_{sup} \\ \rho_{sub} \end{pmatrix} = M \begin{pmatrix} \rho_g \\ \rho_{sup} \\ \rho_{sub} \end{pmatrix} \tag{4.22}$$

and the radiated power is given by

$$P(t) = (\Gamma_{\text{sup}} + \Gamma)\,\rho_{sup}(t) + \Gamma_{\text{sub}}\rho_{sub}(t). \tag{4.23}$$

Solving the system of Eq. (4.21) for the initial state of the switch-on dynamics $(\rho_g, \rho_{sup}, \rho_{sub})^T = (1, 0, 0)^T$

$$\begin{pmatrix} \rho_g \\ \rho_{sup} \\ \rho_{sub} \end{pmatrix}(t) = U e^{Dt} U^{-1} \begin{pmatrix} 1 \\ 0 \\ 0 \end{pmatrix} \tag{4.24}$$

with $M = UDU^{-1}$, D the diagonal matrix obtained from the diagonalization of the system coefficients matrix M. We finally obtain one expression for the radiated power, with $\lambda_{0,\pm}$ the eigenvalues of M:

$$\begin{aligned} P(t) = &\left(\Gamma + \Gamma_{sup}\right) U_{21} U_{11}^{-1} + \Gamma_{sub} U_{31} U_{11}^{-1} + \left[\left(\Gamma + \Gamma_{sup}\right) U_{22} U_{21}^{-1} + \Gamma_{sub} U_{32} U_{31}^{-1}\right] e^{\lambda_- t} + \\ &+ \left[\left(\Gamma + \Gamma_{sup}\right) U_{23} U_{31}^{-1} + \Gamma_{sub} U_{33} U_{31}^{-1}\right] e^{\lambda_+ t} \end{aligned} \tag{4.25}$$

We finally use the Eq. (4.25), apart from one amplitude A to consider the N atoms contribution $f = AP(t)$, to fit the slope decay, with free fitting parameter Γ_{sup}, Γ_{sub} and an amplitude A to account for the N atoms in the system.

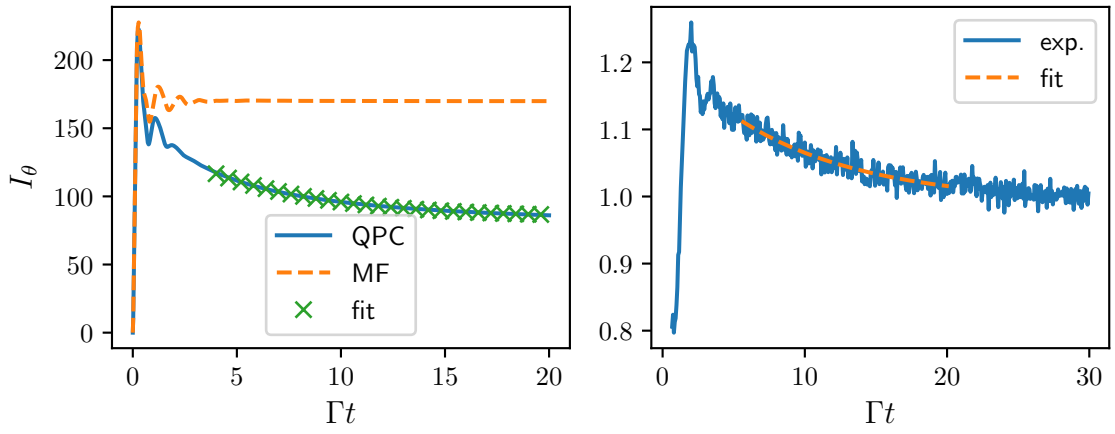

Figure 27 – Comparison of the field dynamics for QPC and MF for high b_0 (a) for the fiting it was obtained a $\Gamma_{sup} = 24.72\Gamma$ and $\Gamma_{sub} = 0.10\Gamma$. The MF method fails to capture the slope. In (b) a experimental run where the same slope behavior is observed, with $\Gamma_{sup} = 37.81\Gamma$ and $\Gamma_{sub} = 0.09\Gamma$.
Source: By the author

In Fig. 27 we observe with numerical simulation (a) and experimental results (b) that, for substantial saturation $s \gtrsim 1$ and high optical thickness b_0, the fitting function for the slope has a good agreement, which shows that the simple three-level model captures the slope. This slope may thus be a signature of optical pumping of subradiant modes, which could be a way to tune the population of these modes.

Also, in Fig. 27(a), the MF simulation does not capture the slope behavior, so it can be understood as a signature of the presence of quantum correlations. The QPC

simulations are limited to hundreds of atoms, we are not able to match the experimental regime of dilute cloud with high optical thickness to obtain a direct comparison. Also, the experimentalist of the Cold Atom Group in Nice are still improving the experimental setup to achieve higher saturation parameters. These preliminaries results will, in a near future, be compared more systematically to the experimental ones to understand whether optical pumping of subradiant modes can be achieved.

4.2 Switch-off dynamics in the quantum regime

Most of the cooperative effects were discussed up to date in the classical linear optics limit and with the switch-off dynamics protocol. In the previous section we described some collective effects with the switch-on dynamics and showed that the nonlinear MF equations describe the system correctly for higher saturation. Only for larger densities does the MF model fails to capture a slope in the switch-on protocol, which is probably related to an optical pumping of subradiant modes.

In the switch-off protocol, the laser is turned-off ($t = 0$) when the system has reached a steady-state (practically, it has received the pump for a time $t \gg 1/\Gamma$). Since the number of excitations can only decay with time, one expects to recover the low-excitation behavior for long-times ($\Gamma t \gg 1$). The correlations build up in the decay dynamics and fade away at late times.

In Fig. 28 we present a benchmark of the MF and QPC models with exact simulations (E) for $N = 7$ atoms, on resonance ($\Delta = 0$) in two different regimes. For small saturation ($\Omega = 0.1\Gamma$) all the results are in good agreement, the MF model presents some deviations for $\Gamma t \gtrsim 2.5$. For the high saturated case ($\Omega = 5.0\Gamma$), while the QPC method has a good agreement with E, the MF model decays like N independent atoms ($e^{-\Gamma t}/2$, dashed line). Also, for $\Gamma t \sim 10$ the MF starts to deviate from the linear decay, so non-linear effects might appear, which are not related to quantum correlations.

By fitting the exponential decay as $Ae^{-\Gamma_N t}$ in a given time interval, one can obtain the collective decay time $\tau_N = 1/\Gamma_N$. In Fig. 29 we divided the field decay in intervals of $\Gamma\delta t = 1$ and fitted an exponential decay to obtain the decay constant $\Gamma_N(t)$ as a function of time. We can observe that, for small saturation parameter, $s = 0.1$, in Fig. 29(a) the MF and QPC methods are in good agreement, while for higher saturation, $s = 5$, in Fig. 29(b), for $\Gamma t \sim 5$ there is a plateau with $\Gamma_N = 1$ for the MF model decaying essentially as N independent atoms. Thus, we choose the interval $\Gamma\delta t \in (5, 10)$ to analyze the role of quantum correlations, since it is the interval in which the MF method does not agree with QPC.

By analyzing the decay dynamics in the quantum regime, in the time interval $\Gamma t \in (5, 10)$, we extract the decay time τ_N and always find subradiant times $\tau_N > 1$ for

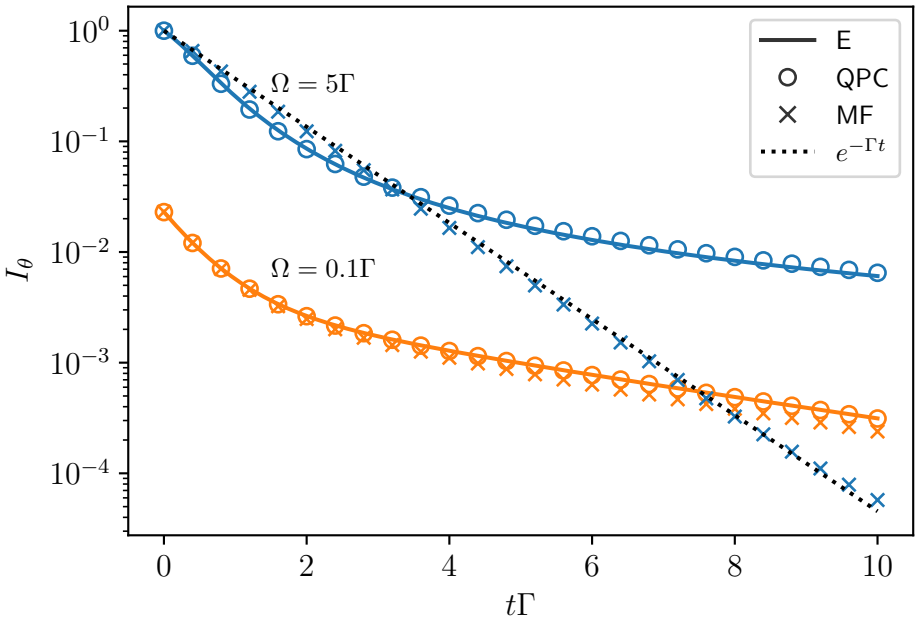

Figure 28 – Far-field radiated intensity in the switch-off configuration, using exact simulations (plain lines), quantum pair correlations (empty symbols) and mean-field approximation (crosses) normalized by the saturated ($\Omega = 5\Gamma$) steady-state value. The black dashed line represents the decay of N independent atoms ($I = e^{-\Gamma t}$. Simulations realized for $N = 7$, $\Delta = 0$, observation angle $\theta = 35°$ for a random Gaussian distribution with root mean square (RMS) $kR = 1.18$, averaging over 62 realizations.
Source: By the author

the QPC model, yet not for the MF: thus, the subradiance in this regime is not captured by the semi-classical model and may present quantum features. In the high saturation regime, $s = 50$ in Fig. 30, the decay constant does not vary with the detuning nor the observation angle θ. Also, we find that when increasing the saturation parameter, the decay time saturates with the QPC model, for a given optical thickness b_0 (Fig. 31(a)), while the subradiance is totally suppressed for the MF approximation ($\tau_N = 1$) (see Fig. 31(b)).

In Fig. 32 we present the scaling behavior of the subradiant collective decay time with the on-resonance optical thickness b_0. To rule out spatial density effects, we run simulation with constant spatial densities ρ varying the number of atoms N (black triangles) and compare them with simulations at constant number of atoms $N = 100$ varying the spatial density (blue circles), both with the QPC method. We also checked that for these simulation parameters the subradiance is suppressed with the MF model (orange squares). We conclude that the subradiant decay rate scales with the optical thickness and is beyond semi-classical physics: in this context, a characterization of entanglement or signatures of non-classicality will be an important step to show the quantum nature of this decay process.

Finally, we investigate whether the decay dynamics of the saturated cloud falls into

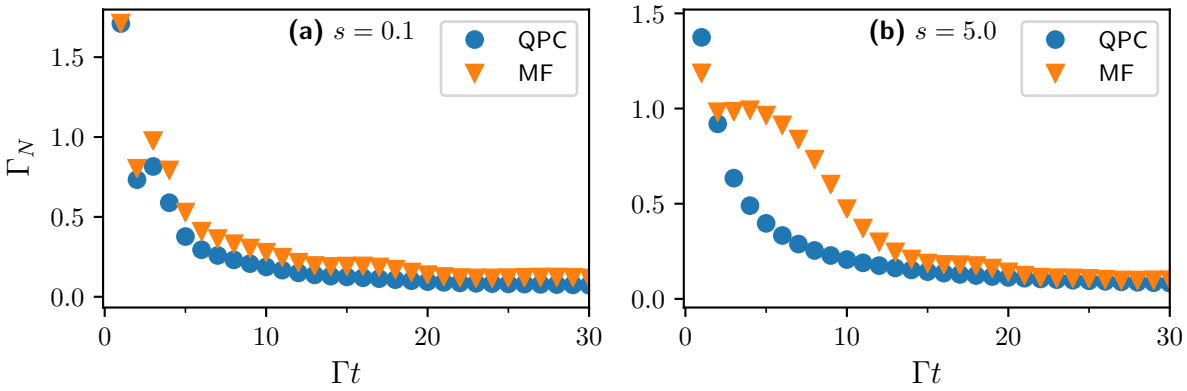

Figure 29 – Collective decay rate Γ_N as a function of time using an exponential fitting of the switch-off radiated far-field intensity in intervals of $\Gamma\delta t = 1$ using quantum pair correlations (QPC) and mean-field approximation (MF). Simulation for $N = 100$, $b_0 = 10$, $\Delta = -4\Gamma$ and saturation parameter (a) $s = 0.1$ and (b) $s = 5$. Average over 62 realizations.

Source: By the author

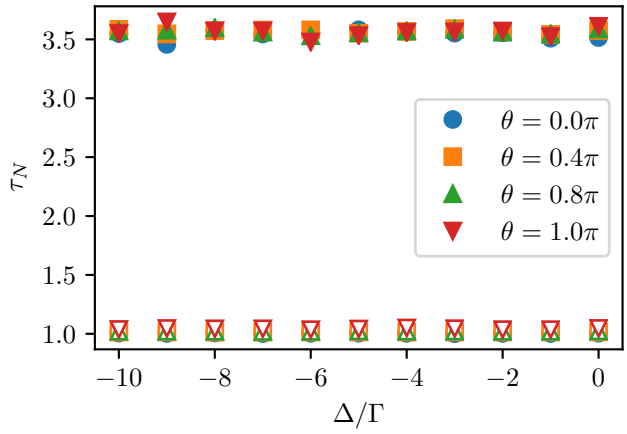

Figure 30 – Collective decay time constant τ_N as a function of the detuning Δ for different detection angles θ. Simulations with $N = 100$ atoms, saturation $s = 50$ and $b_0 = 10$ with average over 72 realizations. For high saturation the decay time constant is independent of the detection angle and of the detuning.

Source: By the author

a subradiant state with a low number of excitations (through a superradiant cascade[9], for example) or if states with many excitations might present subradiance. In the next section we study the population decay of a state with n-excitations in an attempt to clarify this point.

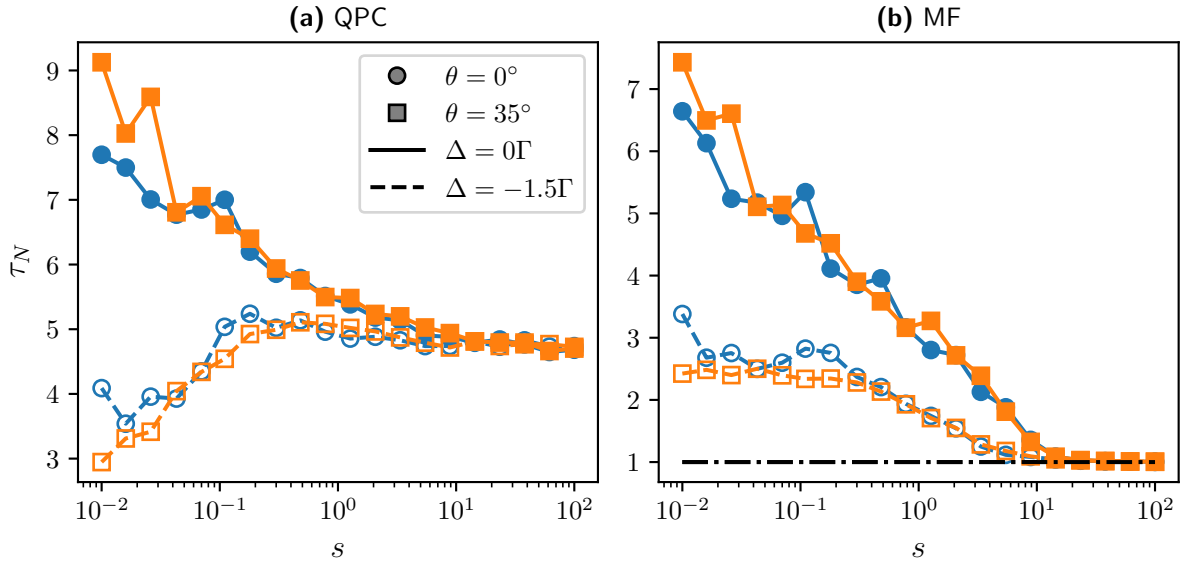

Figure 31 – Decay time constant × saturation parameter for two detection angles $\theta \in (0, 35°)$ and two values of detuning $\Delta \in (0, -1.5\Gamma)$. Simulations for $N = 50$ atoms and $b_0 = 20$ for (a) QPC and (b) MF. For larger saturation the dependency of τ_N with θ and Δ disappears for QPC while for the MF method the subradiance is suppressed $\tau_N = 1$.

Source: By the author

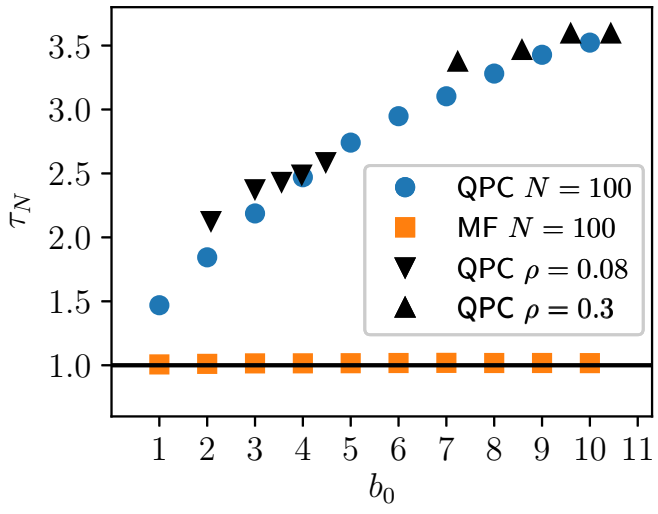

Figure 32 – Subradiant decay time versus the optical thickness for the switch-off dynamics using (MF) mean-field and (QPC) quantum pair correlations method. Simulations realized for $N = 100$, on resonance $\Delta = 0$, with saturation $s = 50$ and detection angle $\theta = 0.6\pi$, using an average over the azimuthal angle and over 62 realizations of a random Gaussian distribution. The triangles denotes simulations with fixed spatial density ρ varying the number of atoms to achieve the desired b_0 with the QPC method.

Source: By the author

4.2.1 Population decay of a state with n excitations

Considering the master equation for the atomic system Eq. (2.52) one can define the population of a n-excited state as the probability to find a state with n-excited atoms. Let us consider the projection operators for the excited state $\mathbb{e} = |e\rangle\langle e|$ and the ground state $\mathbb{g} = |g\rangle\langle g|$ of a single two-level atom. For N atoms we define the population of a n-excited state as the linear combination of all the states with n-excited atoms. This means that we must take into account all the possible $N!/n!(N-n)!$ permutations for each state with n excitations. Each term of the permutation is a tensor product of the projector operators.

$$\hat{f}_n = \sum_{\mathcal{P}} \mathbb{e}_1 \otimes \mathbb{e}_2 \otimes \cdots \otimes \mathbb{e}_n \otimes \mathbb{g}_{n+1} \otimes \mathbb{g}_{n+2} \otimes \cdots \otimes \mathbb{g}_N, \tag{4.26}$$

where the indices represent the Hilbert space of the atom n and $\mathcal{P}$ represents all the possible permutations (with repetition) changing the position of the projectors operators $\mathbb{e}$ and $\mathbb{g}$. The n-excited population is the expected value of the respective state calculated in the usual way, $P_n = \mathrm{Tr}(\hat{\rho}\hat{f}_n)$.

One must keep in mind that each term of the sum over the permutations in the $\hat{f}_n$ state is a $2^N \times 2^N$ matrix, thus to consider and calculate all to possibles $N!/n!(N-n)!$ permutations numerically would demand a lot of computational resources for N beyond a dozen. We limit our analysis to small systems ($N \leq 9$) with exact simulations.

In the superradiance essay by M. Gross and S. Haroche[59] a cascade decay for symmetric states was described, with all atoms excited as the initial state, *i.e.* fully-inverted system. The collective decay rate begins with $\Gamma_c = N\Gamma$ and increases in the upper part of the symmetric states ladder. The maximum value of the decay rate is proportional to N^2 for the half-excited state. In our case, for the switch-off dynamics, the initial state is the steady-state, which is composed of a statistical mixture of all the n-excited states and not only the fully-inverted one.

We present the decay dynamics of the n-excited population for a system with $N = 9$ atoms in Fig. 33. Note that all populations are present in $\Gamma t = 0$ (superposition at the steady-state) and a faster decay is observed with increasing n. By fitting the exponential decay in $\Gamma\delta t \in (5, 10)$ we obtain the n-excited states decay rate Γ_n. In Fig. 34 we vary the number of atoms N and compare all the decay rates. Note that, for the state with N excited atoms we always obtain a decay rate $\Gamma_N = N\Gamma$, consistent with the result for the same state in the superradiant cascade decay[59]. In the symmetric states decay considered by Dicke, with a fully-inverted state as the initial state, the superradiant rate reaches values $\propto N^2$, while in our model, with the steady-state as initial state, we obtain $\Gamma_n \leq n\Gamma$ for all the n-excited populations. Also, it appears that the states with $n > N/2$ presents a superradiant behavior ($\Gamma_n > \Gamma$) while the ones with $n < N/2$ are subradiant ($\Gamma_n < \Gamma$),

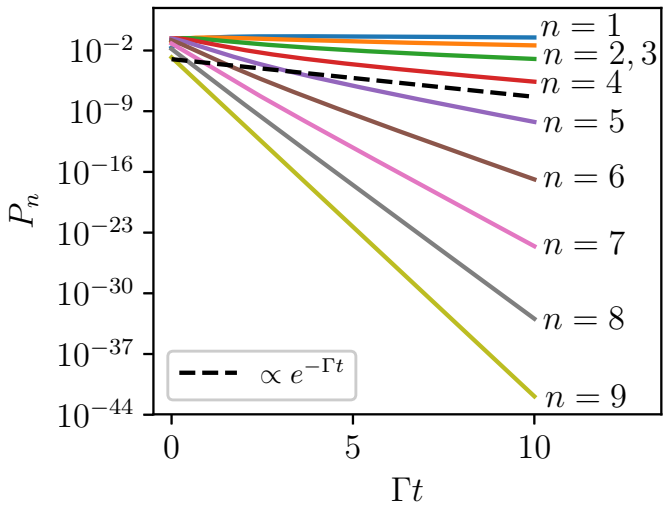

Figure 33 – n-excited state population time decay for $N = 9$ atoms, $\Omega = 5\Gamma$, $\Delta = 0$ and $\rho = 0.4k^3$. Simulation for the switch-off dynamics after the steady-state is reached and average over 8 realizations with a uniform sphere distribution.
Source: By the author

which explains the presence of a higher population of $n < N/2$ states for long times in Fig. 33.

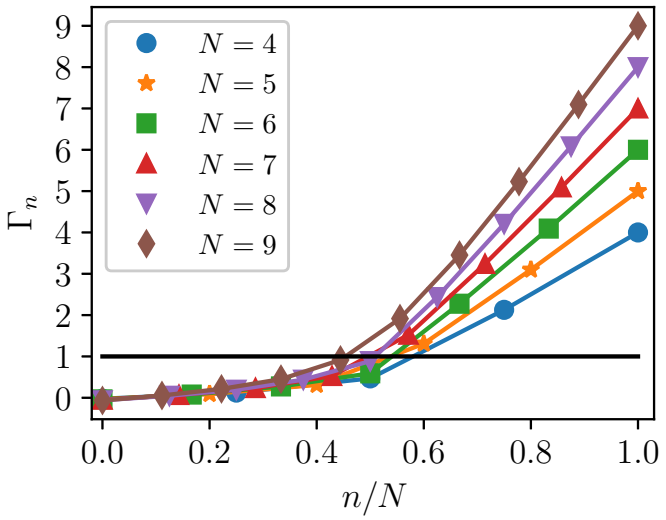

Figure 34 – Collective decay constant of the n-excited population versus n/N for $\Gamma t \in (5, 10)$ and varying the number of atoms. Simulation for $\Omega = 5\Gamma$, $\Delta = 0$ and spatial density $\rho = 0.3k^3$ with average over 8 realizations with a uniform sphere distribution.
Source: By the author

In Fig. 35 we increase the spatial density and we observe smaller decay rates for systems increasing ρ. Since the interaction depends on the atomic distances, a less dilute system presents stronger interaction and the collective behavior of subradiance is enhanced, which is consistent with the scaling of τ_N with b_0 presented in section 4.2.

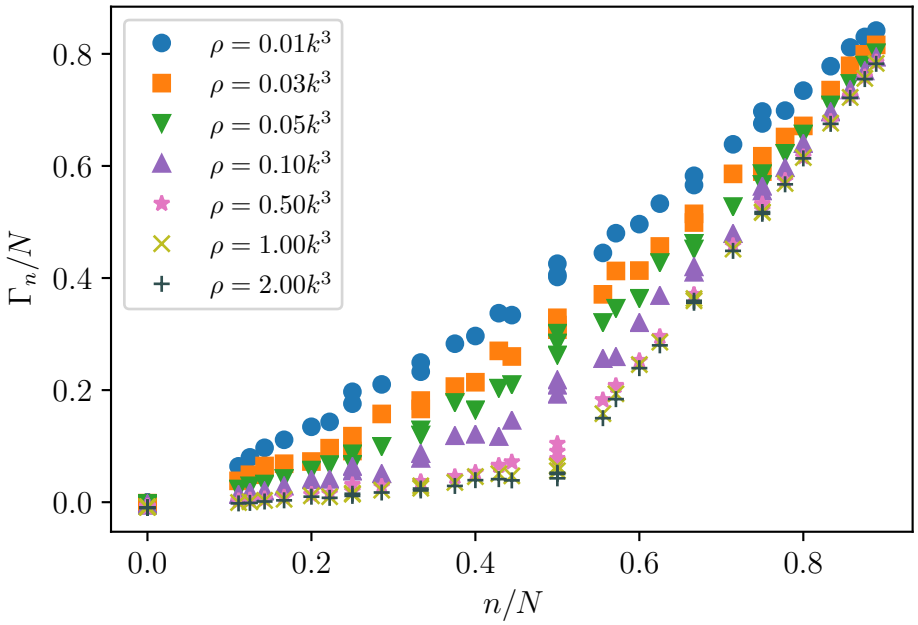

Figure 35 – Decay rate Γ/N versus n/N varying the spatial density ρ. For each density we vary $N \in (4, 9)$. Simulation for $\Omega = 5\Gamma$ and $\Delta = 0$ with average over 8 realizations using a uniform sphere distribution.

Source: By the author

We conclude that states with many excited atoms lead to a beyond-semi-classical subradiance for the states with $n < N/2$ excited atoms, which are the most populated ones in the late-time decay dynamics. It differs from the cascaded decay from Dicke[9] where the decay is superradiant at first, and then only subradiant as the system reaches the states with a low excitation number.

We can also define the contribution to the intensity of the radiated field due to the n-excited state by

$$I_n = \sum_{j=1}^{N}\sum_{k=1}^{N} \mathrm{Tr}\left(\hat{\sigma}_j^+ \hat{\sigma}_k^- \hat{f}_n \hat{\rho}\right) e^{ik_0 \hat{n}.(\mathbf{r}_j - \mathbf{r}_k)} \tag{4.27}$$

with $\hat{n}$ the emission direction. In Fig. 36 we observe a fast decay of the intensity of the radiated field in the early-time dynamics due to the states with $n > 2$ excitations. However, in the interval $\Gamma t \in (5, 10)$ most of the intensity is due to the 1-excited state, indicating that this is a long-lived subradiant state.

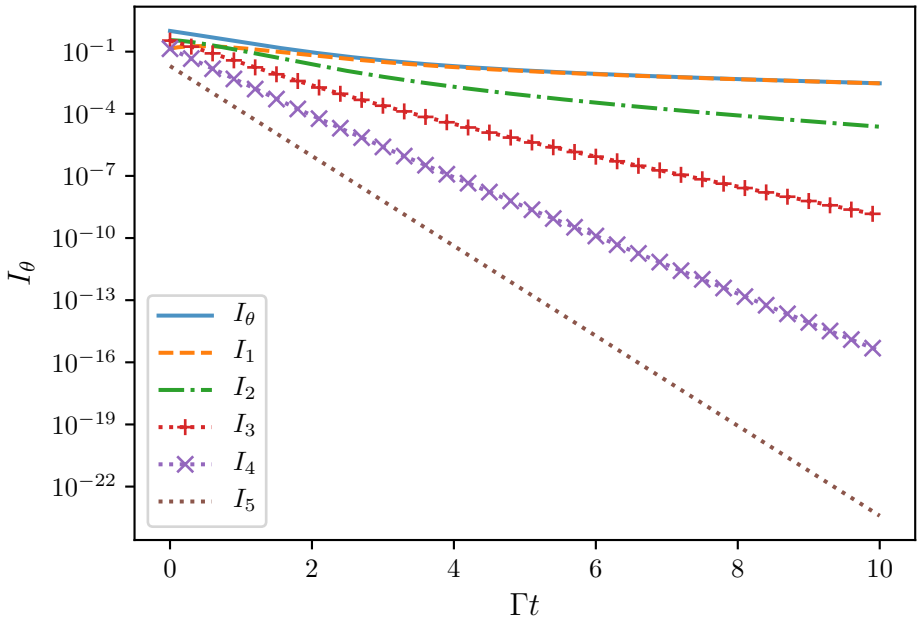

Figure 36 – Intensity of the radiated far-field in a detection angle $\theta = 35°$ for a cloud of $N = 5$ atoms using exact simulation. I_θ is the total intensity while I_n is the contribution of the n-excited state. Spatial density $\rho = 0.1k^3$, saturation parameter $s = 5$ and detuning $\Delta = -4$. Average over 50 realizations using a uniform sphere distribution.
Source: By the author

4.2.2 A non-separability parameter for the decay dynamics

In section 4.1.4 we observed a slope in the switch-on dynamics which is not captured by the MF model. We remind that, in the MF approximation, we evolve the density matrices $\hat{\rho}_n = (\mathbb{1} + \langle\hat{\sigma}_n\rangle\,\hat{\sigma}_n)/2$ of N coupled atoms without any quantum correlation and obtain the N-atom density matrix with a product state $\hat{\rho}^N = \bigotimes \hat{\rho}_n$. With exact simulations (E) we evolve the total $(2^N \times 2^N)$ N-atom density matrix, for quantum correlations of any order. One can calculate the single atom density matrices by evaluating the mean values of the Pauli operator for each atom and define the N-atom product state density matrix for exact simulation. Note that this product state will give a different result from the MF dynamics since for exact simulations the mean values $\langle\hat{\sigma}_n\rangle$ are influenced by the quantum terms in the dynamics. We define a non-separability parameter by subtracting the product state from the total N-atom density matrix, and summing up all off-diagonal terms:

$$Q = \sum_{i \neq j} \rho_{ij} - \rho_{ij}^N \tag{4.28}$$

In Fig. 37 we calculate the decay dynamics with initial condition the steady-state for the given saturation. We also compare with the decay for the product state as initial condition. The results are very similar, the parameter Q is very small at the beginning and the quantum correlations (of any order) build up during the dynamics. We observe

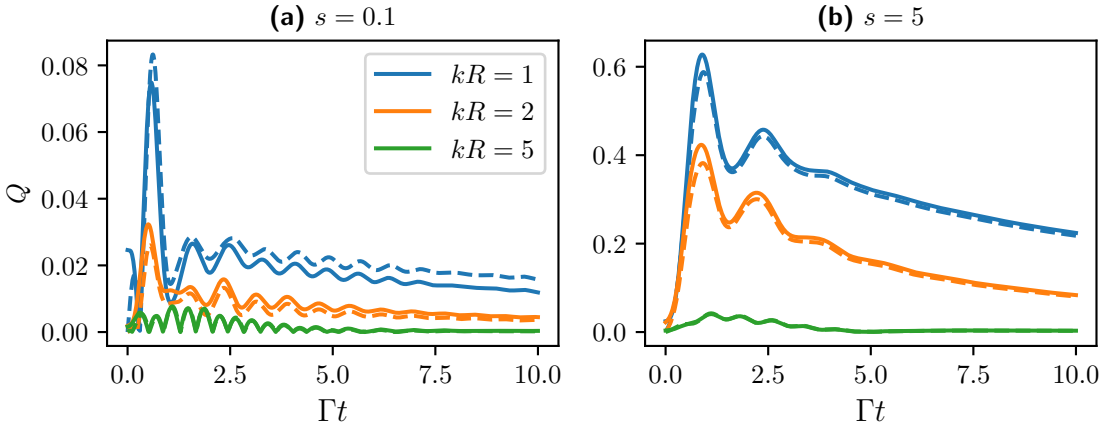

Figure 37 – Time evolution of the parameter Q varying the spherical cloud radius kR. Simulation parameter $N = 4$, $\Delta = -4\Gamma$ and saturation (a) $s = 0.1$; (b) $s = 5.0$. The dashed lines represent the same dynamics with initial condition the product-state density matrix. Average over 50 realizations.
Source: By the author

the same slope behavior in the saturated case (Fig. 37(b)) as the slope behavior of the radiated field for the high b_0 case in section 4.1.4 for the switch-on dynamics.

We can obtain the decay time constant from a exponential fitting of the radiated field in the time interval $\Gamma t \in (5, 10)$ and compare with the non-separability parameter averaged in the same time interval. In Fig. 38 we observe the behavior of the parameter Q as a function of the saturation. For high saturation Q reaches a constant value independent of the detuning (Fig. 38(a)) similar to the subradiant decay time constant in Fig. 31(a). The scaling behavior of $Q/(\tau_n - 1)^2$ in Fig. 38(b) resembles the scaling of τ_n as a function of b_0 in Fig. 32.

The presented results demonstrate a strong relation of the quantum correlations, accounted with the parameter Q, with the subradiant decay time τ_N, which suggest that subradiance in the saturated regime may be related to non-classical atomic states.

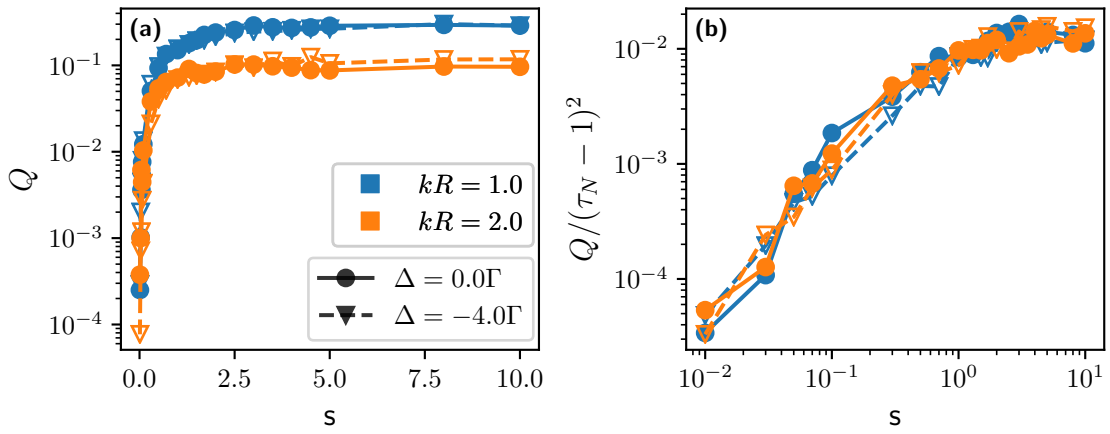

Figure 38 – (a) averaged parameter Q in the interval $\Gamma t \in (5, 10)$ as a function of the saturation. In (b) the scaling behavior of $Q/(\tau_N - 1)^2$ with the saturation. τ_N is obtained from a exponential fit of the intensity of the radiated field in the interval $\Gamma t \in (5, 10)$. Average over 50 realizations.

Source: By the author

5 FLUORESCENCE POWER SPECTRUM

In Section 2.3.2 we presented the fluorescence power spectrum obtained from the Fourier transform (Eq. 2.60) of the first order coherence function Eq. 2.61 using the quantum regression theorem. We discussed some results in the literature: new side bands at multiples of the Rabi frequency Ω_{GR} in the Mollow triplet for a dense small system of two-level atoms; an asymmetry in the forward direction for the spectrum of a large dilute cloud, driven out of resonance, using a perturbative approach that does not include quantum correlations.

Here, we have investigated in more details cooperative effects in the fluorescence spectrum, using the QPC method presented in Section 3.3. By combining the QPC method with the quantum regression theorem, using as a basis for the N-atom state the mean value of the operators $\langle\hat{\sigma}_n^a\rangle$ and $c_{nm}^{ab} = \left\langle\hat{\sigma}_n^a\hat{\sigma}_m^b\right\rangle$ we are able to perform numerical calculations for a dilute cloud of hundreds of atoms. In section 5.1 we present the results for quantum cooperative effects in the power spectrum.[23] Finally, in Section 5.2 we discuss preliminary results for the spectrum obtained with an atomic sensor model, that allows us to monitor dynamically the fluorescence spectrum, beyond the steady-state spectrum calculated with the quantum regression theorem.

5.1 Quantum cooperative effects in the power spectrum

The fluorescence power spectrum is obtained from the first-order coherence function $g^{(1)} \propto \left\langle\hat{E}(t)\hat{E}^{(+)}(t+\tau)\right\rangle$ (Eq. 2.61). Since the electric far-field depends on the atomic operators $\hat{E}^{+} \propto \sum\hat{\sigma}_n^- e^{-ik_0\hat{n}.\mathbf{r_n}}$ (Eq. 2.54), thus it depends on two-time two-atom correlations $\langle\hat{\sigma}_n^+(t)\hat{\sigma}_m^-(t+\tau)\rangle$. The QPC method is a promising approximation to describe this observable, since it addresses accurately two-atom correlations.

Let us consider a cloud of many two-level atoms driven by a monochromatic light and decaying by spontaneous emission through the vacuum modes. The quantum regression theorem is applied when the system is in the steady-state with the driving laser always turned on. In that sense we calculate the steady-state power spectrum in which the single-time operators are stationary. That way the complexity to calculate the two-time correlations to obtain the spectrum is reduced, as reaching the steady-state does not require computing all the dynamics, but rather using a solver such as with the Newton-Krylov method.

We benchmark the QPC method ((N) in Fig. 39) by comparing the fluorescence spectrum to the exact simulation (E), with a small system $N = 7$ and a uniform sphere of spatial density ρ/k^3. We obtain a really good agreement for densities up to $\rho/k^3 = 0.3$. We

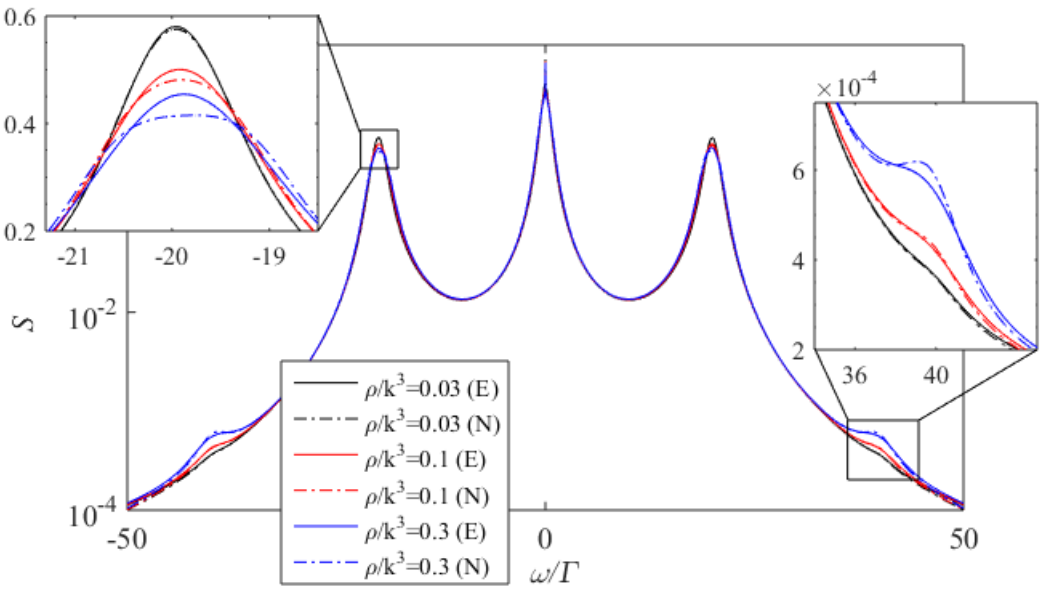

Figure 39 – Benchmark of the QPC method (N) with exact simulations (E) for a cloud of $N = 7$ atoms, $\Omega = 20\Gamma$ and $\Delta = 0$ varying the spatial density ρ/k^3. A good agreement is obtained for densities up to $0.3k^3$.

Source: Adapted from PUCCI *et al.*[23]

also took the average over several position realizations to eliminate statistical deviations and defined a hard-sphere condition with a minimal distance between atoms to avoid pair effects as discussed in Fig. 12.

As mentioned previously, using the QPC method we can address a dilute cloud with hundreds of atoms. For a resonant laser-atom interaction, as can be observed in Fig. 40 (a) the new sidebands at 2Ω are present even in the dilute regime. In addition, the amplitudes of the sidebands scale linearly with the on-resonance optical thickness b_0 (Fig. 40 (b)). Note that, since the spectrum was normalized it is not simply due to the increasing number of atoms, it is a true quantum cooperative effect in the sense that it relies on their interaction. However, the relative amplitude of the new sidebands in comparison with the Mollow triplet is orders of magnitude smaller (10^3) making it challenging to be observed experimentally due to precision issues and random noise. We shift our analyses to the out-off-resonance case, where an asymmetry in the Mollow triplet was reported in the forward direction.[35]

Adding a detuning to the light-atom coupling, the asymmetry is present not only in the forward direction, but also, and more prominent, for other observed angles ($\theta \neq 0$, Fig. 41 (a)), and we also obtain a scaling with b_0 in Fig. 41 (b). This asymmetry might be more accessible to observe in an experiment as it reaches up to 30%. Note that this asymmetry out of the forward cone is not predicted by the perturbative approach[35], which does not include pair correlations.

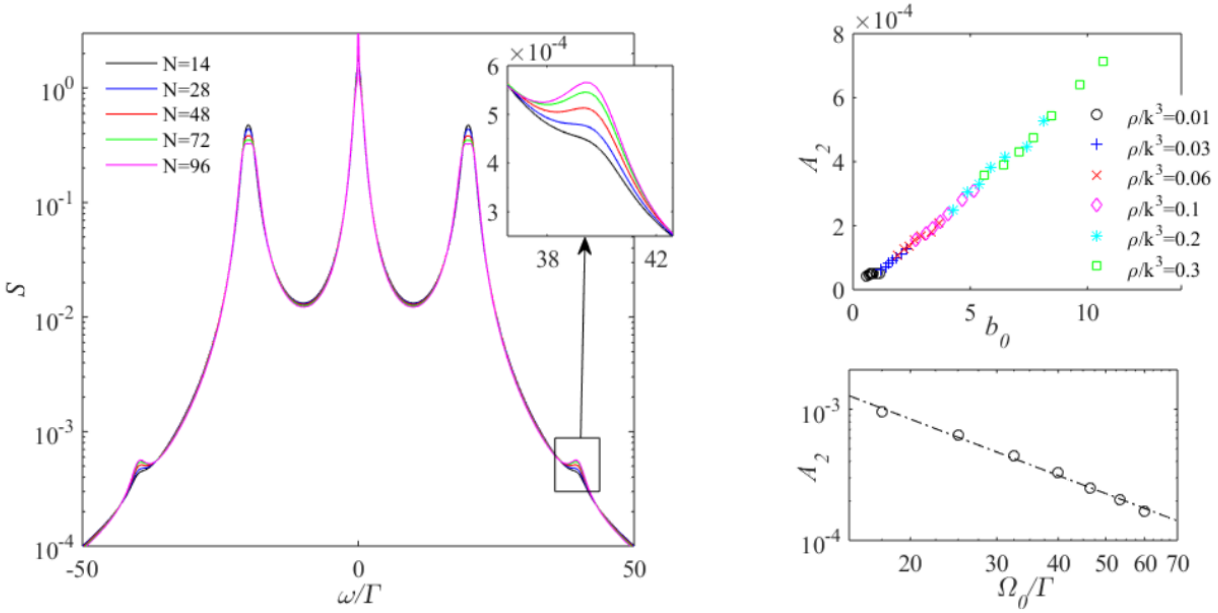

(a) (b)

Figure 40 – Sidebands in the Mollow triplet at 2Ω for a cloud in ressonance $\Delta = 0$. (a) The fluorescence spectrum for a cloud of density $\rho/k^3 = 0.1$ with $\Omega = 20\Gamma$ and $N \in (14, 96)$. (b) The amplitude of the peaks scaling linearly with the on-resonance optical thickness b_0 varying the spatial density for $N = 72$ and driving $\Omega = 20\Gamma$. (c) amplitude dependence with the Rabi frequency Ω for a fixed density $\rho/k^3 = 0.1$ with $N = 72$; the dashed dote line is the scaling behavior with a power law fitting $A_2 = 0.06(\omega/\Gamma)^{1.4}$. The amplitudes are calculated as $\int_{2\Omega-\delta\omega}^{2\Omega+\delta\omega} |S - S_1| d\omega$ with S_1 the single atom spectrum.

Source: Adapted from PUCCI *et al.*[23]

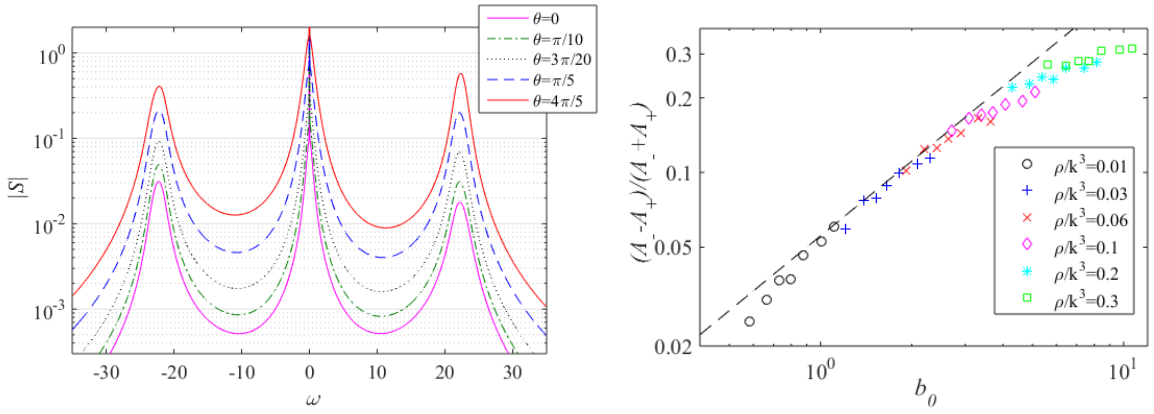

Figure 41 – Asymmetry in the Mollow sidebands at Ω_{GR}/Γ for a cloud out-off resonance $\Delta = \Omega/2$ varying the detection angle. On the left a cloud of density $\rho/k^3 = 0.1$ and $\Omega = 20\Gamma$. On the right the scaling of the asymmetry with the on-resonance optical thickness b_0. We observe a asymmetry not only in the forward direction $\theta = 0$ but also outside the frontal lobe. The asymmetry is defined by difference of the amplitudes for negative and positive frequencies normalized by their sum $(A_- - A_+)/(A_- + A_+)$. The amplitudes are calculated by integrating the spectrum in a suitable interval in the vicinity of $\pm\Omega_{GR}$.

Source: Adapted from PUCCI *et al.*[23]

5.2 Spectrum from a atomic sensor model

In Section 5.1 we obtained the steady-state fluorescence power spectrum making use of the quantum regression theorem. In order to obtain a time-dependent spectrum, for example to monitor the frequency of the photons emitted in the switch-off dynamics, the quantum regression is no longer valid and another approach is necessary. We obtained preliminary results using a model in which a two-level sensor is used to obtain the fluorescence spectrum.[73] The sensor acts as a two-level emitter which is weakly coupled to the system (in order not to disturb it), and has a specific resonant frequency (which is the frequency probed): tuning this frequency allows to compute the spectrum, and this retrieve the Mollow spectrum, for example CARREÑO; VALLE; LAUSSY.[74] Also, an arbitrary number of sensors can be introduced, to prove photon-photon correlations or any higher-order correlations. Thus, the sensors are included in the dynamics as part of the system Hamiltonian, and since each represent an extra degree of freedom, they bring extra complexity to the numerical simulations.

Practically, for a single sensor we define the sensor-atomic cloud interaction Hamiltonian as follows:

$$\hat{H}_s = -(\omega - \Delta)\hat{\sigma}_s^- \hat{\sigma}_s^+ + \sum_n \varepsilon \left(e^{-i\hat{k}_s \cdot \mathbf{r_n}} \hat{\sigma}_n^+ \hat{\sigma}_s^- + e^{i\hat{k}_s \cdot \mathbf{r_n}} \hat{\sigma}_s^+ \hat{\sigma}_n^- \right) \tag{5.1}$$

with ε the sensor-system coupling and ω the frequency at which the correlation is calculated. The Lindbladian operator for the sensor is defined, for a sensor linewidth γ_s, as:

$$\mathcal{L}(\hat{\rho}) = \frac{\gamma_s}{2} \left(2\hat{\sigma}_s^- \hat{\rho} \hat{\sigma}_s^+ - \left\{ \hat{\sigma}_s^+ \hat{\sigma}_s^-, \hat{\rho} \right\} \right) \tag{5.2}$$

Finally, the spectrum is obtained from the correlation:

$$S(\omega, T) = \frac{\langle \hat{\sigma}_s^+(\omega, T) \hat{\sigma}_s^-(\omega, T) \rangle}{\varepsilon^2} \tag{5.3}$$

We point out that some advantages of the sensor method are that (1) the radiated intensity at a given frequency is obtained as a steady-state value, without computing two-time correlations, and (2) the spectrum can be computed dynamically. Some disadvantages, however, are that (1) for each frequency, a simulation with a sensor tuned at that frequency must be run, and (2) each sensor represents an extra degree of freedom, thus increasing the computational cost. In Fig. 42 we calculated the spectrum with two atoms separated by a distance $kd = 0.2$ for the switch-off dynamics using exact simulation (E). For the steady-state $T = 0$ we obtain a similar spectrum comparing to the quantum regression theorem in Fig 12. As the decay dynamics evolves, the system loses its excited population and the Mollow triplet vanishes, the fluorescence spectrum is again centered in the atomic transition frequency ω_a for long times $\Gamma T = 10$. This shows that only resonant light survives on long-time scales.

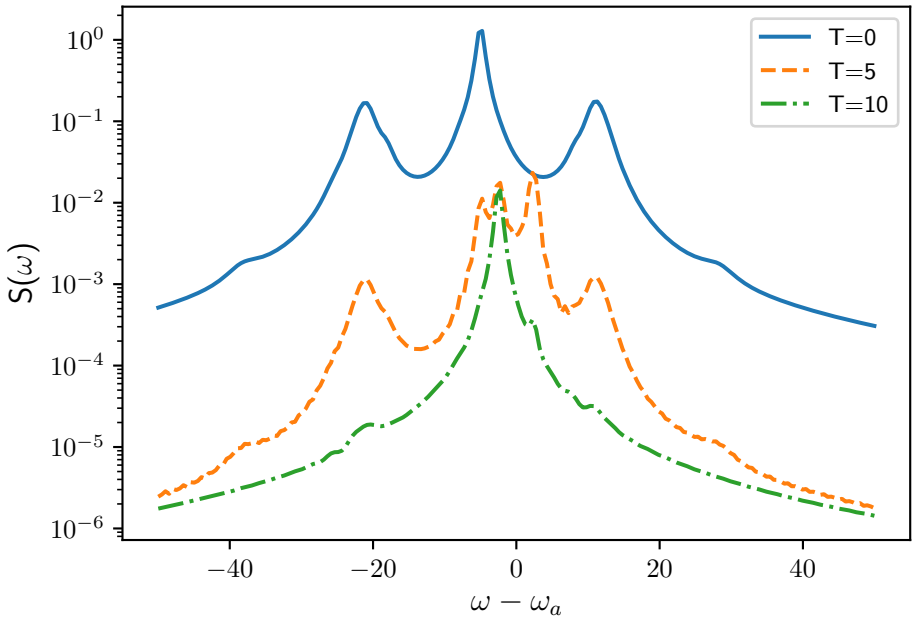

Figure 42 – Fluorescence power spectrum from an atomic sensor for the switch-off dynamics of a $N = 2$ atomic 'cloud'. For $T = 0$ the steady-state is calculated and the laser turned-off. Two atoms separated by $kd = 0.2$, saturation $s = 5$ and detuning $\Delta = -5$. One sensor in the direction $\theta = 35°$ with coupling parameter $\varepsilon = 0.01$ and sensor linewidth $\gamma_s = 1.0$.
Source: By the author.

This figure illustrates the fact that long-time radiation dynamics, *i.e.*, subradiance, presents a non-trivial evolution of the spectrum. This project is in a initial phase and might be addressed in a future work, with the sensor parameters optimization and maybe an extension for the QPC model to investigate larger clouds. More specifically, we intend to understand the features of subradiance for initially strongly driven clouds, as obtained from the experimental setup in Nice, France. Note that, for each ω to scan the spectrum, we do calculate the steady-state (at $T = 0$) and evolve the decay dynamics to the times ($\Gamma T \in (0, 10)$), making the simulation time-consuming. For the exact simulation adding a sensor doubles the size of the Hilbert space. With the QPC method, where the equations scale with N^2, we could add multiple sensors measuring at different frequencies and reduce the simulation time. This is a promising lead we intend to follow to monitor dynamically the spectrum of many-atom dilute clouds.

6 CONCLUSIONS & PERSPECTIVES

We explored the dynamics of a system of N two-level atoms, in the vacuum, driven by a monochromatic laser. By treating a dilute system, cooled below the Doppler limit, we neglected near fields effects, polarization and considered the atoms fixed in position. After tracing-out the infinite degrees of freedom of the vacuum modes we obtained the Lindbladian master equation that gives the dynamics of the collective spontaneous emission. Since we can only perform numerical simulations for a dozen of atoms with the full quantum master equation, we made use of the BBGKY hierarchy to obtain the quantum pair correlation and the non-linear mean-field approximation. We also demonstrate that the classical dipole equation is recovered in the limit of low excitation. Then, we performed simulations searching for quantum collective effects in the radiated field in the far-field limit and in the fluorescence power spectrum.

For the switch-on dynamics, in which all atoms are in the ground-state at $t = 0$ and the driven laser is turned on, we showed that, in the limit of low saturation, superradiance and a frequency shift can be observed. We obtained a good agreement of the numerical results with the experimental data for the intensity of the radiated field. When increasing the saturation parameter, the classical linear equations fails to capture the dynamics while the non-linear mean-field equation gives a good agreement with the switch-on experiment. Surprisingly, the mean-field equation described very well the switch-on dynamics even for high saturation. It presents small deviations when compared to the quantum pair correlation method for $\Omega \approx \Gamma$, where the collective emission term is comparable to the Rabi frequency that drives the system. For high optical thickness, we observed a slope for long-time that might be related to the pumping of a subradiant mode. While the mean-field approximation did not capture the slope, it was observed with the quantum pair correlation method.

For the switch-off dynamics, in which the system is driven to the steady-state and the laser is turned-off at $t = 0$, we have only the decay of the system excitation, with no Rabi oscillations. We looked into the decay of the excited population and observed a faster decay for states with $n > N/2$, with N the total number of atoms. In that sense, the subradiant behavior might be related to the states with few excited atoms. In the intensity of the radiated field, we observed a time interval in which the mean-field equation cannot capture subradiance but it is present when quantum correlations are added. In this quantum subradiant regime, a scaling of the subradiant time with atomic cloud optical thickness was obtained, thus the optical thickness presents itself not only as the cooperative parameter in the classical dipoles limit but also in the quantum regime. Using exact simulations, we also analyzed the decay dynamics of a separability parameter. We

excluded the product state density matrix of N two-level atoms to obtain a parameter that includes only quantum corrections. We obtained a slope similar to the one observed in the switch-on case, which, once more, indicates the importance of quantum correlations in the subradiant radiation.

The fluorescence power spectrum, composed by 3 peaks in the saturated regime, one centered in the transition frequency and two peaks at $\pm\Omega_{GR}$, is obtained from the first order optical coherence function. We showed that the quantum correlations leads to the emergence of new peaks at $\pm 2\Omega_{GR}$, for a resonant laser, even in the dilute regime. When the detuning is considered, we observed an asymmetry in the sidebands not only in the forward direction but also for $\theta \neq 0$. That way, it became clear that quantum cooperative effects can be observed in the first order optical coherence function and not only on the second order one, related to photon bunching and anti-bunching. Preliminary results, of a sensor model able to obtain the fluorescence spectrum as a function of time, can give more clues of the process occurring during the decay dynamics. It will be addressed in the future.

In conclusion, we presented a detailed study of the switch-on dynamics in the low saturation limit and showed that, collective effects like superradiance and a frequency shift, can also be observed for this case, results similar as compared to the switch-off values in the literature. We showed that the classical dipole equation fails with increasing the saturation. The mean-field and quantum pair correlation are good methods to capture correctly the dynamics to explore non-linear and quantum features in this dilute system. We explored a quantum subradiant behavior in the radiated field decay, only possible with quantum correlations, and also obtained quantum cooperative effects in the fluorescence power spectrum. The cooperativity parameter is the optical thickness, as in the classical case.

We focused our analyses in a dilute cloud with two-level atoms randomly distributed in space. The proposed methods can readily be applied to study the phenomenon of collective back scattering and the codes developed for this work will be useful for further investigation in the cold atoms research group.

One could also explore regular lattices, with the lattice parameter greater than the laser wavelength, to study the propagation of the excitation of the correlations in the system after a local quench. For example, the Lieb-Robinson bounds on the speed of propagation of correlations could be explored in more detail. Since the two-level atom algebra is the same, it does not matter if we are dealing with spins, trapped ions or even quantum bits, the method could also be applied in other research fields with some adaptation.

In order to improve the method, one can include near-field terms and polarization of the light. It might allow to address a dense system, however the truncation method

that includes only pair correlation may not be valid anymore in the dense regime. One could also treat the dynamics without the Markov approximation to include retarded field and the state memory in the dynamics, however, it would be a challenging problem.

The truncated Wigner approximation, in the phase space dynamics, might be a good path to improve the quantum simulations. A more detailed approach with a truncation scheme in the Moyal bracket expansion, and the inclusion of stochastic quantum jumps in the dynamics might present better results.

REFERENCES

1 DIRAC, P. A. M.; BOHR, N. H. D. The quantum theory of the emission and absorption of radiation. **Proceedings of the Royal Society of London A**, v. 114, n. 767, p. 243–265, 1927. doi: 10.1098/rspa.1927.0039.

2 SIMON, J. *et al.* Quantum simulation of antiferromagnetic spin chains in an optical lattice. **Nature**, v. 472, n. 7343, p. 307–312, 2011. doi: 10.1038/nature09994.

3 BRITTON, J. W. *et al.* Engineered two-dimensional ising interactions in a trapped-ion quantum simulator with hundreds of spins. **Nature**, v. 484, n. 7395, p. 489–492, 2012. doi: 10.1038/nature10981.

4 ISLAM, R. *et al.* Emergence and frustration of magnetism with variable-range interactions in a quantum simulator. **Science**, v. 340, n. 6132, p. 583–587, 2013. doi: 10.1126/science.1232296.

5 GEORGESCU, I. M.; ASHHAB, S.; NORI, F. Quantum simulation. **Reviews of Modern Physics**, v. 86, n. 1, p. 153–185, 2014. doi: 10.1103/RevModPhys.86.153.

6 JAYNES, E. T.; CUMMINGS, F. W. Comparison of quantum and semiclassical radiation theories with application to the beam maser. **Proceedings of the IEEE**, v. 51, n. 1, p. 89–109, 1963. doi: 10.1109/PROC.1963.1664.

7 DZYALOSHINSKII, I. E.; LIFSHITZ, E. M.; PITAEVSKII, L. P. General theory of Van der Waals' forces. **Soviet Physics Uspekhi**, v. 4, n. 2, p. 153–176, 1961. doi: 10.1070/pu1961v004n02abeh003330.

8 CASIMIR, H. B. G.; POLDER, D. The influence of retardation on the london-van der waals forces. **Physical Review**, v. 73, n. 4, p. 360–372, 1948. doi: 10.1103/PhysRev.73.360.

9 DICKE, R. H. Coherence in spontaneous radiation processes. **Physical Review**, v. 93, n. 1, p. 99–110, 1954. doi: 10.1103/PhysRev.93.99.

10 GUERIN, W.; ARAÚJO, M. O.; KAISER, R. Subradiance in a large cloud of cold atoms. **Physical Review Letters**, v. 116, n. 8, p. 083601, 2016. doi: 10.1103/PhysRevLett.116.083601.

11 COURTEILLE, P. W. *et al.* Modification of radiation pressure due to cooperative scattering of light. **European Physical Journal D**, v. 58, n. 1, p. 69–73, 2010. doi: 10.1140/epjd/e2010-00095-6.

12 BUX, S. *et al.* Cooperative scattering by cold atoms. **Journal of Modern Optics**, v. 57, n. 19, p. 1841–1848, 2010. doi: 10.1080/09500340.2010.503011.

13 BIENAIMÉ, T. *et al.* Interplay between radiation pressure force and scattered light intensity in the cooperative scattering by cold atoms. **Journal of Modern Optics**, v. 61, n. 1, p. 18–24, 2014. doi: 10.1080/09500340.2013.829264.

14 RÖHLSBERGER, R. *et al.* Collective lamb shift in single-photon superradiance. **Science**, v. 328, n. 5983, p. 1248–1251, 2010. doi: 10.1126/science.1187770.

15 ROOF, S. J. *et al.* Observation of single-photon superradiance and the cooperative lamb shift in an extended sample of cold atoms. **Physical Review Letters**, v. 117, n. 7, p. 073003, 2016. doi: 10.1103/PhysRevLett.117.073003.

16 SCULLY, M. O.; SVIDZINSKY, A. A. The effects of the n atom collective lamb shift on single photon superradiance. **Physics Letters A**, v. 373, n. 14, p. 1283–1286, 2009. doi: http://dx.doi.org/10.1016/j.physleta.2009.02.027.

17 SCULLY, M. O. *et al.* Directed spontaneous emission from an extended ensemble of n atoms: timing is everything. **Physical Review Letters**, v. 96, n. 1, p. 010501, 2006. doi: 10.1103/PhysRevLett.96.010501.

18 BIENAIMÉ, T. *et al.* Cooperativity in light scattering by cold atoms. **Fortschritte der Physik**, v. 61, n. 2-3, p. 377–392, 2013. doi: 10.1002/prop.201200089.

19 MOLLOW, B. R. Power spectrum of light scattered by two-level systems. **Physical Review**, v. 188, n. 5, p. 1969–1975, 1969. doi: 10.1103/PhysRev.188.1969.

20 DAS, S.; AGARWAL, G. S.; SCULLY, M. O. Quantum interferences in cooperative dicke emission from spatial variation of the laser phase. **Physical Review Letters**, v. 101, n. 15, p. 153601, 2008. doi: 10.1103/PhysRevLett.101.153601.

21 JONES, R.; SAINT, R.; OLMOS, B. Far-field resonance fluorescence from a dipole-interacting laser-driven cold atomic gas. **Journal of Physics B:** atomic, molecular and optical physics, v. 50, n. 1, p. 014004, 2016. doi: 10.1088/1361-6455/50/1/014004.

22 ESPIRITO SANTO, T. S. *et al.* Collective excitation dynamics of a cold atom cloud. **Physical Review A**, v. 101, n. 1, p. 013617, 2020. doi: 10.1103/PhysRevA.101.013617.

23 PUCCI, L. *et al.* Quantum effects in the cooperative scattering of light by atomic clouds. **Physical Review A**, v. 95, n. 5, p. 053625, 2017. doi: 10.1103/PhysRevA.95.053625.

24 HYDROGEN spectral series. Available from: https://en.wikipedia.org/wiki/Hydrogen_spectral_series. Accessible at: Jan. 22, 2020.

25 GARDINER, C.; ZOLLER, P. **The quantum world of ultra-cold atoms and light book I:** foundations of quantum optics. London: Imperial College Press, 2014. doi: 10.1142/p941.

26 SCULLY, M. O.; ZUBAIRY, M. S. **Quantum optics**. Cambridge: Cambridge University Press, 1997. doi: 10.1017/CBO9780511813993.

27 RABI, I. I. Space quantization in a gyrating magnetic field. **Physical Review**, v. 51, n. 8, p. 652–654, 1937. doi: 10.1103/PhysRev.51.652.

28 HAAR, D. T. Theory and applications of the density matrix. **Reports on Progress in Physics**, v. 24, 1961. doi: 10.1088/0034-4885/24/1/307.

29 BREUER, H.-P.; PETRUCCIONE, F. **The theory of open quantum systems**. Oxford: Oxford University Press, 2007. doi: 10.1093/acprof:oso/9780199213900.001.0001.

30 FRIEDBERG, R.; MANASSAH, J. T. Analytic expressions for the initial cooperative decay rate and cooperative lamb shift for a spherical sample of two-level atoms. **Physical Review A**, v. 374, n. 15, p. 1648–1659, 2010. doi: 10.1016/j.physleta.2010.02.012.

31 LIEB, E. H.; ROBINSON, D. W. The finite group velocity of quantum spin systems. *In*: NACHTERGAELE, B.; SOLOVEJ, J. P.; YNGVASON, J. (ed.). **Statistical mechanics:** selecta of Elliott H. Lieb. Berlin: Springer, 2004. p. 425–431. doi: 10.1007/978-3-662-10018-9_25.

32 FOSS-FEIG, M. *et al.* Nearly linear light cones in long-range interacting quantum systems. **Physical Review Letters**, v. 114, n. 15, p. 157201, 2015. doi: 10.1103/PhysRevLett.114.157201.

33 RICHERME, P. *et al.* Non-local propagation of correlations in quantum systems with long-range interactions. **Nature**, v. 511, n. 7508, p. 198–201, 2014. doi: 10.1038/nature13450.

34 AGARWAL, G. S. Quantum statistical theories of spontaneous emission and their relation to other approaches. *In*: HÖHLER, G. (ed.). **Quantum optics**. Berlin: Springer, 1974. p. 1–128. doi: 10.1007/BFb0042382.

35 OTT, J. R. *et al.* Cooperative fluorescence from a strongly driven dilute cloud of atoms. **Physical Review A**, v. 87, n. 6, p. 061801, 2013. doi: 10.1103/PhysRevA.87.061801.

36 SENITZKY, I. R. Sidebands in strong-field resonance fluorescence. **Physical Review Letters**, v. 40, n. 20, p. 1334–1337, 1978. doi: 10.1103/PhysRevLett.40.1334.

37 AGARWAL, G. S. *et al.* Analytical solution for the spectrum of resonance fluorescence of a cooperative system of two atoms and the existence of additional sidebands. **Physical Review A**, v. 21, n. 1, p. 257–259, 1980. doi: 10.1103/PhysRevA.21.257.

38 JOHANSSON, J.; NATION, P.; NORI, F. Qutip: an open-source python framework for the dynamics of open quantum systems. **Computer Physics Communications**, v. 183, n. 8, p. 1760 – 1772, 2012. doi: 10.1016/j.cpc.2012.02.021.

39 BONITZ, M. **Quantum kinetic theory**. 2nd ed. New York: Springer International Publishing, 2016. doi: 10.1007/978-3-319-24121-0.

40 PUCCI, L.; ROY, A.; KASTNER, M. Simulation of quantum spin dynamics by phase space sampling of bogoliubov-born-green-kirkwood-yvon trajectories. **Physical Review B**, v. 93, n. 17, p. 174302, 2016. doi: 10.1103/PhysRevB.93.174302.

41 SVIDZINSKY, A. A.; CHANG, J.-T.; SCULLY, M. O. Cooperative spontaneous emission of n atoms: many-body eigenstates, the effect of virtual lamb shift processes, and analogy with radiation of n classical oscillators. **Physical Review A**, v. 81, n. 5, p. 053821, 2010. doi: 10.1103/PhysRevA.81.053821.

42 JENNEWEIN, S. *et al.* Coherent scattering of near-resonant light by a dense, microscopic cloud of cold two-level atoms: experiment versus theory. **Physical Review A**, v. 97, n. 5, p. 053816, 2018. doi: 10.1103/PhysRevA.97.053816.

43 MEISER, D. *et al.* Prospects for a millihertz-linewidth laser. **Physical Review Letters**, v. 102, n. 16, p. 163601, 2009. doi: 10.1103/PhysRevLett.102.163601.

44 RYOGO, K. Generalized cumulant expansion method. **Journal of the Physical Society of Japan**, v. 17, n. 7, 2013. doi: 10.1143/JPSJ.17.1100.

45 KRÄMER, S.; RITSCH, H. Generalized mean-field approach to simulate the dynamics of large open spin ensembles with long range interactions. **European Physical Journal D**, v. 69, n. 12, p. 282, 2015. doi: 10.1140/epjd/e2015-60266-5.

46 DUM, R.; ZOLLER, P.; RITSCH, H. Monte Carlo simulation of the atomic master equation for spontaneous emission. **Physical Review A**, v. 45, n. 7, p. 4879–4887, 1992. doi: 10.1103/PhysRevA.45.4879.

47 DUM, R. *et al.* Monte Carlo simulation of master equations in quantum optics for vacuum, thermal, and squeezed reservoirs. **Physical Review A**, v. 46, n. 7, p. 4382–4396, 1992. doi: 10.1103/PhysRevA.46.4382.

48 DALIBARD, J.; CASTIN, Y.; MØLMER, K. Wave-function approach to dissipative processes in quantum optics. **Physical Review Letters**, v. 68, n. 5, p. 580–583, 1992. doi: 10.1103/PhysRevLett.68.580.

49 GARDINER, C. W.; PARKINS, A. S.; ZOLLER, P. Wave-function quantum stochastic differential equations and quantum-jump simulation methods. **Physical Review A**, v. 46, n. 7, p. 4363–4381, 1992. doi: 10.1103/PhysRevA.46.4363.

50 DALEY, A. J. Quantum trajectories and open many-body quantum systems. **Advances in Physics**, v. 63, n. 2, p. 77–149, 2014. doi: 10.1080/00018732.2014.933502.

51 MØLMER, K.; CASTIN, Y.; DALIBARD, J. Monte Carlo wave-function method in quantum optics. **Journal of the Optical Society of America B**, v. 10, n. 3, p. 524–538, 1993. doi: 10.1364/JOSAB.10.000524.

52 POLKOVNIKOV, A. Phase space representation of quantum dynamics. **Annals of Physics**, v. 325, n. 8, p. 1790–1852, 2010. doi: http://dx.doi.org/10.1016/j.aop.2010.02.006.

53 WOOTTERS, W. K. A wigner-function formulation of finite-state quantum mechanics. **Annals of Physics**, v. 176, n. 1, p. 1–21, 1987. doi: http://dx.doi.org/10.1016/0003-4916(87)90176-X.

54 SCHACHENMAYER, J.; PIKOVSKI, A.; REY, A. M. Many-body quantum spin dynamics with monte Carlo trajectories on a discrete phase space. **Physical Review X**, v. 5, n. 1, p. 011022, 2015. doi: 10.1103/PhysRevX.5.011022.

55 SCHACHENMAYER, J.; PIKOVSKI, A.; REY, A. M. Dynamics of correlations in two-dimensional quantum spin models with long-range interactions: a phase-space monte-Carlo study. **New Journal of Physics**, v. 17, n. 6, p. 065009, 2015. doi: 10.1088/1367-2630/17/6/065009.

56 ZHU, B.; REY, A. M.; SCHACHENMAYER, J. A generalized phase space approach for solving quantum spin dynamics. **New Journal of Physics**, v. 21, n. 8, p. 082001, 2019. doi: 10.1088/1367-2630/ab354d.

57 GUERIN, W.; ROUABAH, M. T.; KAISER, R. Light interacting with atomic ensembles: collective, cooperative and mesoscopic effects. **Journal of Modern Optics**, v. 64, n. 9, p. 895–907, 2017. doi: 10.1080/09500340.2016.1215564.

58 KUPRIYANOV, D.; SOKOLOV, I.; HAVEY, M. Mesoscopic coherence in light scattering from cold, optically dense and disordered atomic systems. **Physics Reports**, v. 671, p. 1–60, 2017. doi: https://doi.org/10.1016/j.physrep.2016.12.004.

59 GROSS, M.; HAROCHE, S. Superradiance: an essay on the theory of collective spontaneous emission. **Physics Reports**, v. 93, n. 5, p. 301–396, 1982. doi: 10.1016/0370-1573(82)90102-8.

60 OLIVEIRA, R. A. de *et al.* Single-photon superradiance in cold atoms. **Physical Review A**, v. 90, n. 2, p. 023848, 2014. doi: 10.1103/PhysRevA.90.023848.

61 WEISS, P. *et al.* Subradiance and radiation trapping in cold atoms. **New Journal of Physics**, v. 20, n. 6, p. 063024, 2018. doi: 10.1088/1367-2630/aac5d0.

62 WEISS, P. *et al.* Robustness of dicke subradiance against thermal decoherence. **Physical Review A**, v. 100, n. 3, p. 033833, 2019. doi: 10.1103/PhysRevA.100.033833.

63 SCULLY, M. O. Single photon subradiance: quantum control of spontaneous emission and ultrafast readout. **Physical Review Letters**, v. 115, n. 24, p. 243602, 2015. doi: 10.1103/PhysRevLett.115.243602.

64 MAZETS, I. E.; KURIZKI, G. Multiatom cooperative emission following single-photon absorption: Dicke-state dynamics. **Journal of Physics B:** atomic, molecular and optical physics, v. 40, n. 6, p. F105–F112, 2007. doi: 10.1088/0953-4075/40/6/f01.

65 LEHMBERG, R. H. Radiation from an n-atom system. ii. spontaneous emission from a pair of atoms. **Physical Review A**, v. 2, n. 3, p. 889–896, 1970. doi: 10.1103/PhysRevA.2.889.

66 ARAÚJO, M. O. *et al.* Superradiance in a large and dilute cloud of cold atoms in the linear-optics regime. **Physical Review Letters**, v. 117, n. 7, p. 073002, 2016. doi: 10.1103/PhysRevLett.117.073002.

67 ARAÚJO, M. O.; GUERIN, W.; KAISER, R. Decay dynamics in the coupled-dipole model. **Journal of Modern Optics**, v. 65, n. 11, p. 1345–1354, 2018. doi: 10.1080/09500340.2017.1380856.

68 GOBAN, A. *et al.* Superradiance for atoms trapped along a photonic crystal waveguide. **Physical Review Letters**, v. 115, n. 6, p. 063601, 2015. doi: 10.1103/PhysRevLett.115.063601.

69 SOLANO, P. *et al.* Super-radiance reveals infinite-range dipole interactions through a nanofiber. **Nature Communications**, v. 8, p. 1857, 2017. doi: 10.1038/s41467-017-01994-3.

70 GUERIN, W. *et al.* Collective multimode vacuum rabi splitting. **Physical Review Letters**, v. 123, n. 24, p. 243401, 2019. doi: 10.1103/PhysRevLett.123.243401.

71 GUERIN, W.; KAISER, R. Population of collective modes in light scattering by many atoms. **Physical Review A**, v. 95, n. 5, p. 053865, 2017. doi: 10.1103/PhysRevA.95.053865.

72 MOREIRA, N. A.; KAISER, R.; BACHELARD, R. Localization vs. subradiance in three-dimensional scattering of light. **EPL (Europhysics Letters)**, v. 127, n. 5, p. 54003, 2019. doi: 10.1209/0295-5075/127/54003.

73 VALLE, E. del *et al.* Theory of frequency-filtered and time-resolved n-photon correlations. **Physical Review Letters**, v. 109, n. 18, p. 183601, 2012. doi: 10.1103/PhysRevLett.109.183601.

74 CARREÑO, J. C. L.; VALLE, E. del; LAUSSY, F. P. Photon correlations from the mollow triplet. **Laser & Photonics Reviews**, v. 11, n. 5, p. 1700090, 2017. doi: 10.1002/lpor.201700090.